

# Precision oncology : oncogenic stat3 signalling in brain tumours

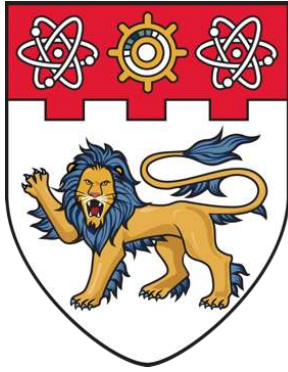
Tan, Melanie Si Yan

2019

Tan, M. S. Y. (2019). Precision oncology : oncogenic stat3 signalling in brain tumours.  
Doctoral thesis, Nanyang Technological University, Singapore.

<https://hdl.handle.net/10356/82741>

<https://doi.org/10.32657/10220/49094>



**NANYANG  
TECHNOLOGICAL  
UNIVERSITY**  

---

**SINGAPORE**

**PRECISION ONCOLOGY: ONCOGENIC STAT3  
SIGNALLING IN BRAIN TUMOURS**

**TAN SI YAN MELANIE**

**SCHOOL OF BIOLOGICAL SCIENCES**

**2019**

**PRECISION ONCOLOGY: ONCOGENIC STAT3  
SIGNALLING IN BRAIN TUMOURS**

**TAN SI YAN MELANIE**

**SCHOOL OF BIOLOGICAL SCIENCES**

A thesis submitted to the Nanyang Technological  
University in partial fulfilment of the requirement  
for the degree of Doctor of Philosophy

2019

## Statement of Originality

I hereby certify that the work embodied in this thesis is the result of original research done by me except where otherwise stated in this thesis. The thesis work has not been submitted for a degree or professional qualification to any other university or institution. I declare that this thesis is written by myself and is free of plagiarism and of sufficient grammatical clarity to be examined. I confirm that the investigations were conducted in accord with the ethics policies and integrity standards of Nanyang Technological University and that the research data are presented honestly and without prejudice.

22 Jan 2019

.....  
Date



.....  
MELANIE TAN

## Supervisor Declaration Statement

I have reviewed the content and presentation style of this thesis and declare it of sufficient grammatical clarity to be examined. To the best of my knowledge, the thesis is free of plagiarism and the research and writing are those of the candidate's except as acknowledged in the Author Attribution Statement. I confirm that the investigations were conducted in accord with the ethics policies and integrity standards of Nanyang Technological University and that the research data are presented honestly and without prejudice.

22 Jan 2019

.....

Date

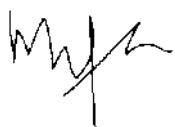


.....

Assoc Prof Andrew Tan

**Thesis Title: PRECISION ONCOLOGY: ONCOGENIC STAT3  
SIGNALLING IN BRAIN TUMOURS**

I have excluded the Authorship Attribution Statement declaration because the thesis does not contain any published material.



.....  
Melanie Tan

Date : 22 Jan 2019



.....  
Assoc Prof Andrew Tan

Date: 22 Jan 2019

## ACKNOWLEDGEMENTS

“It always seems impossible until it is done.” – Nelson Mandela

With utmost gratitude, I would like to thank my supervisors, Dr. Carol Tang and A/Prof Ang Beng Ti, for all their guidance, support, patience and encouragement they have given me throughout my research journey. Their passion for science has kept me engaged throughout this journey. I truly enjoyed working in the research environment which constantly challenged and encouraged me to grow intellectually. Most importantly, I would like to thank both of them for believing in me. Without their guidance and unceasing assistance, this thesis would not have been possible. I would also like to thank my co-supervisor A/Prof Andrew Tan for his insightful advice and guidance during my PhD stint. I am grateful to all my supervisors for sharing their knowledge and advice during this journey.

I would also like to extend my deepest appreciation to my laboratory colleagues (past and present): Yuk Kien, Edwin, Lynnette, See Wee, Tan Boon, Bikai. Thank you all for the encouragement and guidance that allowed me to complete my project with minimal obstacles. You guys have made my research journey more meaningful and fulfilling. Special acknowledgement to Edwin Sandanaraj (Senior Research Associate at NNI), for his expertise in bioinformatical analysis.

I am also grateful to my dear friends who have always been there for me throughout this research journey. Wenhui, Patricia, Christina for always being there when I am weak. Issac, Justina, Charlene, Low See Wee and anyone else I may have unintentionally left out for the help, support as well as good company.

I would also like to thank my family members who have been supportive and provided me their kind concern, being my listening ear and providing your encouragement. Finally, I must express my gratitude to Bernard for his continued support, understanding, patience and strength when mine was failing.

Thank you all for being by my side throughout this research journey.

**TABLE OF CONTENTS**

<b>ACKNOWLEDGEMENTS</b>	<b>i</b>
<b>List of Figures</b>	<b>v</b>
<b>List of Tables</b>	<b>vii</b>
<b>Abbreviations</b>	<b>viii</b>
<b>Abstract</b>	<b>1</b>
<b>1.0 INTRODUCTION</b>	<b>2</b>
<b>1.1. Classification of Glioblastomas</b>	<b>2</b>
1.1.1. Histological Classification of Glioblastomas	3
1.1.2. Molecular Classification of Glioblastomas	5
<b>1.2. GBM Cell Biology</b>	<b>7</b>
<b>1.3. Glioblastoma-Propagating Cells (GPCs)</b>	<b>8</b>
1.3.1. Functional Validation of GPCs	10
<b>1.4. Mouse Models of Gliomas</b>	<b>11</b>
1.4.1. Genetically Engineered Mouse Models (GEMMs)	12
1.4.2. Xenograft Mouse Models	12
<b>1.5. Signalling Pathways Regulating GBM Biology</b>	<b>13</b>
1.5.1. STAT3 Signalling Pathway	14
1.5.1.1. STAT3 Signalling in Glioblastoma	16
1.5.1.2. STAT3 in Tumourigenesis	17
1.5.1.3. STAT3 Inhibitors	18
1.5.2. IGF-1R Signalling Pathway	20
1.5.2.1. IGF-1R Inhibitors	21
<b>1.6. Mechanisms of Chemoresistance in Glioblastoma</b>	<b>22</b>
1.6.1. STAT3 in Treatment Resistance	23
<b>1.7. Gap in Knowledge and Objectives of Study</b>	<b>24</b>
<b>2.0 MATERIALS AND METHODS</b>	<b>26</b>
<b>2.1. Tissue Collection and Primary Gliomasphere Culture</b>	<b>26</b>
<b>2.2. Small Molecule Inhibitors and Reagents</b>	<b>26</b>
<b>2.3. Cell Viability Assays</b>	<b>27</b>
2.3.1. Cell Viability Assessment Post-treatment with Small Molecule Inhibitors	27



2.3.2. Dose-response Curves and IC <sub>50</sub> Calculations	27
2.3.3. Gliomasphere Formation Assay	27
2.3.4. Invasion Assay	28
<b>2.4. Combination Index (CI Values)</b>	<b>28</b>
<b>2.5. Protein Analysis</b>	<b>28</b>
2.5.1. Immunoblot	28
2.5.2. Co-immunoprecipitation	29
2.5.3. Enzyme-Linked Immunosorbent Assay (ELISA)	29
2.5.4. Immunohistochemistry	30
<b>2.6. Quantitative Real Time RT-PCR</b>	<b>30</b>
<b>2.7. Lentiviral-mediated Knockdown and Over-expression</b>	<b>31</b>
<b>2.8. Stereotaxic Intracranial Implantations</b>	<b>31</b>
<b>2.9. Statistical Analysis</b>	<b>32</b>
2.9.1. Kaplan-Meier Analysis	32
<b>2.10. Bioinformatics Analyses</b>	<b>33</b>
<b>(With help from Mr Edwin Sandanaraj)</b>	
2.10.1. Microarray Data Processing and Analysis	33
2.10.2. Predictive Database Analysis	33
2.10.3. Bayesian Information Criterion Analysis	34
2.10.4. Relative Odds Estimation	34
2.10.5. Functional Gene Module Analysis	35
2.10.6. PamChip Kinome Analysis	35
2.10.7. SynergySeq	36
<b>3.0 RESULTS</b>	<b>38</b>
<b>3.1. <i>STAT3</i> Functionally-tuned Gene Signature</b>	<b>38</b>
<b>3.2. Pharmacological Inhibition of <i>STAT3</i> Mitigates Glioma Cell Growth</b>	<b>44</b>
<b>3.3. Mechanism Contributing to <i>STAT3</i>-resistant Profile</b>	<b>49</b>
<b>3.4. IGF-1R Signalling Pathway Contributes to Chemoresistance Mechanism in <i>STAT3</i>-low GPCs</b>	<b>51</b>
<b>3.5. Depletion of IGFBP2 and C-terminal IGF-1R Restores Sensitivity</b>	<b>55</b>
<b>3.6. Utility of <i>STAT3</i> Functionally-tuned Gene Signature</b>	<b>62</b>
<b>3.7. Chemosensitisation of <i>STAT3</i>-stratified Cells Synergises</b>	

<b>with Standard of Care Temozolomide</b>	<b>63</b>
<b>4.0 DISCUSSION</b>	<b>68</b>
<b>4.1. <i>STAT3</i> Functionally-tuned Gene Signature as a Prognostic Indicator</b>	<b>68</b>
<b>4.2. Understanding Mechanisms underlying <i>STAT3</i>-stratified Patients</b>	<b>69</b>
<b>4.3. Tumour Recurrence</b>	<b>70</b>
<b>4.4. Clinical Significance</b>	<b>72</b>
<b>5.0 FUTURE DIRECTIONS</b>	<b>74</b>
<b>6.0 CONCLUSION</b>	<b>76</b>
<b>7.0 REFERENCES</b>	<b>77</b>
<b>8.0 APPENDICES</b>	<b>98</b>
<b>A. List of Genes Comprising the <i>STAT3</i> Functionally-tuned Gene Signature</b>	<b>98</b>
<b>B. Contingency Table, Univariate and Multivariate Analyses</b>	<b>103</b>
I. Contingency analysis	103
II. Univariate and multivariate analyses	104
<b>C. IC<sub>50</sub> Curves of <i>STAT3</i>-stratified GPCs Treated with Various STAT3 Inhibitors</b>	<b>105</b>
<b>D. Winnowed List of Genes Contributing to Resistance in <i>STAT3</i>-low Cohorts</b>	<b>106</b>
<b>E. List of Protein Tyrosine Kinase</b>	<b>108</b>
<b>F. H-score and IC<sub>50</sub> Values of Patient Tumours</b>	<b>110</b>
I. H-score	110
II. IC <sub>50</sub> curves of <i>STAT3</i> -stratified GPCs treated with AZD1480	111
<b>9.0 PUBLICATIONS</b>	<b>112</b>
<b>10.0 POSTERS</b>	<b>113</b>

**List of Figures**

		Pg
Figure 1.	Adapted overview of the latest 2016 World Health Organization classification of adult diffuse gliomas based on histological and genetic features (Louis <i>et al.</i> , 2016).	3
Figure 2.	NNI Brain Tumour Resource Workflow.	9
Figure 3.	Illustration of STAT3 signalling.	16
Figure 4.	Computational workflow to prioritise kinase candidates with functional/biological evidence.	36
Figure 5.	NNI- <i>STAT3</i> functionally-tuned gene signature.	39
Figure 6.	<i>STAT3</i> knockdown reduced viability, gliomasphere-forming ability and clonogenicity.	42
Figure 7.	NNI- <i>STAT3</i> functionally-tuned gene signature stratifies patient survival, independent of current clinical indicators.	43
Figure 8.	<i>STAT3</i> stratification in GBM cohorts.	44
Figure 9.	NNI patient tumours have variable <i>STAT3</i> expression and can be stratified by <i>STAT3</i> functionally-tuned signature.	45
Figure 10.	NNI patient cells can be stratified by their <i>STAT3</i> status, and show variable response to STAT3 inhibitors both <i>in vitro</i> and <i>in vivo</i> .	48
Figure 11.	Recovery Assay.	49
Figure 12.	Mechanistic gene candidates discerning cooperative genes responsible in the <i>STAT3</i> -resistant profile.	51
Figure 13.	Proposed mechanism in <i>STAT3</i> -low (therapeutic resistant) GBM cells.	52
Figure 14.	Mechanistic gene candidates identified by NNI- <i>STAT3</i> gene signature representing resistance to STAT3 inhibitor.	54
Figure 15.	Depletion of mechanistic gene <i>IGFBP2</i> restores sensitivity in <i>STAT3</i> -low GBM cells.	55
Figure 16.	Depletion of IGF-1R C-terminal domain restores sensitivity in <i>STAT3</i> -low GBM cells.	56
Figure 17.	Sensitisation of resistant <i>STAT3</i> -low GBM cells with dual inhibition.	58

Figure 18.	Immunohistochemical (IHC) staining and quantification of pSTAT3 and IGF-1R on patient-derived xenograft (PDX) tumours.	60
Figure 19.	Response to NT157, a selective inhibitor targeting IGF-1R and STAT3 signalling pathways.	61
Figure 20.	NNI- <i>STAT3</i> signature better identifies responsive patient cohorts.	63
Figure 21.	Chemosensitisation of patient-derived GPCs with standard of care temozolomide treatment.	65
Figure 22.	Ranking of LINCS compounds based on their concordance to temozolomide consensus signature.	67
Appendix C.	IC <sub>50</sub> curves of <i>STAT3</i> -stratified GPCs treated with various STAT3 inhibitors	105
Appendix F(II).	IC <sub>50</sub> curves of <i>STAT3</i> -stratified GPCs treated with AZD1480	111

**List of Tables**

		Pg
Table 1.	Adopted summary for WHO classification of glial tumours based on histology	4
Table 2.	Gene-specific primers	31
Table 3.	Kaplan-Meier statistics	59
Table 4.	List of top synergistic compounds able to reverse <i>STAT3</i> -high GBM disease signature	67
Table 5.	Distribution of matched recurrent patients with subtype switching	71
Appendix A.	List of Genes Comprising the <i>STAT3</i> Functionally-tuned Gene Signature	98
Appendix B.	Contingency Table, Univariate and Multivariate Analyses	103
Appendix D.	Winnowed List of Genes Contributing to Chemoresistance	104
Appendix E.	List of Protein Tyrosine Kinase	108
Appendix F(I).	H-score	110

**Abbreviations**

AKT	Protein kinase B
ATP	Adenosine triphosphate
BBB	Blood-brain barrier
Bcl-2, -XL	B-cell lymphoma 2, extra large
BCNU	Carmustine
bFGF	basic fibroblast growth factor
BIC	Bayesian information criterion
BSA	Bovine serum albumin
CCNU	Lomustine
CDK	Cyclin-dependent kinase
CI	Combination index
CIC	Cancer-initiating cells
CI	Classical
CMAP	Connectivity map
CNS	Central nervous system
CPC	Cancer propagating cells
CSC	Cancer stem cells
DC	Dendritic cell
DMEM	Dulbecco's modified eagle medium
DMSO	Dimethylsulfoxide
DNMT1	DNA methyltransferase 1
ECDF	Empirical Cumulative Distribution Functions
ECM	Extracellular matrix
EGF	Epidermal growth factor
EGFR	Epidermal growth factor receptor
ELISA	Enzyme-linked immunosorbent assay
ELK3	E26 transformation-specific containing gene
Fa	Fraction of cell viability affected
FBS	Fetal bovine serum
FDR	False discovery rate
GBM	Glioblastoma Multiforme
GDP	Guanosine diphosphate
GEMMs	Genetically engineered mouse models
GEO	Gene Expression Omnibus
GI	Glioma Intrinsic
GMPPA	GDP-mannose pyrophosphorylase A
gp130	Glycoprotein 130
GPCs	Glioma-propagating cells
GSEA	Gene Set Enrichment Analysis
HPRT	Hypoxanthine phosphoribosyltransferase
HR	Hazard Ratios
HRP	Horseradish peroxidase

IC <sub>50</sub>	Half maximal inhibitory concentration
IDH	Isocitrate dehydrogenase
IFN	Interferon
IGF	Insulin-like growth factor
IGF-1R	Insulin growth factor 1 receptor
IGFBP	Insulin growth factor binding protein
IL-6	Interleukin-6
IRS	Insulin receptor substrate
JAK	Janus Kinase
KD	Knockdown
KLHDC8A	Kelch domain containing 8A
LGG	Low grade glioma
LIF	Leukaemia inhibitor factor
LINCS	Library of Integrated Network-Based Cellular Signatures
mAb	Monoclonal antibody
MAPK	Mitogen-activated protein kinase
Mes	Mesenchymal
MGMT	O <sup>6</sup> -methylguanine methyltransferase
MLH	MutL Homolog
MMP	Matrix metalloprotease
MMR	Mismatch Repair
MSH	MutS Homolog
mTOR	Mammalian target of rapamycin
Mut	Mutant
NCI	National Cancer Institute
Neu	Neural
NEDD9	Neural precursor cell expressed, developmentally down-regulated 9
NF1	Neurofibromatosis 1
NNI	National Neuroscience Institute
NOD-SCID	Non-obese diabetic severe combined immunodeficient
NSC	Neural stem cell
NT	Non-targeting
NTP	Nearest template prediction
OSM	Oncostatin-M
PDGF	Platelet-derived growth factor
PDX	Patient-derived xenograft
PI3K	Phosphatidylinositol 3-kinase
PK	Pharmacokinetics
PLK1	Polo-like kinase 1
PMT	Proneural-mesenchymal transition
PN	Proneural
PFS	Progression-free survival

pSTAT3	Phospho-STAT3
PTEN	Phosphatase and tensin homolog
PVDF	Polyvinylidene difluoride
qRT-PCR	Quantitative Reverse Transcription Polymerase Chain Reaction
RB	Retinoblastoma
Rembrandt	Repository for molecular brain neoplasia data
RTK	Receptor tyrosine kinase
S727	Serine 727
SH2	Src homology-2
shRNA	Short hairpin RNA
siRNA	Small interfering RNA
SNAP23	Synaptosomal-associated protein 23
STAT3	Signal transducer and activator of transcription
TCGA	The Cancer Genome Atlas
TGF	Transforming growth factor
TKI	Tyrosine kinase inhibitors
TMZ	Temozolomide
TNF	Tumour necrosis factor
VAMP	Vesicle-associated Membrane Protein
VEGF	Vascular endothelial growth factor
WHO	World Health Organisation
WT	Wild-type
Y705	Tyrosine 705



**Abstract**

Brain tumour patients diagnosed with grade IV glioblastoma often show dismal prognosis despite the standard of care chemo- and radiation therapies. The Cancer Genome Atlas effort demonstrated that transcriptomic profiles distinguish three glioma-intrinsic subtypes, each with unique genetic aberrations and prognosis. While significant effort has been made to characterize glioblastomas based on their molecular content, functional or biological validation remains lacking. STAT3 activation represents the final molecular switch that precedes transition into the highly aggressive, recurrent mesenchymal subtype. Furthermore, there are several STAT3 small molecule inhibitors in clinical trials for solid malignancies. Our work provides an insight into *STAT3* stratification in GBM using our unique *STAT3* functionally-tuned gene signature. We show that this gene signature stratifies GBM patients, and is not confounded by current clinical and molecular classification. To provide preclinical evidence that stratification leads to more effective STAT3-targeted treatment outcomes, we applied this signature to our collection of tumour cells with matched primary and xenograft tumour molecular information. We identified *STAT3*-sensitive and -resistant tumours, and validated *STAT3* dependence *in vitro* using pharmacologically-treated and genetically manipulated, matched GBM cells. We validated responsiveness to STAT3 inhibition through *in vitro* and animal experimentation. Importantly, by analysing up-regulated genes in the *STAT3*-resistant profile, corroborated by our kinome screen data, dual inhibition of IGF-1R and STAT3 presents a viable strategy to sensitize this cohort. Our study highlights the importance of patient stratification for the utility of STAT3 inhibitors in GBM. This represents a new paradigm challenging the current use of morphological methods such as histology to diagnose and subsequently treat patients.

## 1.0 INTRODUCTION

Among cancers, neoplasms of the central nervous system (CNS) have the worst prognosis. Grade IV glioblastoma (GBM) constitutes 80% of adult primary malignant brain tumours. Patients diagnosed with GBM often survive no more than fifteen months despite advanced surgical intervention with chemotherapy and radiation (Louis *et al.*, 2007; Louis *et al.*, 2016). Tumour recurrence and the development of resistance towards standard of care treatment regimens are key reasons for the poor outcome, and this has been attributed to the molecular heterogeneity of morphologically-identical tumour tissue. This underscores the importance of developing patient stratification methods based on the individual's molecular content, to better identify potential responders, thus sparing non-responders from financial costs and chemotherapeutic side effects. This forms the core of precision medicine where the focus is on targeted therapy.

### 1.1 Classification of Glioblastomas

Ineffective therapy in GBM is often attributed to the infiltrative nature of the tumour cells into the adjacent brain parenchyma that obviates complete resection of malignant tissue. Additionally, these cells are resistant to standard of care treatment regimens. A better understanding of the diversity of mechanisms governing GBM growth would facilitate identification of more efficacious therapeutics. Over the last decade, several large, publicly-funded efforts established that histologically identical GBM tumours are in fact molecularly heterogeneous, with gene expression driving brain tumour progression and clinical outcome (Atlas, 2008; Ceccarelli *et al.*, 2016; Noushmehr *et al.*, 2010; Verhaak *et al.*, 2010). Primary adult malignant GBM which are predominantly isocitrate dehydrogenase-wild-type (*IDH*-WT) can be subdivided into three transcriptomic subtypes (proneural, classical and mesenchymal) after separating out microglial and stromal cell type contribution (Wang *et al.*, 2018). In addition, the Ivy GBM Atlas recently published an annotation of molecular profiles correlating with anatomically distinct features, such as necrosis, endothelial cell proliferation and tumour cell infiltration (Puchalski *et al.*, 2018). These findings contribute to the complexity of treating malignant brain tumours, and further highlight the inadequacy of depending on morphological approaches to diagnose and subsequently treat patients. Importantly,

the revised World Health Organisation (WHO) classification scheme for brain tumours (Figure 1) incorporates molecular markers such as IDH mutant status, 1p/19q co-deletion status, to influence treatment decision (Louis *et al.*, 2016). These efforts highlight the cellular and molecular heterogeneity in GBM tumours, and further underscores the necessity to prescribe treatment regimens based on a stratified population.

Key to therapeutically targeting each tumour subtype is the ability to test treatment response in a preclinical animal model established from patient material. GBM has been shown to arise from cells with considerable self-renewal capacity, termed glioblastoma-propagating cells (GPCs). Orthotopic intracranial xenograft models established from GPCs are important as they recapitulate the patient's original tumour morphology and transcriptomic profile (Verhaak *et al.*, 2010). Furthermore, a recent study supports that therapeutic resistance is reflected in gene expression profiles of molecular subtypes, and may not correspond to differences in somatic mutations (Stathias *et al.*, 2018). Thus, GPC-derived mouse xenograft models provide a core capability of precision oncology-driven preclinical studies.

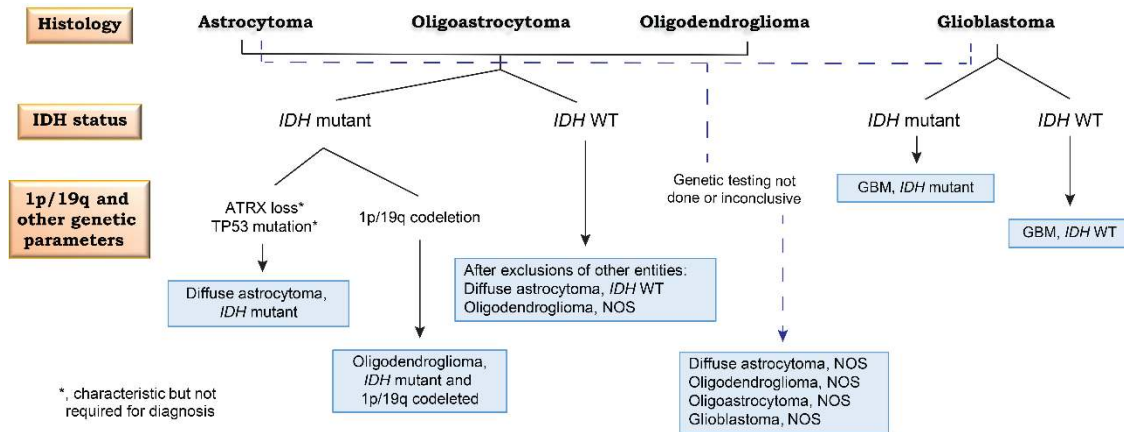


**Figure 1. Adapted overview of the latest 2016 World Health Organization classification of adult diffuse gliomas based on histological and genetic features (Louis *et al.*, 2016).**

### 1.1.1. Histological Classification of Glioblastomas

Prior to the updated 2016 WHO classification, the 2007 classification system relied on the laboratory evaluation of brain tumours which entails a pathological diagnosis based on microscopic and immunohistochemical features, and an

assessment of their clinical behaviour (grade). The histological grading of brain tumours includes their appearances based on cellularity, anaplasia, proliferative index and even presence of necrosis, along with other features. Under the microscope, gliomas can resemble astrocytes, oligodendrocytes, or ependymal cells (Louis, 2006). Gliomas are histologically separated into grades I through IV according to the WHO criteria, with grade I being the least malignant, and grade IV the most malignant. The WHO system divides these diffuse gliomas into astrocytic tumours, oligodendrogliomas and oligoastrocytomas. These are then graded into histological degrees of malignancy. Table 1 summarises the WHO classification of glial tumours based on histology.

**Table 1. Adapted summary for WHO classification of glial tumours based on histology (Kleihues *et al.*, 2002).**

WHO Grading	Type of glioma	Criteria
Grade I	Pilocytic astrocytoma	Benign; slow-growing; low cellularity; absence of microvascular proliferation
Grade II	Diffuse astrocytoma	Well differentiated neoplastic astrocytic cells; increased hypercellularity; absence of mitosis, necrosis and microvascular proliferation
Grade III	Anaplastic astrocytoma	Distinct nuclei atypia; high rate of hypercellularity and mitosis; absence of necrosis and microvascular proliferation
Grade IV	Glioblastoma	Pleomorphic astrocytic tumour cells with marked nuclei atypia; high rate of hypercellularity and mitosis; presence of microvascular proliferation and necrosis

Grade I tumours typically have a good prognosis with benign cytological features, and occurs more frequently in children (Wen and Kesari, 2008). Grade II tumours (diffuse astrocytoma) occurs most frequently in young adults, and are characterised by moderate cellularity, with no anaplasia or mitotic activity. Grade III tumours (anaplastic astrocytoma) is clinically and pathologically an intermediate of grade II and glioblastoma. They are characterised on histologic examination to

be similar to grade II but with greater hypercellularity and anaplasia, with presence of nuclear atypia and a higher mitotic rate and Ki67 proliferative index. Grade IV tumours (GBMs) is the most malignant and with high cellularity, cellular and nuclear anaplasia, presence of mitoses with addition of microvascular proliferation and presence of necrosis. Glioblastoma has a wide range of histological appearance; on one end, small cell glioblastoma are composed of poorly differentiated, uniform small cells, while on the other spectrum, giant cell glioblastoma is characterised by extreme anaplasia (Agamanolis, 2005).

### 1.1.2. Molecular Classification of Glioblastomas

In the past decade, there has been a considerable number of studies evaluating the molecular characteristics of GBM tumours, providing a more accurate and objective method to identify distinct molecular subgroups that correlate with prognostic outcome. The National Cancer Institute in the United States first initiated a multi-consortial effort in 2006 to deep profile the molecular content of a collection of tumours (The Cancer Genome Atlas, TCGA), and GBM was of initial focus due to its dismal survival outcome (Atlas, 2008). Indeed, over the past decade, the standard of care for GBM patients remained unchanged, with temozolomide and radiation as frontline therapy. Despite this, GBM patients have almost always demonstrated recurrence with no curative outcome; yet temozolomide has a worldwide annual revenue of US\$1 billion. This highlights a significant unmet clinical need to improve the lives of patients. TCGA efforts have shown that histologically identical tumours can be molecularly heterogeneous, and that these molecular traits predict patient survival independent of current clinical indicators. The initial publication from TCGA demonstrated that GBM patients sustained mutations that could be grouped into 3 major signalling pathways: Retinoblastoma (RB), p53 tumour suppressor pathway and Receptor tyrosine kinases (RTKs) (Atlas, 2008). These findings thus present a novel paradigm in diagnosis and clinical management of patients, where tumour morphology no longer remains the sole criteria to diagnose and subsequently determine clinical management of the disease.

A follow-up study demonstrated that histologically identical GBM tumours could be divided into 4 transcriptomic subtypes, each displaying unique genomic aberrations and clinical outcome (Verhaak *et al.*, 2010). Using consensus pattern

clustering, the 4 distinct classes identified included the proneural (PN), classical (Cl), neural (Neu) and mesenchymal (Mes) subtypes. The proneural cohort is characterised by patients of better prognosis, often associated with the presence of *IDH1* mutations and active platelet-derived growth factor (PDGF) signalling. On the other spectrum, the mesenchymal cohort is characterised by patients with GBM of a highly aggressive and recurrent nature, a subset (approximately 30% of Mes) which is typified by either homozygous loss of wild-type, or loss-of-function mutations of the tumour suppressor gene neurofibromatosis gene (*NF1*) (Brennan *et al.*, 2009). It is important to note that despite these landmark findings, the clinical application of tumour molecular information at identifying and targeting responder cohorts remains untested. TCGA studies thus provide an initial starting point to establish such stratification methods.

A recent study by Wang *et al.* distinguished transcriptomic profiles unique to only tumour cells and not cells in the microenvironment, such as stromal cells and microglia (Wang *et al.*, 2018). The authors further segregated glioma-specific mRNAs from normal cells by comparing patient tissue with matched cell cultures; core versus peripheral tumour samples, and RNA-sequencing of single GBM cells isolated by flow cytometric sorting. The authors observed that “by removing the contributions of the microenvironment, we developed a much clearer picture of the ecosystem of hundreds of tumours”. With this method, the molecular markers that defined the original neural subtype were attributed to the presence of normal neural tissue, therefore rendering them unrepresented as a “true subtype”. Thus, the neural subtype was removed. Additionally, the study of gene expression patterns in GBM post-treatment demonstrated that the presence of macrophages correlated with poorer outcomes, adding that an increased number of activated T cells was associated with hypermutations (Wang *et al.*, 2018). This study therefore demonstrates that immunotherapy with checkpoint inhibitors could be useful to target the tumour microenvironment. Collectively, these efforts emphasize that GBM disease progression and prognosis are primarily driven by gene expression profiles of tumour tissue.

## 1.2. GBM Cell Biology

Over the last decade, our knowledge of the molecular biology of glioblastoma has increased drastically. GBM cells are characterized by a large variety of cellular dysfunction resulting in resistance to many therapies. Such mechanisms include loss of cell cycle control, over-expression of growth factor receptors, angiogenesis, invasion and migration, genetic instability and abnormal apoptosis.

Dysregulation of cell cycle progression often contributes to self-renewal of tumour cells. The G1-S phase of cell cycle checkpoint has been implicated as a common mechanism. This checkpoint is controlled by the p16/cyclin-dependent kinase (CDK)/retinoblastoma (RB) pathway. In malignant GBM, genetic growth regulatory defects frequently occur when compared to low grade gliomas (LGGs) (Ueki *et al.*, 1996). Another mechanism that results in aberrant proliferation is the over-expression of growth factor receptors such as PDGF, transforming growth factor (TGF), insulin-like growth factor (IGF) and epidermal growth factor receptor (EGFR). GBM cells often display autocrine feedback pathways promoting growth by over-expressing both the receptors and ligands. Ability to escape apoptosis of defective cells in altered checkpoint pathways is another contributor. The loss of p53 function disrupts normal glial apoptotic response that ensues growth factor over-expression (Gomez-Manzano *et al.*, 1997). *TP53* mutations often also lead to genomic instability and promote tumour progression. Selection of these malignant clones characterizes the progression of LGG to higher grades (Leung *et al.*, 2000).

Glioblastomas are vascular tumours. Angiogenic molecules such as the vascular endothelial growth factor (VEGF) is often implicated, and expressed in areas adjacent to necrosis (Louis, 2006). Interestingly, three studies characterized the increased vasculature and presence of endothelial cells to be of tumour origin; thus, it is highly probable that current anti-VEGF therapies such as bevacizumab are ineffective as they target normal endothelial cells. In early clinical studies using bevacizumab, impressive radiographic responses were noted, with prolongation of progression-free survival (PFS). However, it was soon realized that VEGF pathway inhibitors results in transitory clinical and radiographic response prior to inevitable progression. This demonstrated that treatment with anti-angiogenic inhibitors had little anti-tumour activity (Weathers and de Groot, 2015). In animal modelling studies, it has been shown that administration of bevacizumab in tumour-laden mice

resulted in the gradual selection of resistant tumour cell clones, thus giving the initial impression of tumour involution but ultimately, the tumour recurs with heightened aggressiveness (Bao *et al.*, 2006b; Ricci-Vitiani *et al.*, 2010; Soda *et al.*, 2011). The diffuse nature of GBM growth has also been attributed to cell surface and extracellular matrix (ECM) molecules that regulate signal transduction and influence migration and invasion (Nakada *et al.*, 2007; Rao, 2003). Indeed, our team has demonstrated the importance of specific ECM molecules in promoting invasion and metastasis (Ma *et al.*, 2016a; Monzo *et al.*, 2016).

### 1.3. Glioblastoma-Propagating Cells (GPCs)

The CNS has a multifaceted cellular hierarchy of cells ranging from neural stem cells (NSCs), to lineage-committed progenitors with restricted differentiation potential, and the terminally-differentiated cells (Rietze *et al.*, 2001; Uchida *et al.*, 2000). Cancer stem cells (CSCs) and/or cancer-initiating cells (CICs) were initially defined to exhibit extensive self-renewal capacity, tumour-initiating ability, and the ability to generate various differentiated progeny similar (Li *et al.*, 2014) to astrocytes, oligodendrocytes and neurons (Reya *et al.*, 2001). We have shown that these “stemness” properties include the ability to extensively self-renew (symmetrical and asymmetrical divisions) and/or differentiate. Furthermore, several investigators have shown that CSCs can be induced to differentiate upon addition of TGF, leading to tumour involution and cessation of tumour growth (Anido *et al.*, 2010). The definition of patient-derived CSCs precludes their evaluation of the cell-of-origin. Such studies can only be revealed through transgenic lineage-tracing mouse experiments where somatic mutations are generated in various neural cell types with a living colour fluorescence tag (Alcantara Llaguno *et al.*, 2009; Jacques *et al.*, 2010; Zheng *et al.*, 2008). Tumour initiation and propagation can then be traced throughout the lifetime of the mouse, thus revealing the *bona fide* cell-of-origin in GBM formation. Therefore, in our GBM study, we have appropriately termed our patient-derived cancer cells as “glioblastoma-propagating cells” (GPCs), having the capability to be serially transplanted and perpetuate tumours in an orthotopic mouse xenograft model which we showed previously to recapitulate the patient’s original tumour pathophysiology and molecular profile (Chong *et al.*, 2016; Foong *et al.*, 2011).



Patient-derived glioblastoma-propagating cells (GPCs) are cultivated as spheres, suspended in serum-free media supplemented with growth factors (Galli *et al.*, 2004). This media composition is similar to that used to maintain NSCs, and promotes self-renewal and tumorigenic potential of GPCs, without cellular differentiation induced by serum (Reynolds and Weiss, 1992; Reynolds and Weiss, 1996; Svendsen *et al.*, 1998). Likewise, we and other investigators have demonstrated that tumour “stem-like” cells sustained in serum-free conditions mimic the morphological features, transcriptomic and genotype of the parent tumours (Chong *et al.*, 2009; Foong *et al.*, 2011; Lee *et al.*, 2006). Thus, GPCs provide a core capability of precision oncology where in preclinical studies, the ability to re-establish the tumour in a mouse model becomes essential to further exploratory efforts.

Our lab since inception has developed a technique of collecting GPCs isolated from patient tumours, with our methods preserving the karyotypic and transcriptomic hallmarks comparable to the patient’s original primary tumour (Chong *et al.*, 2009). Our previous publications have also validated that within our patient-derived glioblastoma cells lies transcriptomic programs influencing the primary tumour phenotype and prognostic outcome (Chong *et al.*, 2016; Foong *et al.*, 2012; Foong *et al.*, 2011; Koh *et al.*, 2013; Ng *et al.*, 2012). Figure 2 illustrates our NNI Brain Tumour Resource workflow.

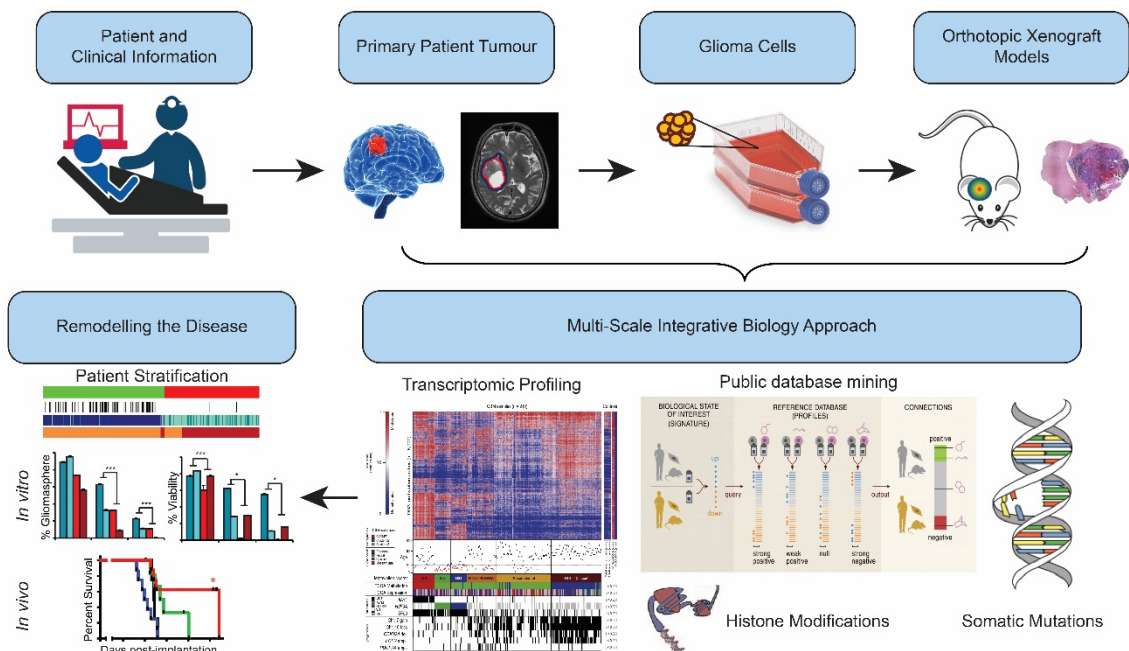


**Figure 2. NNI Brain Tumour Resource Workflow.**

### 1.3.1. Functional Validation of GPCs

Multiple cell surface markers have been implicated in glioma tumour-initiating and -forming capability. The pivotal effort by Singh *et al.* established that CD133, a putative neural stem cell marker derived from the malignant GBM cells was necessary and sufficient to initiate and reform the tumour upon orthotopic transplantation in immunodeficient mice (Singh *et al.*, 2003). In view of these initial observations, many groups have suggested additional markers representing the tumour-propagating cells in brain tumours. These include CD15, nestin, Sox2, CD44 and integrin- $\alpha$ 6 (Anido *et al.*, 2010; Bar *et al.*, 2007; Gangemi *et al.*, 2009; Lathia *et al.*, 2010; Son *et al.*, 2009). Nonetheless, several of these stem cell markers are likely expressed on normal cells, and thus do not represent the most ideal therapeutically targetable candidates. Present studies focus on characterizing tumour-initiating cells using criteria such as extensive self-renewal *in vitro* and serial tumour propagation in mouse models (Verhaak *et al.*, 2010).

Cultured GPCs remain clinically relevant as they: (a) contain karyotypic, phenotypic and transcriptomic information mirroring the original patient's tumour; (b) have the ability to re-establish orthotopic tumour xenografts recapitulating the patient's original histopathology; and (c) provide transcriptomic data through GPC-derived gene signatures contributing to disease progression and patient survival outcome, independent of current clinical indicators like histology and age (Chong *et al.*, 2016; Koh *et al.*, 2013). These properties make GPCs an attractive cellular tool for drug screening and evaluation of signalling mechanisms. As GPCs are slow-growing and frequently represent a minority cellular subset, new end-point measures are needed that detect sustained self-renewal capacity, as opposed to routine oncology experiments that rely on short-term viability assays.

A common method to determine *in vitro* GPC frequency is an adaptation of the neurosphere assay (Reynolds and Weiss, 1992). The neurosphere assay is often utilized to estimate neural stem cell frequency in normal neural stem cell and progenitor cells of the CNS. To develop precision from the neurosphere assay which is often confounded by the heterogeneity of cell type mixtures, the sphere-forming frequency and sphere size are determined over at least 3-4 population doublings. This ensures that only *bona fide* neural stem cells are scored for their self-renewal potential, comparing against other mitotically terminal progenitors

that eventually lose sphere-forming ability (Reynolds and Rietze, 2005). GPCs are typically seeded at clonal density, with no more than 2,000-5,000 cells per cm<sup>2</sup>. Sphere number and size are determined to measure the self-renewing population (Gritti *et al.*, 1996; Rietze *et al.*, 2001). Sphere numbers reflect GPC frequency, while the size of individual gliospheres approximates proliferation of self-renewing cells. Notably, GPCs must form serially transplantable tumours reflecting the extensive self-renewal potential, with their xenografted tumours resembling the original primary tumour pathophysiology (Lee *et al.*, 2006). These assays thus provide a fundamental way to assess *bona fide* tumour-propagating cells amidst the more abundant terminal cell lineages.

#### 1.4. Mouse Models of Gliomas

In the past decade, biological heterogeneity in glioma tumours have been demonstrated by molecular genetic analyses. However, experimental mouse models are still vital to conclusively associate mutational events with tumorigenicity arising from evidence implicated by bioinformatics analyses on the genetics of tumour initiation and progression. Unlike the invertebrate model system, mouse tumour development is similar to that of human cancer, as it is associated with other complex processes such as metastasis and angiogenesis (Wee *et al.*, 2011). Essentially, these models provide a genetically-controlled system and a temporal view to study the tumourigenic process, along with the ability to evaluate responses to specific therapies. Advantages of mouse models for the study of cancer includes the precise manipulation of the mouse genome in creating specific genetic modifications, availability of inbred strains that are genetically identical and the extensive physiological and molecular resemblance mice share with humans (Miyai *et al.*, 2017; Rosenthal and Brown, 2007). Modelling brain tumours *in vivo* reveals molecular mechanisms that contribute to oncogenesis. The development of applicable mouse models thus presents the opportunity to interrogate abnormalities of specific pathways contribution to gliomagenesis.

#### 1.4.1. Genetically Engineered Mouse Models (GEMMs)

Genetically engineered mouse models or GEMMs, are popular models to study tumour biology as they can be engineered to reflect genetic similarity to the human disease (Wee *et al.*, 2011). However, they often offer an inaccurate recapitulation of the clinical situation especially in cancer biology whereby disease progression is often sustained by multiple genetic mutations and external factors. Even so, GEMMs are valuable as they reveal the significance of tumour-initiating/driver versus passenger mutations within a disease. Some advantages of the GEMM comprise: (a) the capacity to offer appropriate material for comparative onco-genomic studies, aimed at identifying supplemental genes that are transformed during tumour development; (b) the utility of tumours derived from GEMMs to substantiate the functions of specific genes in tumourigenesis; (c) the ability to investigate the network of genes with specific genetic mutations, therefore permitting the distribution of genetic lesions into distinct pathways and drug target testing. Altogether, GEMMs are useful to understand the molecular association of tumour initiation, progression, histology and therapeutic response.

On the other hand, a limitation to using GEMMs is the requirement of two or more driver mutations for the initiation of tumourigenesis (Alcantara Llaguno *et al.*, 2009; Zheng *et al.*, 2008). The expression levels of the transgene are often elevated and exceeding those in patients. Tumours arising from GEMMs are frequently irregular, giving rise to difficult study designs that require considerable number of animals for statistical reproducibility. The Cancer Genome Atlas (TCGA) endeavour has likewise revealed that the scale of driver mutations varies among patients considerably; therefore the application of a particular GEMM could be limited (Atlas, 2008; Network, 2013). Nonetheless, GEMMs are still crucial to provide insights to the tumour cell-of-origin and -initiating events.

#### 1.4.2. Xenograft Mouse Models

Xenograft mouse models are created by implanting tumour cells into immune-compromised mice such as the non-obese diabetic severe combined immunodeficient (NOD-SCID) strains, either subcutaneously or orthotopically. These models are often characteristically utilised in preclinical trials to assess the efficacy of novel therapeutic agents. Dating back to the late '60s, xenograft mouse

models derived from implantation of commercially procured serum-grown cell lines had been established. Despite the long practice of using these serum-grown cells, several studies have shown that such xenografted tumours display substantial morphological and molecular features unobserved in patient tissues (Hodgson *et al.*, 2009; Lee *et al.*, 2006). In addition, karyotypic and transcriptomic features are altered such that they no longer resemble the patient's original tumour (Behnan *et al.*, 2017; Lee *et al.*, 2006). These concerns were mitigated by the establishment of patient-derived xenograft (PDX) mouse models. Numerous investigations have demonstrated that orthotopic implantation of patient-derived GBM cell lines or tumour explants orthotopically, displays greater clinical relevance (Horten *et al.*, 1981; Kaye *et al.*, 1986; Shapiro *et al.*, 1979). This can be attributed to the availability of the microenvironment supported by the normal mouse brain parenchyma, drug delivery measurements and clearance kinetics to be better evaluated. Studies have demonstrated that PDX tumours phenocopy the pathophysiology and molecular features of the primary tumour (Joo *et al.*, 2013; Lee *et al.*, 2006). The use of patient-derived GPCs to re-establish orthotopic xenografts yield valuable information of GBM histology. Additionally, the significance of recreating the tumour in the anatomically correct site is important to generate PDX tumours that recapitulate the molecular heterogeneity as described by TCGA efforts (Galli *et al.*, 2004; Verhaak *et al.*, 2010). Particularly, their serially propagated tumours retain karyotypic hallmarks and gene expression profiles characteristic of the original primary tumours. Such systems provide an advantage as the cells are derived from human gliomas. These orthotopic xenograft models thus facilitate clinically relevant insight into glioma biology.

### **1.5. Signalling Pathways Regulating GBM Biology**

The integrated analysis of the multi-dimensional genomic data from TCGA described the dysregulation of p53, retinoblastoma (RB), and RTK/RAS/PI(3)K pathways central to GBM initiation (Atlas, 2008). Numerous oncogenic signalling pathways; for instance, the mitogen-activated protein kinase (MAPK), protein kinase B (AKT), receptor tyrosine kinase (RTK), and transforming growth factor- $\beta$  (TGF- $\beta$ ) influence the progression of GBM (Verhaak *et al.*, 2010). Receptor tyrosine kinases (RTKs) have essential roles in neoplasia as activated receptors

transduce signals resulting in cell proliferation and survival. These membrane-bound receptors depend on activation by hormones, cytokines and growth factors. Once a ligand binds, the RTK is activated which then in turn induces receptor monomers to oligomerise, usually dimerization. Upon kinase activation, trans-phosphorylation (cross-phosphorylation of tyrosine residues in the cytoplasmic tail of the opposite monomer) occurs, leading to triggering of various signalling cascades. Indeed, our earlier collaboration with Eli Lilly pharmaceutical company screened our GPCs for small molecule inhibitors targeting key oncogenic pathways and uncovered roles for PI3K/AKT, GSK3 $\beta$ , mammalian target of rapamycin (mTOR) and polo-like kinase 1 (PLK1) (Foong *et al.*, 2012; Foong *et al.*, 2011). Several studies have also substantiated our findings on the regulatory pathways promoting GPC growth (Bao *et al.*, 2006a; Eyler *et al.*, 2008; Kotliarova *et al.*, 2008; Lee *et al.*, 2012a).

#### 1.5.1. STAT3 Signalling Pathway

The Janus kinase-signal transducer and activator of transcription (JAK/STAT) signalling pathway was initially uncovered within the background of downstream interleukin-6 (IL-6)-mediated signalling and has been largely implicated in inflammatory responses (Darnell *et al.*, 1994; Taga *et al.*, 1989). The *STAT* family of genes instructs the making of proteins essential in chemical signalling pathways within cells. When STAT proteins are activated, they translocate to the nucleus and binds regulatory domains (Figure 3). Structurally, STAT3 is similar to other STAT proteins, having a conserved amino-terminus, a DNA-binding domain, a SH2 domain and a carboxy-terminal transactivation domain. STAT3 is activated upon tyrosine phosphorylation (Y705) close to the carboxy-terminus, and serine phosphorylation (S727) within the transactivation domain. In response to cytokine stimulation, tyrosine phosphorylation is mediated by Janus kinase (JAK1), and is required for STAT3 dimerization, nuclear translocation and DNA binding (Guschin *et al.*, 1995). STAT3 proteins are involved in numerous cellular functions, regulating genes that are involved in cell division and growth, cellular movement and apoptosis (Yang *et al.*, 2007). In the immune system, the STAT3 protein transmits signals for the maturation of immune system cells, especially T and B cells, and is involved the regulation of inflammation (Hodge *et al.*, 2005). STAT3

and STAT5 have been established to be vital for cancer progression among the seven STAT family of proteins (Buettner *et al.*, 2002; Haura *et al.*, 2005; Yu and Jove, 2004). Direct evidence of oncogenic STAT3 signalling was demonstrated from the spontaneously dimerizing-mutant form of STAT3, STAT3-C, which does not require tyrosine phosphorylation to be activated (Bromberg *et al.*, 1999).

In cancer cells, the transduction of signalling messages from various receptor and non-receptor tyrosine kinases and vital roles played by STAT3 and STAT5. Additionally, they also modulate the expression of an extensive range of genes implicated in tumour progression (Bromberg and Darnell, 2000; Yu and Jove, 2004; Yu *et al.*, 2009). Despite STAT3 and STAT5 both contributing towards tumour cell proliferation and survival, STAT3 has a noteworthy role of being a favourable target for cancer therapeutics (Herrmann *et al.*, 2010). STAT3 also plays a vital function in stromal cells, which includes immune cells, promoting tumour progression via recruitment to the tumour microenvironment (Bowman *et al.*, 2000; Coffey *et al.*, 1997). Additionally, STAT3 participates in several anti-tumour immune responses as an immune checkpoint (Bowman *et al.*, 2000; Herrmann *et al.*, 2010; Yu *et al.*, 2009). The importance of STAT3 signalling is not restricted to tumour cells and their microenvironment; it also contributes to the self-renewal property of cancer stem-like cells. STAT3 plays an indispensable role in the maintenance of genes crucial for the stem cell phenotype, and is transcriptionally involved in genes important for differentiation (de la Iglesia *et al.*, 2008; Kim *et al.*, 2013; Murray *et al.*, 1990; Smith *et al.*, 1988; Zong *et al.*, 2000).

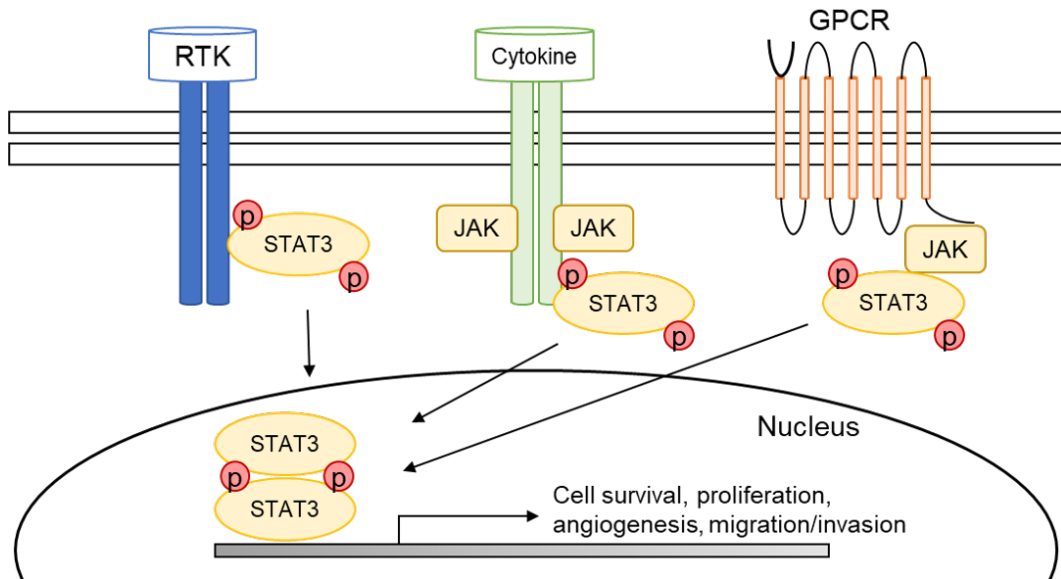


**Figure 3. Illustration of STAT3 signalling.** STAT3 activation is regulated by upstream kinases such as RTKs, cytokine receptors and GPCRs.

#### 1.5.1.1. STAT3 Signalling in Glioblastoma

The Interleukin 6/Janus Kinase/STAT3 (IL-6/JAK/STAT3) signalling pathway plays a significant role in the growth and development of multiple cancers (Hedvat *et al.*, 2009; Jamieson *et al.*, 2006). In various chronic inflammatory conditions such as inflammatory bowel disease and rheumatoid arthritis, as well as in a vast number of patients with solid tumours or hematologic malignancies, including GBM, elevated levels of IL-6 are often detected (Kumari *et al.*, 2016). In the pathogenesis of cancer, elevation of IL-6 stimulates JAK/STAT3 hyperactivation, commonly associated with poorer prognosis (Chen *et al.*, 2013; Kusaba *et al.*, 2006; Ludwig *et al.*, 1991; Macha *et al.*, 2011). Moreover, genes that encode for JAK enzymes, in particular *JAK2*, are commonly mutated in myeloproliferative neoplasms, resulting in constitutive activation of JAK/STAT3 signalling (Jamieson *et al.*, 2006). Specifically, in polycythaemia vera, hematopoietic stem cells are characterized by a hyperactivating *JAK2* V617F mutation (Jamieson *et al.*, 2006); thus the use of JAK/STAT inhibitors effectively target these aberrant self-renewing hematopoietic stem cells, subsequently leading to cessation of tumour growth (Geron *et al.*, 2008; Levine and Gilliland, 2008; Morgan and Gilliland, 2008). However, our preliminary analysis indicated the absence of such mutations in GBM tumours. Clearly, other distinct molecular



events leading to STAT3 up-regulation in glioblastomas remain to be identified. This also suggests the importance of developing novel STAT3 inhibitors in addition to current clinical stage molecules targeting the *JAK2* V617F mutation.

In recent years, much emphasis has been given to the elucidation of the tumour cell-of-origin. The bulk of glioblastoma tumours arise from neural stem cells or astrocytes (Bachoo *et al.*, 2002; Bajenaru *et al.*, 2003; Kwon *et al.*, 2008). Several studies revealed that STAT3 plays a pivotal role in neural stem cell and astrocyte development (Bonni *et al.*, 1997; Rajan and McKay, 1998; Yoshimatsu *et al.*, 2006); furthermore a similar role in GPCs (Guryanova *et al.*, 2011; Sherry *et al.*, 2009). Phosphorylation by receptor-associated tyrosine kinases results in the translocation of STAT3 to the nucleus, regulating transcription of downstream target genes (Darnell *et al.*, 1994). STAT3 activation by cytokines is mediated via JAK family kinases (Schindler and Darnell, 1995).

#### 1.5.1.2. STAT3 in Tumourigenesis

Under normal physiologic situations, the activity of STAT3 is often well-regulated. The communication with its interacting partners allows for feedback inhibition loops and several checkpoints. However, loss of this tight regulation could lead to the initiation of multiple oncogenic mechanisms promoting cell survival, proliferation, invasion, angiogenesis and immune suppression. Contributing to its role in cell survival, STAT3 activity is coupled to anti-apoptotic molecules Bcl-X<sub>L</sub> and survivin (Chen *et al.*, 2010). Numerous studies have demonstrated that STAT3 downregulation results in apoptosis and cell cycle arrest, and noted that even momentary inhibition could effect loss of self-renewal properties and growth arrest (Iwamaru *et al.*, 2006; Sherry *et al.*, 2009).

STAT3 also contributes to invasion via the upregulation of matrix metalloprotease-2 and -9 (MMP-2 and MMP-9) (Liu *et al.*, 2011; Senft *et al.*, 2011). Crucial for survival of tumour cells, vascular endothelial growth factor (VEGF)-mediated angiogenesis provides the required nutrients for enhanced growth and progression (Wei *et al.*, 2011). VEGF is often upregulated in GBM tumours and has been shown to be co-expressed with STAT3 (Schaefer *et al.*, 2002). Anti-VEGF therapy has implicated increased levels of STAT3 in GBM patients, and the coupled use of STAT3 inhibitors with current standard of care therapy could improve the

efficacy of anti-angiogenic treatments (de Groot *et al.*, 2012). The role of VEGF is not limited to angiogenesis alone; it launches a positive feedback loop for increased STAT3 activation in immature dendritic cells (DCs) (Gabrilovich *et al.*, 1996). STAT3 inhibition has been shown to trigger the release of soluble factors such as IL-6, IL-8, interferon (IFN)- $\beta$  and tumour necrosis factor (TNF)- $\alpha$ , and these paracrine signalling molecules could induce DC activation and maturation (See *et al.*, 2012).

#### 1.5.1.3. STAT3 Inhibitors

While copious evidence proposes that STAT3 is a potential target for cancer therapeutics, effective inhibitors that target STAT3 besides the *JAK2* V617F mutation remain to be further developed and evaluated. Recent studies demonstrated the importance of STAT3 as the final molecular switch preceding the proneural-mesenchymal transition (PMT), frequently seen in tumour recurrence; thus its selective targeting presents an attractive therapeutic approach in light of several candidates in clinical trials (Segerman *et al.*, 2016). STAT3 has also been shown to regulate the self-renewal potential of glioblastoma cells, suggesting that its inhibition could lead to a more curative and sustained outcome (Sherry *et al.*, 2009; Wang *et al.*, 2009). Currently, clinical inhibitors of JAKs such as tofacitinib, ruxolitinib and pacritinib are the most studied, with numerous other inhibitors in preclinical development. Presently, the clinical application of JAK inhibitors has centred predominantly on diseases including myeloproliferative cancers and chronic inflammation, with fewer assessment of these inhibitors in solid tumours. We are therefore interested in assessing JAK/STAT3 inhibitory agents in GBM tumours, with an ultimate goal in developing patient stratification methodologies leading to the identification of potential responders and non-responders.

Therapeutic approaches for inhibiting STAT3 activity are grounded on either directly blocking the STAT3 protein or indirect targeting of the upstream regulators in the STAT3 signalling pathway. Activation of STAT3 is contingent on its phosphorylation by JAK2, which promotes monomers of STAT3 to dimerise by the Src homology-2 (SH2) domain, causing STAT3 to go into an active conformation for transcription (Pan *et al.*, 2013). Therefore, STAT3-targeted therapies are often categorised according to their sites of action: (i) SH2 domain or dimerization

inhibitors, (ii) upstream tyrosine kinase inhibitors, (iii) oligonucleotides and inhibitors of DNA domain binding, and (iv) peptide-mimetics of physiological negative modulators. Stattic is a non-peptidic small molecule demonstrated to inhibit the SH2 domain irrespective of the STAT3 phosphorylation state *in vitro*. Stattic selectively inhibits STAT3 activation and nuclear translocation, thereby inducing apoptosis in cancer cell lines (Schust *et al.*, 2006). WP1066 was developed from the modification of AG490, which blocks the JAK2/STAT3 interaction and subsequent phosphorylation of STAT3 at tyrosine 705 (pSTAT3), modulating multi-factorial immunosuppression and eliciting an anti-tumour immune response (Iwamaru *et al.*, 2006). A novel pyrazol pyrimidine adenosine triphosphate (ATP) competitive inhibitor of the JAK/STAT3 pathway (McFarland *et al.*, 2011), AZD1480 has been demonstrated to inhibit STAT3 phosphorylation both *in vitro* and *in vivo* of solid tumours (Hedvat *et al.*, 2009). Due to its efficient blood-brain barrier penetrance, AZD1480 presents a viable therapeutic option for GBM.

Although direct targeting of the STAT3 protein is the most appealing, challenges exist such as large and diffuse protein-protein interaction compared to a “druggable” classic binding pocket. Moreover, STAT3 proteins share a highly homologous domain structure, rendering specific targeting more challenging. Multiple small molecule inhibitors identified through virtual screening targeting the SH2 domain have demonstrated physiochemical properties suitable for clinical use. However, most of these compounds such as curcumin have yet to be further explored due to concerns over the lack of potency and specificity (Furqan *et al.*, 2013). Although signs of efficacy were observed in tyrosine kinase inhibitors (TKIs), further development was limited by concerns of unpredictable pharmacokinetics (PK) profiles, severe toxicities and susceptibility to opportunistic infections (Wong *et al.*, 2015). A possible explanation could be the ubiquitous expression of STAT3 and its diverse roles in normal and cancer biology. Novel strategies have since emerged using antisense and decoy oligonucleotides or using small interfering RNA (siRNA) for post-transcriptional gene silencing. The existing evidence strongly justifies the role of STAT3 inhibition as an anti-cancer therapeutic approach, but a lack in progress indicates the urgent need to re-examine the strategies for direct STAT3-targeted drugs. The extensive cross-talk and alternate signalling pathways present in STAT3-activation renders single-agent STAT3 inhibition less effective in general.

### 1.5.2. IGF-1R Signalling Pathway

In the evaluation of upstream kinases that lead to active STAT3 signalling (Figure 3), the human epidermal growth factor receptor (EGFR), a member of the ErbB/HER family of RTKs; the family of IL-6-type cytokine receptors that form complexes with gp130 and JAKs; and several GPCRs have been described in previous literature (Wieduwilt and Moasser, 2008). Multiple growth factors (e.g. EGF, TGF $\alpha$ , PDGF, and CSF1) and cytokines (e.g. IGF-1, IL-6, LIF, CT-1, CNTF, IL-10, IL-11, and OSM) have been shown to activate STAT3. In addition, Src family kinases, SFKs (e.g., Src, Lck, Hck, Lyn, Fyn, and Fgr) either activate STAT3 directly or by the activation of RTKs or GPCRs downstream. Much evidence has demonstrated a significant role for autocrine and/or paracrine cytokine loops in driving the aberrant activation of STAT3 in human cancers. Elevated levels of STAT3-activating ligands, such as IGF-1, TGF $\alpha$  or IL-6, have also been detected in the serum and/or the tumour microenvironment of patients with a variety of human malignancies (Berishaj *et al.*, 2007; Gao *et al.*, 2007; Lam *et al.*, 2008). The increased amounts of IGF-1, TGF $\alpha$  or IL-6 that sustain activation of STAT3 in these cases may be produced in an autocrine, paracrine, or endocrine manner (See *et al.*, 2012; Wei *et al.*, 2011); although in the case of IGF-1R where several small molecule candidates are under evaluation in pharmaceutical pipelines, the downstream cell-intrinsic activation of STAT3 remains unclear in GBM tumours.

In the last decade, much evidence arose supporting IGF-1R signalling in various cancers playing a vital role in the transformation of cells, cancer cell proliferation and metastasis (Kaleko *et al.*, 1990; Pollak *et al.*, 2004; Scotlandi *et al.*, 2002). Therefore IGF-1R can be considered as a possible therapeutic target in cancer. A myriad of growth factors and cytokines which include insulin and IGF-1 are able to trigger STAT3 activation. It has been suggested that IGF-1R mediates activation of STAT3 via an adaptor, as there are no consensus STAT3 binding sites found in *IGF-1R* (Zhang *et al.*, 2006b; Zong *et al.*, 2000). Through activated IGF-1R, STAT3 can be constitutively activated (Coffer *et al.*, 1997; Zong *et al.*, 2000). IGF binding proteins (IGFBPs) modulate the activity of IGF ligands and their receptors. IGFBPs are usually bound directly to IGF-1 in extracellular fluids, mediating the half-life and localized availability of the ligands, implicating cellular proliferation, apoptosis and interaction with the microenvironment (Hwa *et al.*, 1999). Several studies have demonstrated that circulating IGF and IGFBP levels

correlate with sensitivity to IGF axis inhibition (McCaffery *et al.*, 2013). Numerous literature have emphasized the capability of IGF-1R in mediating resistance to other treatment modalities; these discoveries thus provide sound basis for trials designed using IGF-1R inhibitory drugs in combination with other targeted agents.

#### 1.5.2.1. IGF-1R Inhibitors

Downstream intracellular signalling of the IGF system could result in the activation of various pathways such as the RAS/RAF/MAPK and/or PI3K/AKT/mTOR (Furstenberger and Senn, 2002). Therefore, targeting the IGF-1R pathway has appeared as a promising therapeutic target. Numerous approaches to inhibit IGF-1R signalling have been examined, these include monoclonal antibodies against the receptor or the ligand and the IGF-1R tyrosine kinase inhibitors (TKIs). Among the several small molecule TKIs under clinical investigation, Linsitinib (OSI-906) and BMS-754807 are the most specific (Chen and Sharon, 2013). In a study by Buck *et al.*, Linsitinib demonstrated superior anti-tumour activity compared to a selective anti-IGF-1R monoclonal antibody (Buck *et al.*, 2010).

The IGF-1R pathway is a valid target in human cancers; however, clinical benefits of IGF-1R inhibitors are often restricted to a small subset of patients. Common factors such as the presence of an “escape” mechanism or constitutively activated downstream effector confer *de novo* or acquired resistance (Chen and Sharon, 2013). Crosstalk with other RTK signalling pathways including EGFR and pathway redundancy could also be reasons for the failure of IGF-1R inhibitors (Liu *et al.*, 2014). This therefore results in compensatory mechanisms which limit response and possibly mediates acquired resistance characteristic of targeting a single pathway (Park *et al.*, 2016). In GBM, this crosstalk is specifically evident with EGFR. Both IGF-1R and EGFR signalling pathways mediate the PI3K/AKT signalling axis (Chakravarti *et al.*, 2002; Ma *et al.*, 2016b). Several studies therefore support the combination of IGF-1R inhibitors with other key pathway blockers such as MEK or mTOR inhibitors (Villanueva *et al.*, 2010; Wan *et al.*, 2007).

## 1.6. Mechanisms of Chemoresistance in Glioblastoma

Successful treatment of cancer remains a challenge and this can be attributed to acquired or intrinsic resistance to cytotoxic agents. As discussed previously, high grade malignant glioblastomas are among the most devastating cancers despite standard of care treatment comprising of maximal surgical resection followed by concomitant chemo- and radiotherapy with alkylating agents. Despite these alkylating agents readily crossing the blood-brain barrier (BBB) and showing the ability to attain therapeutic concentrations in the brain, glioblastoma tumours frequently develop resistance. An important mechanism for the resistance towards these alkylating agents can be attributed to O<sup>6</sup>-methylguanine methyltransferase (MGMT), a DNA repair enzyme (Friedman *et al.*, 1998b). Commonly used bifunctional alkylating agents include lomustine (CCNU) and carmustine (BCNU) that form double-strand crosslinks (Sariban *et al.*, 1987). In contrast, temozolomide (TMZ) - a methylating agent, causes O<sup>6</sup>-methylguanine adducts, initiating the ineffective cycling of the DNA mismatch repair (MMR) mechanism that eventually induces apoptosis due to DNA double-strand breakage (Karran and Hampson, 1996). However, MGMT can directly reverse the methylation damage caused by TMZ. The direct repair of alkylated guanine residues occurs through the transfer of the alkyl group from O<sup>6</sup>-alkylguanine to a cysteine residue at its active site, to which the alkyl group becomes covalently attached, resulting in MGMT protein inactivation (Daniel *et al.*, 2019). In the absence of MGMT, base mismatches invoke the MMR pathway. MMR proteins including MutS Homolog 2 and 6 (MSH2 and MSH6), MutL Homolog (MLH1) and PMS2 recognise and bind to the mismatched guanine, causing cells to enter a cycle of DNA repair. However, mismatches in newly synthesised daughter DNA strands are repaired, while methyl adducts persist on the parental DNA. This therefore leads to a futile repair and mismatching which eventually induces DNA double strand break, cell arrest and death (Daniel *et al.*, 2019).

Numerous studies in the last decade have demonstrated that sensitivity of GBMs to alkylating agents could be correlated to a deficiency of MGMT; nonetheless, chemoresistance are still observed in tumours expressing low levels of MGMT. Thus, these findings support that chemoresistance in tumours could involve other mechanisms (Dolan *et al.*, 1990; Friedman *et al.*, 1998a). In cases of recurrent glioblastoma, researchers have suggested that *MSH6* inactivation could

mediate TMZ resistance due to compromised MMR function (Yip *et al.*, 2009). Because a large proportion of glioblastomas have a hypermethylated promoter for the *MGMT* gene resulting in transcriptional silencing, the MMR pathway thus serves as a primary mediator of O<sup>6</sup>-methylguanine cytotoxicity. Defects in the MMR pathway, such as a somatic mutation of *MSH6*, would therefore provide cancer cells an alternative mechanism for resistance (Allan and Travis, 2005; Cahill *et al.*, 2007; Yip *et al.*, 2009).

Other mechanism contributing to chemoresistance in glioblastoma include the dysregulation of apoptosis-regulating proteins and genes, such as upregulation of Bcl-X<sub>L</sub> or Bcl-2, loss of p53 function, or *EGFR* over-expression. p53 has been well-studied to play a crucial function in detecting DNA damage and to regulate signalling pathways that mediate apoptosis. Deficient or mutant Trp53 in murine tumours are less sensitive to chemotherapy (Lee and Bernstein, 1993), while the restoration of wild-type Trp53 could re-establish sensitivity to cytotoxic agents (Asgari *et al.*, 1997; Yang *et al.*, 1995). Wild-type p53 interacts with the promoters of numerous genes (*Bcl-2*, *MDM2* and *EGFR*), increasing their transcriptional activity (*EGFR* and *MDM2*) or repressing transcription (*Bcl-2*). *EGFR* commonly harbours activating mutations in *de novo* malignant GBM, and several investigators have shown that the *EGFR* amplification could affect sensitivity of GBMs to chemotherapy (Schlegel *et al.*, 1994). Consistently, EGFR or Bcl-2 upregulation in glioblastoma correlates with decreased apoptotic response and drug resistance (Nagane *et al.*, 1996; Weller *et al.*, 1995). While abnormal levels of Bcl-2 and EGFR are common in GBM, their contribution to disease progression and prognostic outcome have not been evaluated (Newcomb *et al.*, 1998). Therefore, further investigation remains to establish new strategies to overcome resistant phenotypes in GBM.

#### 1.6.1. STAT3 in Treatment Resistance

Several studies implicate STAT3 activation and treatment resistance by RNA interference, dominant-negative mutants, or treatment with STAT3 inhibitors. One such study demonstrated the enhanced radiation sensitivity of treatment-resistant glioblastoma cells by exogenously expressing dominant-negative STAT3 (Zhou *et al.*, 2007). Activated STAT3 has been shown by Kohsaka *et al.* and others to be a

driver of resistance to TMZ via the upregulation of MGMT, albeit independent of its transcriptional activity (Kohsaka *et al.*, 2012; Lee *et al.*, 2011). Additionally, work by others demonstrated STAT3 as an emerging central player in GBM resistance towards radiation (Halliday *et al.*, 2014) and anti-angiogenic therapy (de Groot *et al.*, 2012). Although TCGA investigators have associated several key signalling pathways with clinical outcome in GBM, it remains to be validated and applied to patient stratification methods to overcome the frequently observed inter-patient variability to treatment response, and most likely reason for subsequent failure of current clinical trials. Currently, there are several clinical trials for the inhibition of JAK/STAT3 in glioblastoma (NCT01712542, NCT01904123, NCT00897663). The application of TCGA concepts will present a shift in paradigm in the way patients should be assessed for targeted therapy. This will in turn spare non-responders from financial burden and chemotherapeutic side effects.

### 1.7. Gap in Knowledge and Objectives of Study

In the field of brain tumours, specifically GBM where patient prognosis is dismal, molecular heterogeneity has been implicated as a cause of inter-patient variability to treatment response. The Cancer Genome Atlas effort has identified molecular subtypes based on transcriptomic profiles, with each subtype correlating with unique genomic aberrations and survival outcome. The activation of a key regulator, STAT3, is crucial in the proneural-mesenchymal transition that typifies the highly aggressive and recurrent tumour. Furthermore, current STAT3 inhibitor clinical trials have largely focused on the *JAK2* V617F mutation in haematological disorders, with no implication on the oncogenic nature of amplified wild-type *JAK2-STAT3*. These trials also do not address patient stratification methods which our study shows to be beneficial at identifying responder cohorts. My thesis will address several goals:

1. A unique *STAT3* gene signature derived from clinical databases intersected with differentially expressed candidates upon perturbation of *STAT3*, resulting in phenotypic effects. This signature stratifies patient survival of key glioma databases, and is not confounded by current clinical and molecular indicators defined in the newly revised World Health Organization classification scheme.



2. Identification of *STAT3*-high responsive, and *STAT3*-low non-responsive cohorts.
3. Biological validation of our stratification predictions using primary GBM cells and orthotopic patient-derived xenograft (PDX) mouse tumour model (Chong *et al.*, 2009; Chong *et al.*, 2016; Koh *et al.*, 2013; Xu *et al.*, 2018).
4. Development of therapeutic methods to sensitize the *STAT3*-low non-responsive cohort.

This study is unique as it incorporates several novel analytical pipelines to evaluate multi-dimensional clinical databases, and biologically validate them using primary cells and PDX models established in the NNI Brain Tumour Resource. We define new approaches in precision oncology-based trials where serial profiling is essential to accurately target individuals who may demonstrate molecular subtype switching.

## 2.0 MATERIALS AND METHODS

### 2.1. Tissue Collection and Primary Gliomasphere Culture

Brain tumour specimens were obtained with informed consent and de-identified, as part of a study protocol approved by the SingHealth Centralised Institutional Review Board A. In this study, tumour specimens were from patients with primary GBM. Tumours were processed according to Gritti *et al.* with slight modifications (Gritti *et al.*, 1996). Cells were seeded at a density of 2,500 per cm<sup>2</sup> to promote clonal sphere formation. GPCs were cultured in chemically defined serum-free selection growth medium consisting of basic fibroblast growth factor (bFGF; 20 ng/ml; Peprotech, New Jersey), epidermal growth factor (EGF; 20 ng/ml, Peprotech), heparin (5 µg/ml; Sigma-Aldrich, St Louis), and serum-free supplement (B27; 1x; Gibco, NY) in a 3:1 mix of Dulbecco's modified Eagle's medium (DMEM; Sigma-Aldrich) and Ham's F-12 Nutrient Mixture (F12; Gibco). The cultures were incubated at 37°C with 5% CO<sub>2</sub>. To maintain the undifferentiated state of the gliomasphere cultures, growth factors were replenished every 2 days. Successful gliomaspheres (1 to 4 weeks) were expanded by mechanical trituration with a flame-drawn glass Pasteur pipette and reseeded at 100,000 cells per ml in fresh culture medium supplemented with growth factors. All experiments were conducted with low-passage GPCs (within 10 passages) for which we previously demonstrated retention of the phenotypic, transcriptomic, and karyotypic features similar to the original primary tumour (Chong *et al.*, 2009). Briefly, we used vitrification as a cryopreservation technique, and we demonstrated that this method ensured our GPCs maintained self-renewal and multipotentiality properties, with spectral karyotypic analyses confirming the presence of GBM hallmarks

### 2.2. Small Molecule Inhibitors and Reagents

The small molecule inhibitors AZD1480, Stattic, WP1066 and Linsitinib were obtained from Selleck Chemicals. GPCs were treated with AZD1480 at concentrations of either 0.5, 1 or 2 µM; Linsitinib was used at 0.5 µM; the other inhibitors Stattic and WP1066 were used at their IC<sub>50</sub> concentrations. Temozolomide was obtained from Sigma-Aldrich and used at concentrations of 20, 50, 100 and 200 µM.

### 2.3. Cell Viability Assays

#### 2.3.1. Cell Viability Assessment Post-treatment with Small Molecule Inhibitors

Gliomaspheres were dissociated with Accutase<sup>TM</sup> (eBioscience) and seeded into 96-well plate format at 2,000 cells per well. Cells were allowed to recover for 24 hours prior to addition of compounds, along with replenishment of growth factors. Viability was measured at days 5 and 10 post-treatment using AlarmaBlue® (Serotec, Oxford, UK) according to manufacturer's instructions. Briefly, cells were incubated with 10% volume of AlarmaBlue® for approximately 16 hours before absorbance readings were measured at 570 and 650 nm.

#### 2.3.2. Dose-response Curves and IC<sub>50</sub> Calculations

Gliomaspheres were dissociated into single cells and seeded into 96-well plates similar to the cell viability assay. Cell viability post-drug treatment was assessed on day 5 using AlamarBlue® (Serotec, Oxford, UK). Briefly, cells were incubated with 10% volume of AlamarBlue® for approximately 16 hours before absorbance readings were measured at 570 and 600 nm. Dose-response curves for each line were generated from a mean of triplicate experiments using GraphPad Prism (GraphPad Software, Inc; USA) and IC<sub>50</sub> values were computed from 12-point titration curves ranging from 10<sup>-4</sup> to 10<sup>2</sup> μM.

#### 2.3.3. Gliosphere Formation Assay

Serial gliosphere-forming ability, which approximates the *bona fide* GPC frequency within heterogeneous gliomaspheres, and sphere size, which reflects GPC proliferation, were assessed as described in previous work (Chong *et al.*, 2016; Foong *et al.*, 2012; Koh *et al.*, 2013). Gliomaspheres were dissociated into single cells by Accutase<sup>TM</sup> (eBioscience) and 30 live cells were flow-sorted into each well of 96-well plates based on negative staining with 7-aminoactinomycin D (7-AAD) cell viability dye. Cells were then treated with the indicated concentration of drugs, or dimethylsulfoxide (DMSO) as vehicle control. Gliosphere-forming ability and gliosphere sizes were determined after 7, 14, and 21 days. Scoring and diameter measurements were performed using the Nikon Eclipse Ti Microscopy,

accompanied with digital camera (DS-Qi1) and NIS-Element Imaging Software (Nikon Instruments Incorporation; New York, USA). A *bona fide* gliomasphere is defined as a single sphere of diameter exceeding 20  $\mu\text{m}$ , formed from cellular divisions of single cells. The initial seeding density precludes the cellular aggregation artefact.

#### 2.3.4. Invasion assay

Fifty thousand cells were added to the upper compartment of the BD BioCoat Matrigel invasion chamber (BD Bioscience) and chemo-attractant of 2% FBS was added to the lower compartment. Cells were incubated for 48 hours before being wiped off from the upper surface of the filter with a cotton swab. The lower surface of the filter was fixed with 4% paraformaldehyde and subsequently stained with 0.005% crystal violet (Sigma-Aldrich). The number of cells that migrated to the bottom of the chamber was counted from 5 randomly selected fields.

### 2.4. Combination Index (CI Values)

Combination index (CI) values based on Loewe's additivity model were determined to assess the nature of drug-drug interactions that can be additive (CI=1), antagonistic (CI>1), or synergistic (CI<1) and effect levels (Fa, indicating fraction of cell viability affected). CI and Fa values were calculated using the CompuSyn software (ComboSyn Inc., Paramus, NJ), following the Chou-Talalay method (Chou, 2010).

### 2.5. Protein Analysis

#### 2.5.1. Immunoblot

Cells were lysed in buffer containing 0.5% sodium deoxycholate, 1% NP-40 detergent, 0.1% SDS, 0.15M NaCl, 10mM Tris-HCl pH7.4, protease and phosphatase inhibitor cocktail tablets (Roche, Indianapolis, IN). Approximately 25  $\mu\text{g}$  of heat-denatured protein lysate was resolved on 8% SDS polyacrylamide gel and electro-transferred onto polyvinylidene difluoride (PVDF) membrane (Millipore). The following antibodies were used for protein analysis: anti-pSTAT3

(Tyr705; 1:1000; CST, #9138), anti-STAT3 (1:1000; CST, #9139), anti-IGFBP2 (1:1000; CST, #3922), anti-pIGF-1R (Tyr1135/1136; 1:1000; CST, #3024), anti-IGF-1R (1:1000; Santa Cruz, #712), and anti- $\beta$ -actin (1:10000; Sigma Aldrich A5441). Anti-mouse or rabbit (1:10000; CST) IgG horseradish peroxidase (HRP)-linked secondary antibody was used. All antibodies were diluted in 5% bovine serum albumin (Hyclone BSA, GE Healthcare) in 10 mM Tris-HCL pH 7.4, 100 mM NaCl, 0.1% Tween® 20 (Merck) (TBS-T buffer). Blots were blocked with 5% BSA for 1 hour, probed over upon stripping with Restore™ Plus Stripping buffer (ThermoFisher Scientific) for 15 minutes and washed thrice with TBS-T buffer for 5 minutes. Membranes were detected using chemiluminescence detection kit SuperSignal West Pico or Femto (Thermo Scientific) according to manufacturer's instructions. Protein bands were visualized using SYNGENE G:Box, iChemiXT. Protein expression was quantitated with Quantity One® software (Bio-Rad Laboratories), normalized against  $\beta$ -actin levels.

### 2.5.2. Co-immunoprecipitation

Protein lysates were pre-cleared by incubating 1 mg of protein with sepharose beads (Protein A-Sepharose®; Zymed Laboratories Inc.; San Francisco; USA) for 30 minutes. Subsequently, protein lysates were incubated overnight with agitation at 4°C using 5  $\mu$ g anti-STAT3 (124H6, Cell Signalling Technology, CST 9139) or anti-IGF-1R (1:1000; Santa Cruz, #712) antibodies. Fresh sepharose beads were then added to the protein-antibody mixture and incubated at 4°C with agitation for 4 hours to bind the protein-antibody complex to the beads. Sepharose beads were collected and washed 5 times with lysis buffer. The beads were subsequently resuspended in 2x SDS loading buffer (4% SDS, 20% Glycerol, 0.15 M Tris-HCl (pH6.8), 0.05% Bromophenol Blue, 20%  $\beta$ -mercapthoethanol) and boiled for 5 minutes prior to gel loading.

### 2.5.3. Enzyme-Linked Immunosorbent Assay (ELISA)

Cells were lysed in buffer containing 0.5% sodium deoxycholate, 1% NP-40 detergent, 0.1% SDS, 0.15M NaCl, 10mM Tris-HCl pH7.4, protease and phosphatase inhibitor cocktail tablets (Roche, Indianapolis, IN). 1  $\mu$ g of protein

lysate was analysed using IGFBP2 and IGF-1R ELISA kits (Sigma-Aldrich) as per manufacturer's protocol in triplicates with standard curves.

#### 2.5.4. Immunohistochemistry

Tissue sections were stained with the following antibodies: Anti-pSTAT3 antibody (1:100, CST, #9145) and anti-IGF-1R antibody (1:400, CST, #14534). For quantitative analysis, the percentage of stained tumour cells and intensity of staining were evaluated under high-power field (400x) on tissue sections using optical microscopy. H-scores were then derived from both the staining intensity (scale of 0-3) and the percentage of positive cells (0-100%), generated based on a score ranging from 0 to 3. Briefly, the percentage of weakly stained cells was multiplied by 1, plus moderately stained cells multiplied by 2, plus strongly stained cells multiplied by 3. At least 5 random fields were counted, and scoring was performed blinded to clinical data.

#### 2.6. Quantitative Real Time RT-PCR

RNA was isolated using TRI Reagent® (Sigma-Aldrich) as per manufacturer's protocol and reverse transcribed into cDNA using the Superscript® III First-Strand Synthesis System kit (Life Technologies). Cycle parameters were: 40 cycles of 95°C for 10 seconds, 55°C for 10 seconds, and 72°C for 5 seconds. Real-time PCR was performed on Roche LightCycler® 96 Instrument using FastStart Essential DNA Green Master (Roche Life Science). Each real-time PCR was conducted in triplicate, and the level of each gene's expression was determined relative to the house-keeping gene, hypoxanthine phosphoribosyltransferase (HPRT). Gene-specific primers used are shown in Table 2.

**Table 2. Gene-specific primers**

<b>Gene</b>	<b>Forward primer sequence (5'-3')</b>	<b>Reverse primer sequence (5'-3')</b>
<i>STAT3</i>	GGG AGA GAT TGA CCA GCA GT	CTG CAC TCT CTT CCG GAC AT
<i>ELK3</i>	TCA AGA CGG AGA AGC TGG AG	CCG AGA TGA GAA GGG TGA GG
<i>BIRC2</i>	CTC CAG CCT TTC TCC AAA CC	AGT TAC TGA GCT TCC CAC CA
<i>FZD1</i>	GCC CTC CTA CCT CAA CTA CC	ACA GCC GGA CAA GAA GAT GA
<i>SLC35F5</i>	CTG TGG GGA AAC TTA CTG CA	CCA GTA CAA CGC CTC CAA TG
<i>KLHDC8A</i>	CGG GTC TAC TGC TCC CTG	TGT ACA TCT CCA CGA CCT
<i>GMPPA</i>	TCA CCC AGT TCC TAG AAG CC	CTG TTA GCC GTA GTG CCA AG
<i>SNAP23</i>	AGG ATG CAG GAA TCA AGA CCA	CTC CAC CAT CTC CCC ATG TT
<i>NEDD9</i>	AGC TCA GGA CAA AAG GCT CT	GCA ACA GCT CCC TTG ACA AA
<i>DTX3L</i>	TCA CAA GCA GAA ACA CCG TC	AGT CAC ACA CCT TCT CA
<i>CTNNA1</i>	GCA GCC AAA AGA CAA CAG GA	TGT GAG GCA TCG TCT GAG G
<i>NAA38</i>	GTC AAG CAG CAA GAT GGA GG	GCG CAT AGT CTT GTT GAG CA
<i>ITFG3</i>	ACA CCA ACA GCA ACA ATT	AAT GAA AGA ACT GGG TCT GCC
<i>IGFBP2</i>	GGC TTG GTT GGA AGA CTG AT	CAT TTT CAA AGG CCT CAC GC

## 2.7. Lentiviral-mediated Knockdown and Over-expression

Human lentiviral shRNA clones targeting *STAT3* and *IGFBP2* in pLKO.1 backbone were from GE Life Science; Dharmacon (TRCN0000020840, TRCN0000020842, TRCN0000020843, RHS4080, TRCN0000011033, TRCN0000006574). These vectors were co-transfected using the Lenti-X™ HTX Packaging System (Clontech, CA, USA) into HEK293T cells according to the manufacturer's instruction (Clontech). Viral titre of supernatant collected was determined using Lenti-X™ p24 Rapid Titre Kit (Clontech) according to manufacturer's instructions. *IGF-1R* full-length (*IGF-1R\_FL*) and C-terminal deleted (*IGF-1R\_C-Del*) over-expression vectors were constructed using pCDH-CMV-MCS-EF1-GFP+Puro vector (System Biosciences). The amplified product was digested with XbaI and NotI, and subsequently ligated into the pCDH vector. Lentiviral particles were generated as described above.

## 2.8. Stereotaxic Intracranial Implantations

Mice were handled according to guidelines of the Institutional Animal Care and Use Committee of the National Neuroscience Institute, Singapore. Animal implantation was carried out as previously described (Chong et al, 2009; Ng et al, 2012), using NOD/SCID gamma mice (NOD.Cg-Prkdcscid<sup>112rgtm1Wjl/SzJ</sup>, Jackson Laboratories). 500,000 pre-treated cells resuspended in 2 µL of phosphate-

buffered saline were delivered into the right frontal lobe (0.1  $\mu\text{L}/\text{minute}$ ) by stereotaxic injection through a glass electrode connected to a Hamilton syringe. The coordinates used were: +1.0 mm antero-posterior; +2.0 mm medio-lateral; -2.5 mm dorso-ventral. Mice were euthanized by means of transcardiac perfusion with 4% paraformaldehyde upon presentation of neurological deficits with ataxia, cachexia, lethargy, or seizure. A portion of mice brains was harvested and processed for paraffin blocks for immunohistochemistry, or snap frozen for use in immunoblotting. Kaplan-Meier survival curves were plotted to show survival differences. A logrank test was adapted to estimate the survival difference between the *STAT3*-high and *STAT3*-low patient groups using Prism 5 (GraphPad Software, San Diego, CA). Multivariate Cox Regression model was fitted to identify the significant clinical covariates associated with survival. A  $p\text{-value} < 0.05$  was defined as significant association of covariates with survival. The statistical significance of correlation was evaluated using Spearman's rank correlation test.

## 2.9. Statistical Analysis

Data are expressed as means  $\pm$  standard error of the mean (SEM) of at least 3 independent experiments. Student's  $t$  or Mann-Whitney  $U$  test was used where appropriate,  $p\text{-value} \leq 0.05$  was accepted as statistically significant. Kaplan-Meier survival curves were analysed using the logrank test with Prism 5 (GraphPad Software, San Diego, CA). The statistical significance of correlation was evaluated using Spearman's rank correlation test.

### 2.9.1. Kaplan-Meier Analysis

Kaplan-Meier survival curves were plotted to show the survival differences between patient groups. A logrank test was adapted to estimate the survival difference between the *STAT3*-high and *STAT3*-low patient groups. Multivariate Cox Regression model was fitted to identify the significant clinical covariates associated with survival. A  $p\text{-value} < 0.05$  was defined as significant association of covariates with survival.



## 2.10. Bioinformatics Analyses (With help from Mr Edwin Sandanaraj, G1403220A, Research Associate at NNI)

### 2.10.1. Microarray Data Processing and Analysis

*STAT3* knockdown GPCs were profiled on Affymetrix GeneChip® Human Genome U133 Plus 2.0 Array using 3' IVT express kit. The Gene Expression Omnibus (GEO) accession number for the microarray data is available at <https://www.ncbi.nlm.nih.gov/geo/query/acc.cgi?acc=GSE117905> using the 'kbuzuwkqbxaxxav' access token. Raw CEL files were summarized with mas5 algorithm and log<sub>2</sub>-scaled and gene expression dataset was created. All data pre-processing analysis was carried out by R/Bioconductor packages (Gautier *et al.*, 2004). A linear model was regressed to assess the differentially expressed genes between *STAT3* knockdown and non-targeting control profiles (adjusted *p*-value<0.01) in NNI GPCs (N=3) as described in R/limma packages (Ritchie *et al.*, 2015). False discovery rate (FDR) adjusted *p*-value<0.05 were considered as statistically significantly perturbed genes upon *STAT3* KD. A subset of differential genes was extracted as *STAT3* KD gene signature by applying a stringent criterion of 2-log<sub>2</sub> fold change between KD clones and the control profiles.

### 2.10.2. Predictive Database Analysis

The *STAT3* functionally-tuned gene signature (Appendix A) was derived by extracting the list of genes that displayed an inverse trend upon *STAT3* knockdown in patient-derived GPCs, from the *STAT3* co-expressed genes in primary tumour samples. Linear model for microarray analysis extracted a total of 997 mRNA transcripts that were differentially altered upon the genetic KD of *STAT3* (FDR adjusted *p*-value<0.01). We next leveraged on transcriptome data of primary tumours from the public database, Rembrandt as our training model to ascertain *STAT3* co-expressed gene modules (Madhavan *et al.*, 2009). The spearman rank correlation co-efficient cut-off was set at 0.3 to yield transcripts that were co-regulated along with *STAT3*. We considered the intersection of genes modulated in GPCs upon genetic KD of *STAT3* and *STAT3* co-regulated transcript modules from the primary tumour collection as the *STAT3* functionally-tuned gene signature (N=207). We used Gene Set Enrichment Analysis (GSEA) to confirm that the gene signature is enriched for JAK/STAT and cytokine signalling modules. We adapted

the Connectivity Map (CMAP) approach first developed by the Broad Institute; patients with positive activation scores tended to have low *STAT3* activation while patients with negative activation scores had high *STAT3* activation (contrary to *STAT3* KD) (Lamb, 2007; Lamb *et al.*, 2006). A univariate analysis was performed using logrank test to evaluate the *STAT3* signature classes having association for survival in GBM patients.

### 2.10.3. Bayesian Information Criterion Analysis

Bayesian Information Criterion (BIC) score was calculated for each regression model to understand the information contributed by covariates for the survival variability. A multivariate model using Cox proportional hazards analysis was tested to evaluate the contribution of *STAT3* signature in the presence of known clinical predictors including age, tumour grade and the Karnofsky score (measure of patient's functional status). The BIC score was calculated for each regression model to identify whether the model was improved with the inclusion of covariates. A highly favoured model was identified by the presence of the lowest BIC score. A likelihood ratio test was also used to evaluate the statistical significance of delta BIC (difference between BIC of baseline model and BIC of updated model including new covariate).

### 2.10.4. Relative Odds Estimation

To understand the clinical association of WHO classification marker *IDH1* status with *STAT3* signature-stratified classes, we employed the use of relative odds estimation as recommended (Wald *et al.*, 1999). First, we calculated the density distribution of CMAP activation score values for both *IDH*-WT and mutant cohorts. Then, relative odds score was estimated from the proportion of highest 5<sup>th</sup> distribution and lowest 5<sup>th</sup> distribution of *STAT3*-signature score values for *IDH* phenotypes. The glioma-intrinsic (GI) subtype signatures for each subtype were interrogated using single sample Gene Set Enrichment Analysis (ssGSEA) with resampling classification strategy as described (Barbie *et al.*, 2009; Wang *et al.*, 2018). Briefly, the Empirical Cumulative Distribution Functions (ECDF) of subtype signatures were estimated from rank-normalized expression values of each

sample. The empirical  $p$ -value was calculated by evaluating ECDFs of GI-signatures and the remaining genes in the transcriptome. To facilitate an unbiased comparison across the three subtype signatures, a random resampling strategy was applied to estimate the robust signature score for each GI subtype. The R/library for GI subtype stratification scheme in patient was employed. The subtype for each patient was assigned based on the ssGSEA score with lowest  $p$ -value.

#### 2.10.5. Functional Gene Module Analysis

To identify the functional gene modules of *STAT3* stratification, we performed preliminary analysis on public glioma databases Rembrandt, Gravendeel and TCGA (Gravendeel *et al.*, 2009; Madhavan *et al.*, 2009; Verhaak *et al.*, 2010). We looked for all upregulated genes in the *STAT3*-high patient cohort. For increased stringency of the *STAT3* functionally-tuned genes, we applied 4 criteria for inclusion: (i) Most highly variable genes, (ii) Differential expression between normal and tumour tissue, (iii) Neurodevelopmentally-regulated, and (iv) Patient survival-related. FDR adjusted  $p$ -value < 0.05 was considered as significantly perturbed genes.

#### 2.10.6. PamChip Kinome Analysis

We measured the phosphorylation kinetics of 144 kinases using the PamChip technology to understand the kinase spectrum in *STAT3* signature-stratified GBM cells. The computational pipeline is represented in the flowchart (Figure 4). Briefly, we integrated phosphorylated peptide measurements estimated from PamChip with *STAT3* knockdown transcriptome using published database resources (Hornbeck *et al.*, 2012; Milacic *et al.*, 2012; Prasad *et al.*, 2009). We resolved the multiple peptide-substrate complexity by estimating the pairwise correlations for every peptide catalogued in kinase-peptide matrix. The quantitative mean of peptide cluster was calculated by evaluating the ranks for the presence of large number of correlated peptides having strong expression and dynamic variation across the experimental conditions. We interrogated a linear differential model to estimate the statistical significance between AZD1480 and DMSO-treated cells. A  $p$ -value < 0.1 was considered as statistically significant. We mapped the AZD1480-altered kinase

profiles with *STAT3* knockdown transcriptomic profiles using two key gene-specific databases (Marbach *et al.*, 2016; Olow *et al.*, 2016).

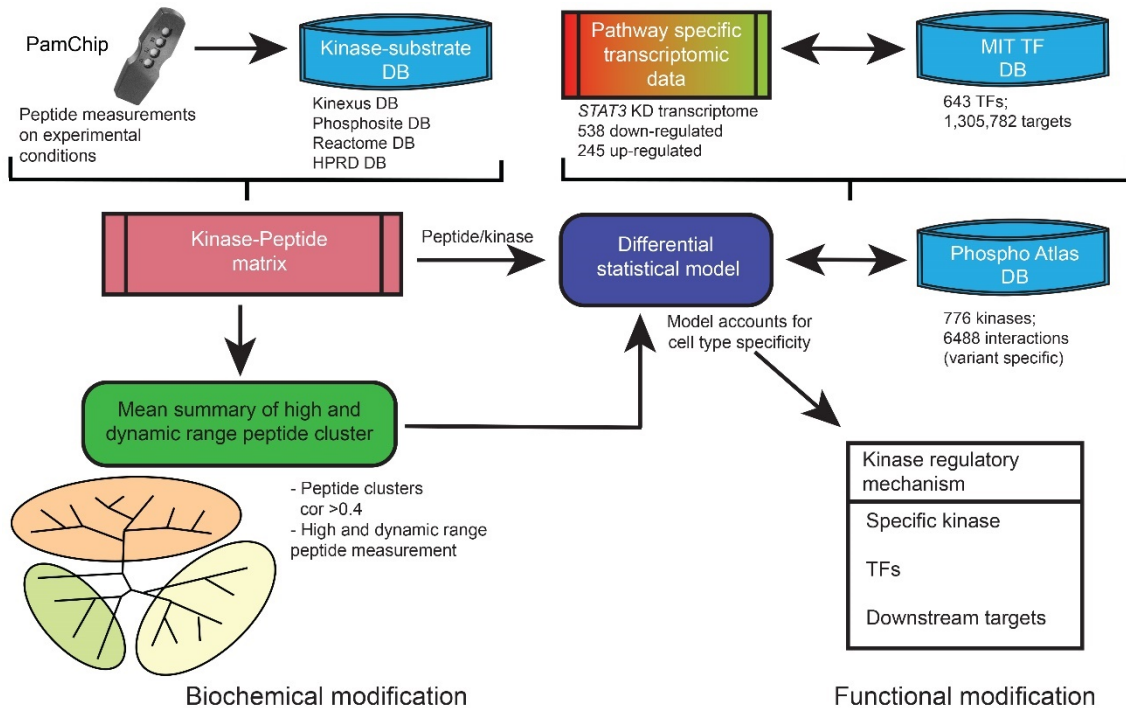


**Figure 4. Computational workflow to prioritise kinase candidates with functional/biological evidence.** The workflow includes biochemical modification module and functional module to integrate phosphorylated kinetics measured from PamChip with *STAT3* knockdown transcriptomic profile. A linear regression model evaluates the kinase activity between the cells with AZD1480 treatment condition.

#### 2.10.7. SynergySeq

We utilized the SynergySeq platform to identify synergistic compounds with temozolomide (TMZ) to reverse *STAT3*-high disease signature in GBM patients (Stathias *et al.*, 2018). The R/shiny package of SynergySeq platform along with drug perturbed signature scores were downloaded from github (<https://github.com/schurerlab/SynergySeq>; cloned on 29/April/2019). First, we interrogated TCGA GBM patients (N=558) in microarray database with our functionally-tuned *STAT3* signature using nearest template prediction (NTP) method available in R/CMScaller package (Eide *et al.*, 2017; Hoshida, 2010). The predicted classes for patient tumours with statistical significance ( $p$ -value<0.05 using 1000 permutation tests) were further evaluated to identify the differential

disease gene signature. A disease signature of 6359 genes were identified to be differential between *STAT3*-high versus *STAT3*-low GBM patients (FDR  $p$ -value<0.0001). This *STAT3*-high GBM signature was interrogated as a disease signature, with TMZ as the reference compound in the SynergySeq pipeline. The Library of Integrated Network-Based Cellular Signatures (LINCS) compounds that displayed high disease discordance and low concordance to the reference compound, were determined as synergy compounds suitable to reverse the disease signature based on Loewe additive model (Subramanian *et al.*, 2017). The current evaluation included compounds from both the LINCS database and GBM-JQ1 study from SynergySeq project (N=1679).

### 3.0 RESULTS

#### 3.1. *STAT3* Functionally-tuned Gene Signature

Brain tumour gene expression drives disease progression and patient survival outcome (Wang *et al.*, 2018). This underscores the molecular heterogeneity of tumour cells, suggesting that druggable pathways may be revealed through genomic and transcriptomic profiles. To address the concept of tumour heterogeneity and subsequent need for patient stratification for more effective targeted therapies, we evaluated JAK/STAT small molecule inhibitors for which several are in clinical trials, mainly in haematological disorders. Importantly, STAT3 represents the final molecular switch that is activated prior to PMT that typifies highly aggressive and recurrent GBMs (Segerman *et al.*, 2016). We hypothesize that the STAT3 pathway promotes oncogenic growth through regulation of self-renewal traits, and stratifies patients for their likely response to STAT3 inhibition therapy.

As any signalling pathway is better represented by a set of genes rather than a single candidate, we established a transcriptomic signature representing the STAT3 pathway activation status (Appendix A). A recent study demonstrated that drug-treated GBM cells contain transcriptomic information that portends prognostic outcome in clinical databases (Stathias *et al.*, 2018). This further suggests that corresponding responder and non-responder patient cohorts can be identified for targeted therapy; thus sparing non-responder patients from unwarranted financial burden and chemotherapeutic side effects. First, we prioritised genes that contribute functionally to the STAT3 pathway and correlate with prognostic outcome. We intersected the *STAT3* co-expressed genes from the Rembrandt patient database (Figure 5A middle panel) that displayed an inverse expression from genes established using 3 patient GBM lines with *STAT3* knockdown (Figure 5A left panel). These genes were identified to form the *STAT3* “functionally-tuned” gene signature (Figure 5A right panel and 5B) (Madhavan *et al.*, 2009). This approach would allow us to select candidates present in the original clinical material yet ensure that only genes downstream and modulated by the STAT3 pathway would be selected.

Consistent with our hypothesis that the *STAT3* pathway as represented by a transcriptomic signature can act as a prognostic indicator in glioma disease, our bioinformatics analysis revealed that patients with high *STAT3* activation (*STAT3*-

high) were enriched for the mesenchymal and classical subtypes and *IDH*-WT status (Figure 5B), commonly associated with aggressive and recurrent GBM (Phillips *et al.*, 2006). In contrast, *STAT3*-low tumours, comprised mostly of low-grade gliomas (LGGs), *IDH*-mutant (1p/19q co-deleted and non-co-deleted) and the proneural molecular subtypes that typify the more sensitive cohort.

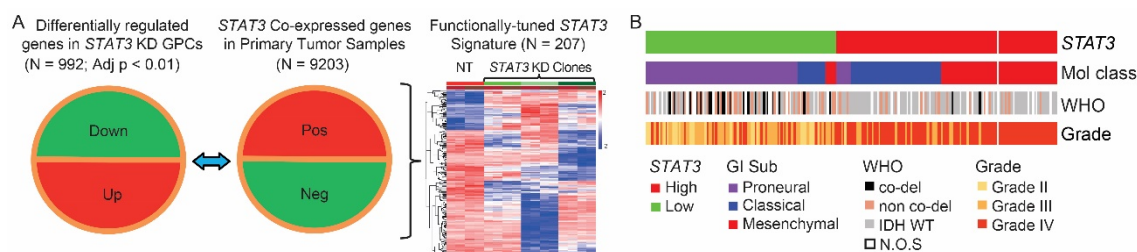


**Figure 5. NNI-*STAT3* functionally-tuned gene signature.** (A) *STAT3* co-expressed genes from Rembrandt patient database (middle panel, training patient database) were intersected with genes that displayed an inverse expression from transcriptomic data obtained from 3 patient GBM cell lines with *STAT3* knockdown (KD) (left panel); these gene sets were identified to form the NNI-*STAT3* functionally-tuned gene signature (right panel). (B) Our functionally-tuned gene signature could stratify patients into two cohorts: *STAT3*-high patient cohort was enriched in the mesenchymal and classical molecular subtypes, with *IDH*-WT status. *STAT3*-low tumours, in contrast, comprised mostly low grade gliomas (LGGs), *IDH*-mutant (1p/19q co-deleted and non-co-deleted) and the proneural molecular subtype.

Prior to subjecting our GBM cell lines to microarray analyses, we verified *STAT3* protein expression upon lentiviral-mediated knockdown in our 3 patient GBM cell lines. All three clones targeting different areas of the *STAT3* coding regions. Upon lentiviral transduction and selection for *STAT3* knockdown clones, we validated with immunoblot analyses for the reduction in phospho-*STAT3* levels (Figure 6A-C i). We observed significant mitigation of viability (Figure 6A-C ii), sphere-forming frequency (Figure 6A-C iii) and reduction in sphere size (Figure 6A-C iv). These assays assess the self-renewal frequency and proliferation of glioma stem-like cells, commonly associated with tumour-initiating and – propagating potential (Rietze *et al.*, 2001). We established a positive enrichment of the JAK/*STAT* signalling pathway in our functionally-tuned gene signature, and

defined it as *STAT3*-high, while an inverse correlation defined the *STAT3*-low gene signature (Figure 6D) (Gravendeel *et al.*, 2009; Madhavan *et al.*, 2009). Based on the gene set enrichment analysis (GSEA), we demonstrated that *STAT3*-high stratified patients had a positive correlation to enriched JAK/STAT signalling. Accordingly, *STAT3*-high defines a patient cohort enriched in the mesenchymal and classical molecular subtypes, typifying highly aggressive and recurrent GBMs (Appendix B). These tumours also demonstrated a significant enrichment of 1p/19q non-co-deletion and *IDH*-WT status, key indicators of diagnostic outcome in the revised WHO classification scheme (Louis *et al.*, 2016). *STAT3*-low tumours, in contrast, comprise mostly of low grade gliomas (LGGs), and the proneural molecular subtype with enrichment of 1p/19q co-deletion and *IDH*-Mut (mutant) status, representing tumours of better prognosis with greater chemosensitivity (Figure 5B) (Cairncross *et al.*, 1998).

Our *STAT3* functionally-tuned gene signature could stratify glioma patient survival. *STAT3*-high defines poorer prognosis patients (median survival of 8.04 months), while *STAT3*-low patients survived significantly longer (median survival of 57.48 months) (logrank  $p$ -value  $< 2e^{-16}$ ) (Figure 7A). A goodness-of-fit evaluation estimates the quality of model addressing the variability with the inclusion of covariates. We demonstrate using an information theory measure, Bayesian Information Criterion (BIC) scoring to identify the best representation of statistical model addressing survival variability. The WHO classification scheme incorporating molecular parameters was the best univariate model addressing for overall survival variability in patient databases. This method revealed that a combination of *STAT3*, the revised WHO classification system that incorporates the isocitrate dehydrogenase (*IDH*) and 1p/19q co-deletion status, and Karnofsky score (measures a patient's functional status) and age presented the best statistical model accounting for patient survival (Figure 7Bi). In such an analysis, a reduction in the BIC score by an absolute value of 10 fulfils the industry standard for advancing a therapeutic strategy into clinical trial (Kass and Raftery, 1995). Furthermore, our *STAT3* signature outperformed the existing Alvarez *STAT3* gene signature previously established to be a pan-solid, tumour-specific profile for glioma patient prognosis (Figure 7Bii) (Alvarez *et al.*, 2007). We estimated the probabilities of our *STAT3* signature to predict for *IDH* status. The relative odds of correlation between *STAT3* signature and *IDH* mutation is 2.42 in a diagnostic metrics test (Figure 7C).



These results indicate that patients with a negative signature score (*STAT3*-high) are 2.42 times more likely to be *IDH*-WT than those with a positive signature score (*STAT3*-low, *IDH*-Mut). This finding emphasizes the clinical relevance of the *STAT3*-score with the WHO diagnostic classification marker-*IDH* mutation status.

As grade IV GBM patients portend the poorest prognosis, with little improvement even with the best standard of care drug temozolomide, we extended our analyses to GBM tumours exclusively (Figure 8). Similar prognostic association was observed in GBM patients for *STAT3*-high and -low subtypes (logrank  $p$ -value=0.0017, Figure 8A). *STAT3*-high significantly enriched for the mesenchymal and classical subtypes, with predominantly *IDH*-WT and 1p/19q non-co-deletion status (Figure 8B and Appendix B). Taken together, the ability to stratify patients using the *STAT3* functionally-tuned gene signature suggests that the *STAT3* pathway contributes to the molecular heterogeneity of GBM tumours that cannot be accounted for by current clinical indicators and should not be ignored in targeted treatment therapeutic decisions.

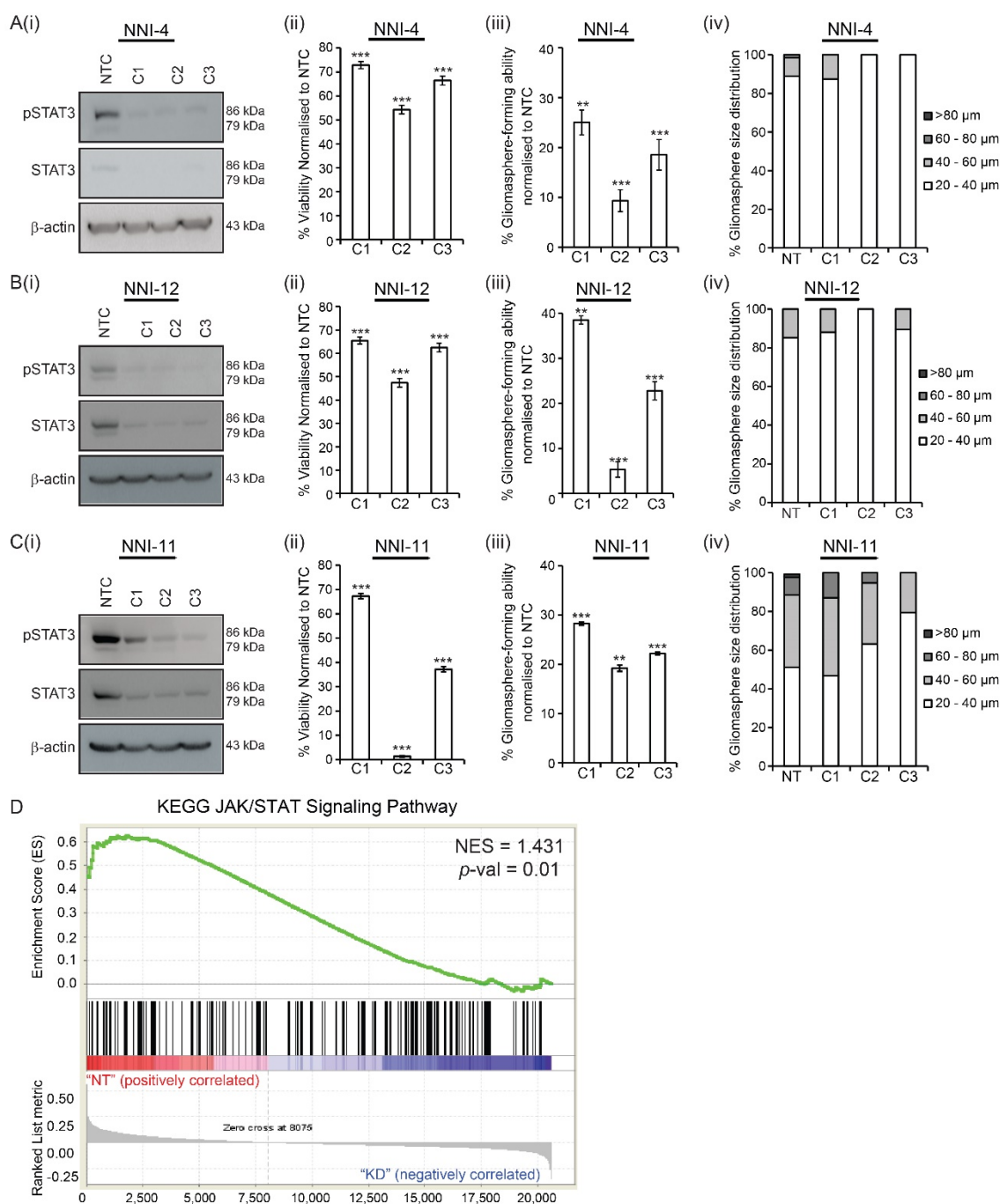


**Figure 6. *STAT3* knockdown reduced viability, gliosphere-forming ability and clonogenicity.** (A) NNI-4, (B) NNI-11 and (C) NNI-12 GPCs were subjected to lentiviral-mediated *STAT3* knockdown (NTC, non-targeting control; 3 sh*STAT3* knockdown clones, C1, C2 and C3). The knockdown clones were verified by (i) immunoblotting; (ii) cell viability assay; (iii) clonogenicity, and (iv) gliosphere size distribution. Phosphorylation of *STAT3* (p*STAT3*) at Tyr705. \*\*,  $p$ -value<0.01; \*\*\*,  $p$ -value<0.001; versus NTC. For statistical analysis, two-sided Student's  $t$  test was used, Error bars represent standard deviation of the mean. (D) Gene Set Enrichment Analysis (GSEA) in *STAT3*

knockdown expression profile revealed down-regulation of the JAK-STAT signalling pathway.

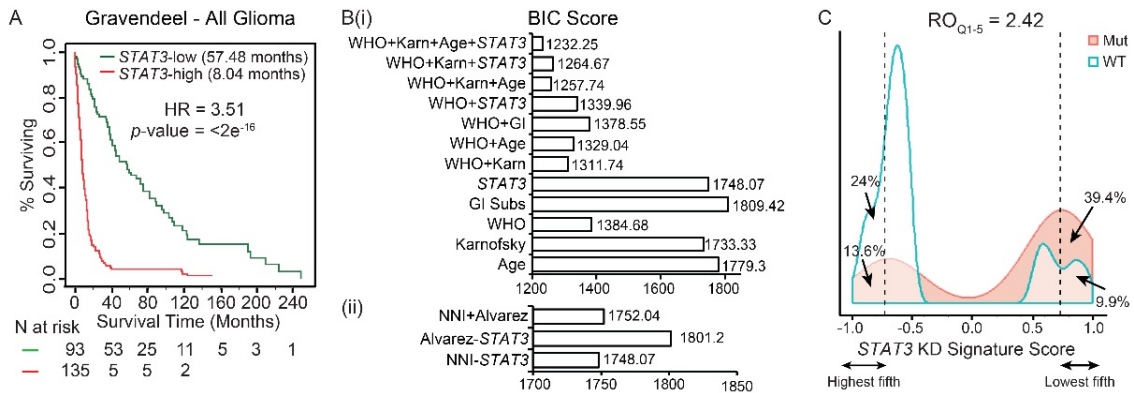


**Figure 7. NNI-*STAT3* functionally-tuned gene signature stratifies patient survival, independent of current clinical indicators. (A)** NNI-*STAT3* signature stratified patient survival in “Gravendeel” clinical database (validation patient database). An enrichment of *STAT3* pathway activation defined the poor prognosis patients (*STAT3*-high) while patients of *STAT3*-low survived significantly longer. **(Bi)** A combination of NNI-*STAT3* gene signature, WHO status, Karnofsky (Karn) score and age presented the best statistical model to account for the variability in patient survival, using the Bayesian Information Criterion (BIC) method. **(ii)** NNI-*STAT3* signature performed better than the existing “Alvarez” *STAT3* signature for glioma patient prognosis. **(C)** The relative odds of correlation between *STAT3* signature and *IDH*-mutation is 2.42 in a diagnostic metrics test. Patients with a negative signature score (*STAT3*-high), are 2.42 times more likely to be *IDH*-WT than those with a positive signature score (*STAT3*-low).

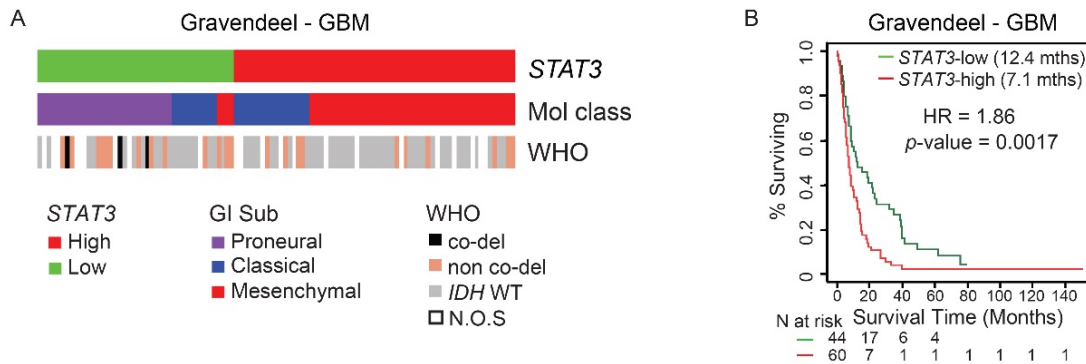


**Figure 8. *STAT3* stratification in GBM patient cohorts. (A)** *STAT3*-high GBM patient cohort was enriched in mesenchymal and classical molecular subtypes. *STAT3*-low tumours, in contrast, comprised mostly the proneural molecular subtype. **(B)** NNI-*STAT3* signature stratified GBM patient survival. An enrichment of *STAT3* pathway activation defined poor prognosis patients (*STAT3*-high, 7.1 months) while patients of *STAT3*-low survived significantly longer (12.4 months).

### 3.2. Pharmacological Inhibition of STAT3 Mitigates GBM Cell Growth

To test the concept of patient stratification and identify individuals most likely to respond to STAT3 inhibition therapy, we applied the functionally-tuned gene signature to our biobank of patient tumours and cells (Figure 9A). In Figure 9Ai, we were able to stratify the patient tumours into *STAT3*-high or -low groups. We demonstrated that *STAT3*-high tumours indeed had higher mean *STAT3* mRNA expression as compared to *STAT3*-low stratified tumours. In Figure 9Aii, we probed the GPCs for their *STAT3* mRNA expression, to select for cells with respective high/low expression for our subsequent *in vitro* analyses. Our cells are typically maintained at low passages to minimize accumulation of cytogenetic aberrations and epigenetic silencing. We utilized our novel technique of vitrification, facilitating cryopreservation of GPC spheroid structures in the absence of serum, a confounding factor in cellular differentiation contributing to mitotically terminal cells. Based on our bioinformatics analysis of both GBM tumours and cells, our *STAT3* functionally-tuned gene signature could consistently stratify our patient material into *STAT3*-high and -low subgroups. Specifically, our immunoblot analysis validated that patient-derived GPCs displayed varied levels of pSTAT3/STAT3 protein expression, with *STAT3*-high groups (NNI-12, -21, -24), displaying higher phospho-STAT3 (pSTAT3) levels in contrast to the *STAT3*-low

cells (NNI-11, -20 and -23) (Figure 9B). In this study, we focused on STAT3 phosphorylation at tyrosine residue 705 (Tyr705) for its role in facilitating homodimerization and being conserved across all SH2 domains (Becker *et al.*, 1998; Kuriyan and Cowburn, 1997). We subsequently selected to work with NNI-20 and -23 as *STAT3*-low cell lines and NNI-21, and -24 as *STAT3*-high cells for subsequent experiments based on their ability to form orthotopic xenograft tumours within an experimentally feasible time span (3.5 months).

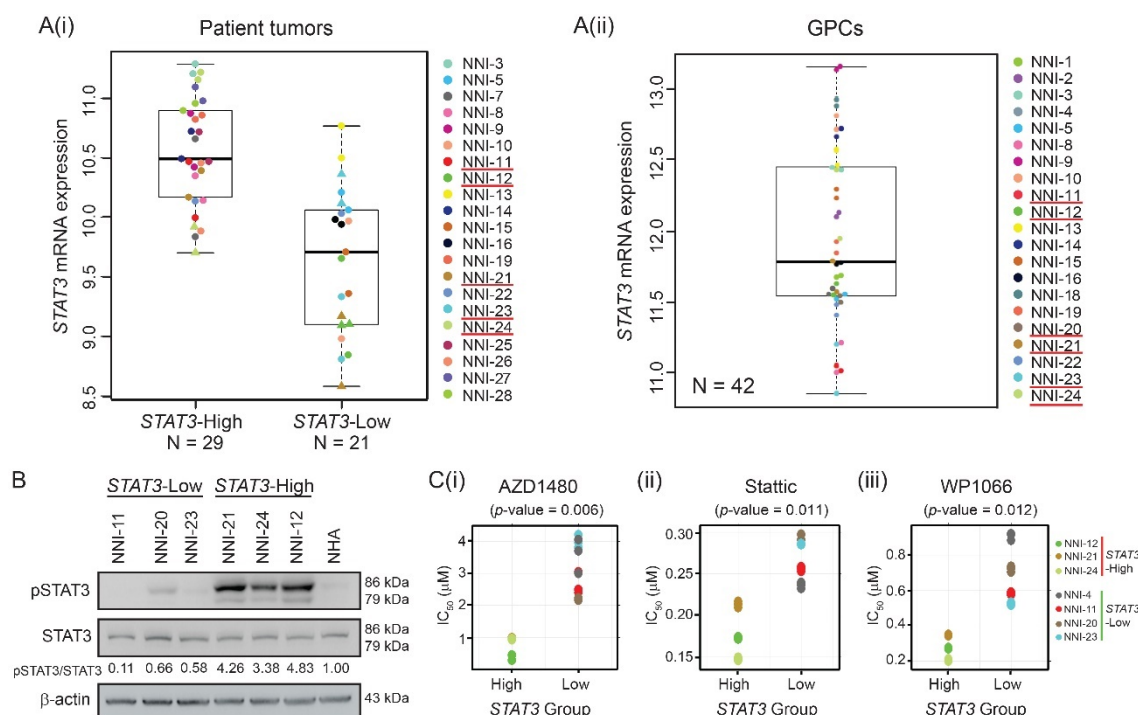


**Figure 9. NNI patient tumours have variable *STAT3* expression and can be stratified by *STAT3* functionally-tuned gene signature. (Ai)** NNI patient tumours and **(ii)** patient-derived glioblastoma-propagating cells (GPCs) have variable *STAT3* expression levels and can be classified into *STAT3*-high and -low based on our *STAT3* functionally-tuned gene signature. **(B)** Immunoblot analysis of patient GBM cell lines. *STAT3*-high cell lines (NNI-21, -24, -12) showed elevated phospho-STAT3, compared to *STAT3*-low cell lines (NNI-11, -20, -23), normal human astrocytes (NHA) served as control. Phosphorylation of STAT3 (pSTAT3) at Tyr705. **(C)** Seven patient GBM cell lines were treated with **(i)** AZD1480; **(ii)** Stattic; and **(iii)** WP1066 and their IC<sub>50</sub> values determined. Consistent with our bioinformatics prediction, *STAT3*-high cell lines that included NNI-12, -21 and -24 were sensitive to *STAT3* inhibitors as demonstrated by lower IC<sub>50</sub> values. *STAT3*-low cell lines included NNI-4, -11, -20 and -23 that were more resistant.

We hypothesized that the STAT3 pathway promotes GBM growth through regulation of self-renewal traits, and stratifies patients for their likely response to STAT3 inhibition therapy. This was based on our initial observation that while STAT3 small molecule inhibitors effectively mitigated GPC viability and growth, they were also equally ineffective in a subset of patient GPC lines, thereby suggesting some degree of heterogeneity in response. To address this concept of tumour heterogeneity and subsequent need for patient stratification for more effective targeted therapies, we evaluated the performance of our *STAT3*-functionally-tuned gene signature and identified specific candidates contributing to chemo-resistant and –sensitive profiles (Foong *et al.*, 2012; Geron *et al.*, 2008; Levine and Gilliland, 2008; Morgan and Gilliland, 2008). Consistent with our hypothesis, *STAT3*-high tumour cells demonstrated significantly lower half maximal inhibitory concentrations (IC<sub>50</sub>) upon treatment with various STAT3 inhibitors, compared to *STAT3*-low cells (Figure 9C and Appendix C). AZD1480, Stattic and WP1066 represent JAK/STAT inhibitors commonly used; in particular, AZD1480 demonstrated specific activity against Jak2 kinase, mitigating tumour cell proliferation in a variety of solid tumours. We proceeded to use AZD1480 as a mechanistic tool for our study due to its high specificity (AZD1480 has enzymatic IC<sub>50</sub> value in nM range (Derenzini *et al.*, 2011), compared to μM range of Stattic (Schust *et al.*, 2006) and WP1066 (Hatiboglu *et al.*, 2012)) and blood-brain barrier penetration efficiency. Similarly, *STAT3*-high cells showed greater reduction in cell viability (Figure 10A) and gliomasphere-forming ability (Figure 10B) after treatment with STAT3 inhibitors when compared to *STAT3*-low cell lines.

Finally, we utilized the pre-treated orthotopic patient-derived xenograft (PDX) mouse model routinely established in our lab (Chong *et al.*, 2009; Chong *et al.*, 2016; Foong *et al.*, 2012; Foong *et al.*, 2011; Koh *et al.*, 2013) to illustrate how mice bearing *STAT3*-stratified tumours respond to AZD1480, a JAK/STAT small molecule currently in clinical trials (Hedvat *et al.*, 2009). We selected two GBM lines that each represented either *STAT3*-high or –low group, and pre-treated these cells with AZD1480 prior to stereotaxic implantation in NOD-SCID gamma mice (Larochelle *et al.*, 1996). The results demonstrated a dose-dependent extension of survival in *STAT3*-high (NNI-24) mice bearing cells treated with AZD1480 (Figure 10C and Table 3). The median survival of mice bearing either NNI-20 or NNI-24 dimethylsulfoxide (DMSO) control cells was 134 days. Compared to NNI-20

(*STAT3*-low) mice, NNI-24 mice demonstrated an approximate 2.5-fold increased median survival difference between matched DMSO solvent control and AZD1480-treated groups (Figure 10D and Table 3). In mice implanted with cells treated with AZD1480 at 1  $\mu$ M, the median survival was 181 days in *STAT3*-high NNI-24 mice compared with 154 days in *STAT3*-low NNI-20 bearing mice. Although we saw a marginal significance ( $p$ -value=0.041) in NNI-20 AZD1480 treated mice, the added survival benefit was not impactful. We demonstrated subsequently that NNI-20 (*STAT3*-low) treated with dual inhibitors performed significantly better with dual inhibitor treatment (Section 3.5, Figure 17 and Table 3). These findings support the application of our *STAT3* functionally-tuned gene signature to stratify and identify patient cohorts ostensibly to receive treatment benefit from STAT3 inhibition therapy, whilst further cautioning against the use of such inhibitors in *STAT3*-low patients due to the development of resistance mechanisms.

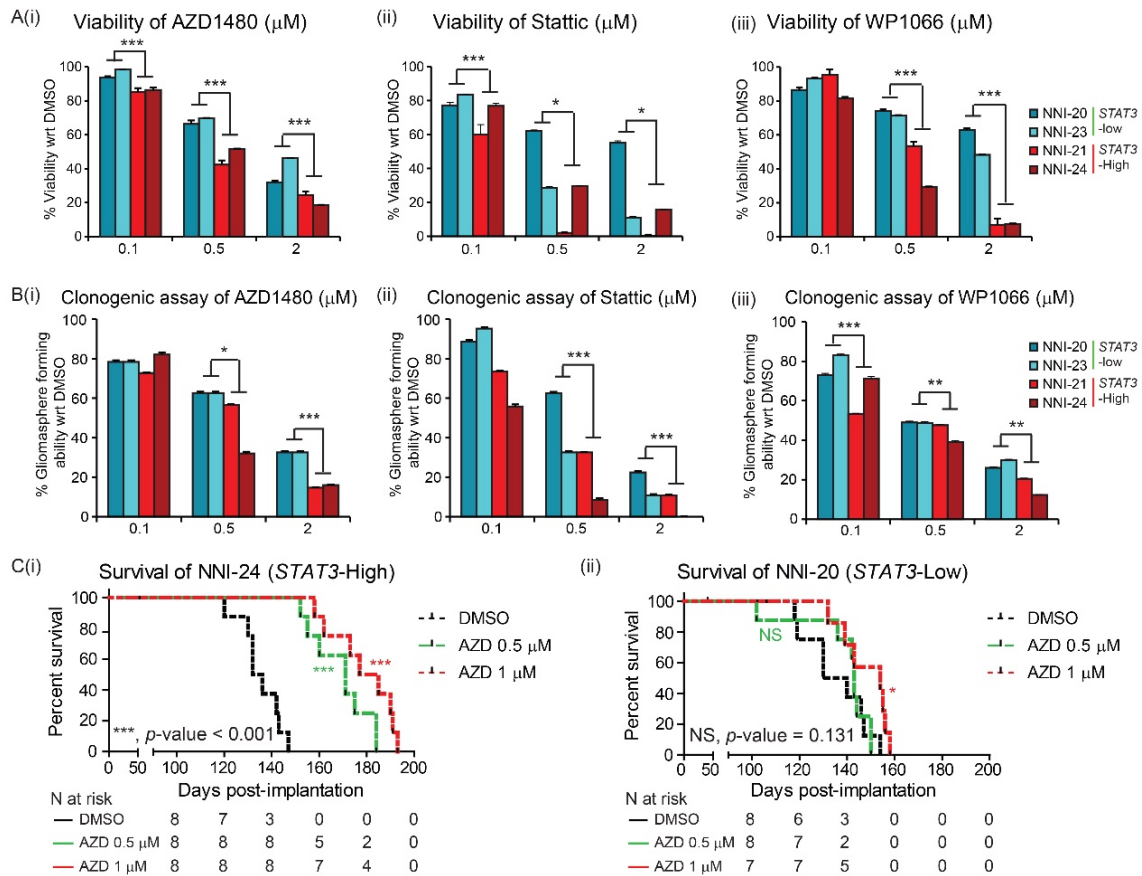


**Figure 10. NNI patient cells can be stratified by their *STAT3* status, and show variable response to *STAT3* inhibitors both *in vitro* and *in vivo*.** (A) *STAT3*-high and -low cell lines were validated by cell viability assay after treatment with various *STAT3* inhibitors. *STAT3*-low lines (NNI-20 and -23) demonstrated greater viability after treatment with (i) AZD1480; (ii) Stattic; (iii) WP1066. Conversely, *STAT3*-high lines (NNI-21 and -24) displayed greater sensitivity to *STAT3* inhibitors, resulting in reduced cell viability. (B) Consistently, clonogenic assays of GPCs upon treatment with (i) AZD1480; (ii) Stattic; (iii) WP1066 showed that *STAT3*-high cell lines displayed reduced gliomasphere-forming capability, compared to *STAT3*-low cell lines. \*, *p*-value<0.05; \*\*, *p*-value<0.01; \*\*\*, *p*-value<0.001; *STAT3*-high versus *STAT3*-low. For statistical analysis, two-sided Student’s t-test was used. Error bars represent standard deviation of the mean. (C) *STAT3*-high-stratified orthotopic PDX mouse model demonstrated favourable response to AZD1480. (i) *STAT3*-high (NNI-24) patient xenograft model demonstrated greater median survival difference to AZD1480. The median survival difference was ~2.5-fold for NNI-24 (47 days) compared to (ii) NNI-20 (19 days) animal groups (groups of 8 in 3 arms). \*, *p*-value<0.05; \*\*\*, *p*-value <0.001 versus DMSO.



### 3.3. Mechanism Contributing to *STAT3*-resistant Profile

To demonstrate therapeutic resistance and the recurrent nature of GBM, our GPCs were treated with *STAT3* inhibitor AZD1480 at their respective  $IC_{50}$  concentrations and allowed to recover for 5 days in drug-free growth media. Our recovery assay revealed that *STAT3*-high cells (NNI-21 and -24) showed significant mitigation of viability and self-renewal (Figure 11A and B). In contrast, *STAT3*-low cells (NNI-20 and -23) were minimally inhibited by the *STAT3* inhibitors. Instead, these *STAT3*-low cells developed resistance as demonstrated by the ability to recover and continued to proliferate, and gained greater invasive potential (Figure 11C). As important as identifying patient cohorts who potentially respond favourably to *STAT3* inhibition therapy, we sought to evaluate resistance mechanisms in the *STAT3*-low group, so that therapeutic options may be defined to sensitize these individuals to chemotherapy.

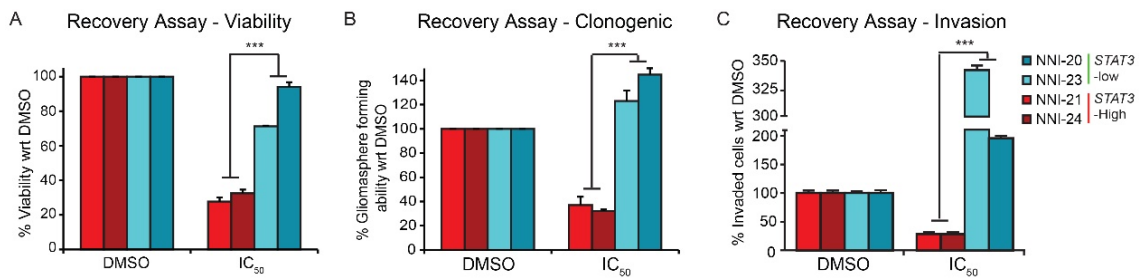


**Figure 11. Recovery Assay.** Upon releasing GPCs into drug-free media after AZD1480 treatment for 5 days, the (A) viability, (B) clonogenic capacity of *STAT3*-high GPCs were significantly mitigated. In contrast, *STAT3*-low GPCs developed resistance and (C) demonstrated greater ability to invade. This highlights the potential of our gene signature to accurately identify susceptible individuals, and to avoid those who might develop resistance against *STAT3* inhibition therapy. \*,  $p$ -value < 0.05; \*\*,  $p$ -value < 0.01; \*\*\*,  $p$ -value < 0.001; *STAT3*-high versus *STAT3*-low. For statistical analysis, two-sided Student's t-test was used. Error bars represent standard deviation of the mean.

We evaluated our *STAT3* functionally-tuned gene signature and prioritised those candidates most highly variable between *STAT3*-high and *STAT3*-low groups. We winnowed down candidate genes based on four criteria: (i) Most highly variable genes, (ii) Differential expression between normal and tumour tissue, (iii)

Neurodevelopmentally-regulated, and (iv) Patient survival-related. This reduced the gene list (includes up- and down-regulated candidates), selecting potential targets contributing to self-renewing potential of stem-like GPCs (Appendix D). We validated the genes via quantitative real-time PCR (qRT-PCR) and focused on candidates that exhibited a dose-dependent increase in *STAT3*-low cells after treatment with various *STAT3* inhibitors (Figure 12) for the reason that up-regulated genes better serve as therapeutic targets. Six genes were identified; insulin-like growth factor binding protein 2 (*IGFBP2*), neural precursor cell expressed, developmentally down-regulated 9 (*NEDD9*), synaptosomal-associated protein 23 (*SNAP23*), guanosine diphosphate (GDP)-mannose pyrophosphorylase A (*GMPPA*), E26 transformation-specific containing gene (*ELK3*, ETS domain containing protein) and kelch domain containing 8A (*KLHDC8A*).

We assessed the functions of these genes:

- a) *IGFBP2* – binding protein of insulin-like growth factors I and II (IGF-I and IGF-II).
- b) *NEDD9* – a member of CRK-associated substrates family as adhesion docking molecules, mediating protein-protein interaction of signal transduction pathways. A focal adhesion protein acting as a scaffold for regulating signalling complexes for cell attachment, migration and invasion.
- c) *SNAP23* – a synaptosomal protein that tightly binds to multiple vesicle-associated membrane protein (synaptobrevins/VAMPs) to target compartment membrane protein (syntaxin). This complex serves a binding site for membrane fusion.
- d) *GMPPA* – GDP-mannose pyrophosphorylase catalysing the transformation of mannose-1-phosphate and GTP to GDP mannose during the production of N-linked oligosaccharides.
- e) *ELK3* – Member of the E26 transformation-specific (ETS) domain transcription factor family and the ternary complex factor (TCF) subfamily. Upon recruitment by serum response factor, *ELK3* is involved in the regulation of transcription.
- f) *KLHDC8A* – Kelch domain-containing protein, often upregulated in cancers providing an alternative pathway for tumours to maintain aggressiveness as a delta-EGFR substitute.

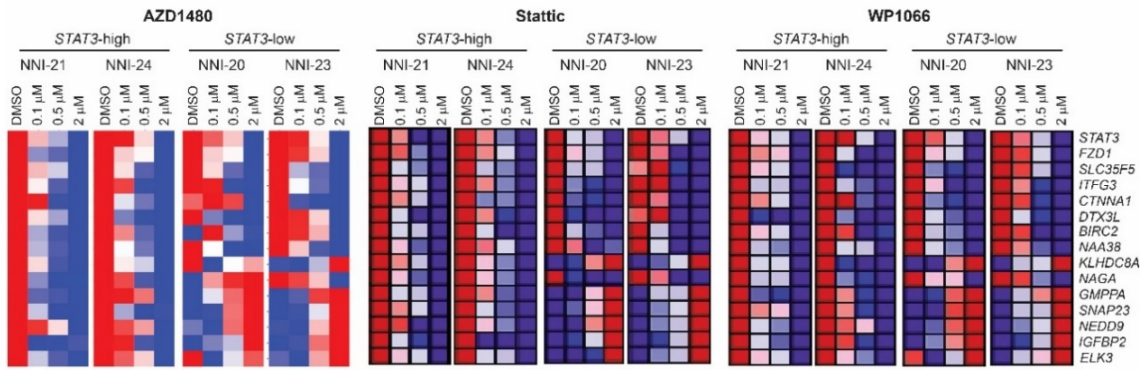


**Figure 12. Mechanistic gene candidates discerning cooperative genes responsible in the *STAT3*-resistant profile.** Dose-dependent differential gene expression after various *STAT3* inhibitor treatment across *STAT3*-high and -low cell lines.

### 3.4. IGF-1R Signalling Pathway Contributes to Resistance Mechanism in *STAT3*-low GPCs

By surveying literature, we prioritised *IGFBP2* for resistance as it is one of six genes that sequester intracellular insulin-like growth factor 1 (IGF-1), and for which clinical trials are currently in progress to evaluate anti-IGF-1R inhibitors in a variety of solid tumours. We hypothesise that the chemoresistant profile of *STAT3*-low cells can be attributed to a self-regulatory circuit that involves IGF-1R and *STAT3* (Lee *et al.*, 2015; Nair *et al.*, 2001; Zhang *et al.*, 2006b).

Insulin-like Growth Factor Binding Protein-2 (IGFBP2) has been shown to promote cell growth and metastatic potential in ovarian, prostate and bladder cancer, as well as in glioblastoma by modulating the action of IGF-1 (Chakrabarty and Kondratyck, 2006; Chatterjee *et al.*, 2004; Fukushima *et al.*, 2007; Miyake *et al.*, 2005). Nuclear expression of IGFBP2 has been demonstrated to contribute to tumourigenic potential by promoting angiogenesis and invasion (Azar *et al.*, 2011; de Groot *et al.*, 2010; Pažanin *et al.*, 2011). With this understanding, we propose that in chemoresistant GPCs (*STAT3*-low), *STAT3* activation increases the transcription of *IGFBP2*, regulating the production of IGF-1 as part of a feed-forward mechanism. More importantly, IGFBP2 is part of the *STAT3* functionally-tuned transcriptomic signature, and was up-regulated upon treatment of *STAT3*-low cells with AZD1480. In Figure 13A, we propose the mechanism involving IGF-1R and *STAT3* pathways. Indeed, we verified direct binding of *STAT3* to *IGFBP2*

(Figure 13B) by co-immunoprecipitation. To provide firm evidence, we demonstrated in *STAT3*-low cells (NNI-20), IGFBP2 protein expression was upregulated in the nuclear fraction but not cytosolic fraction (Figure 13C). This was not observed in the *STAT3*-high cells (NNI-24).

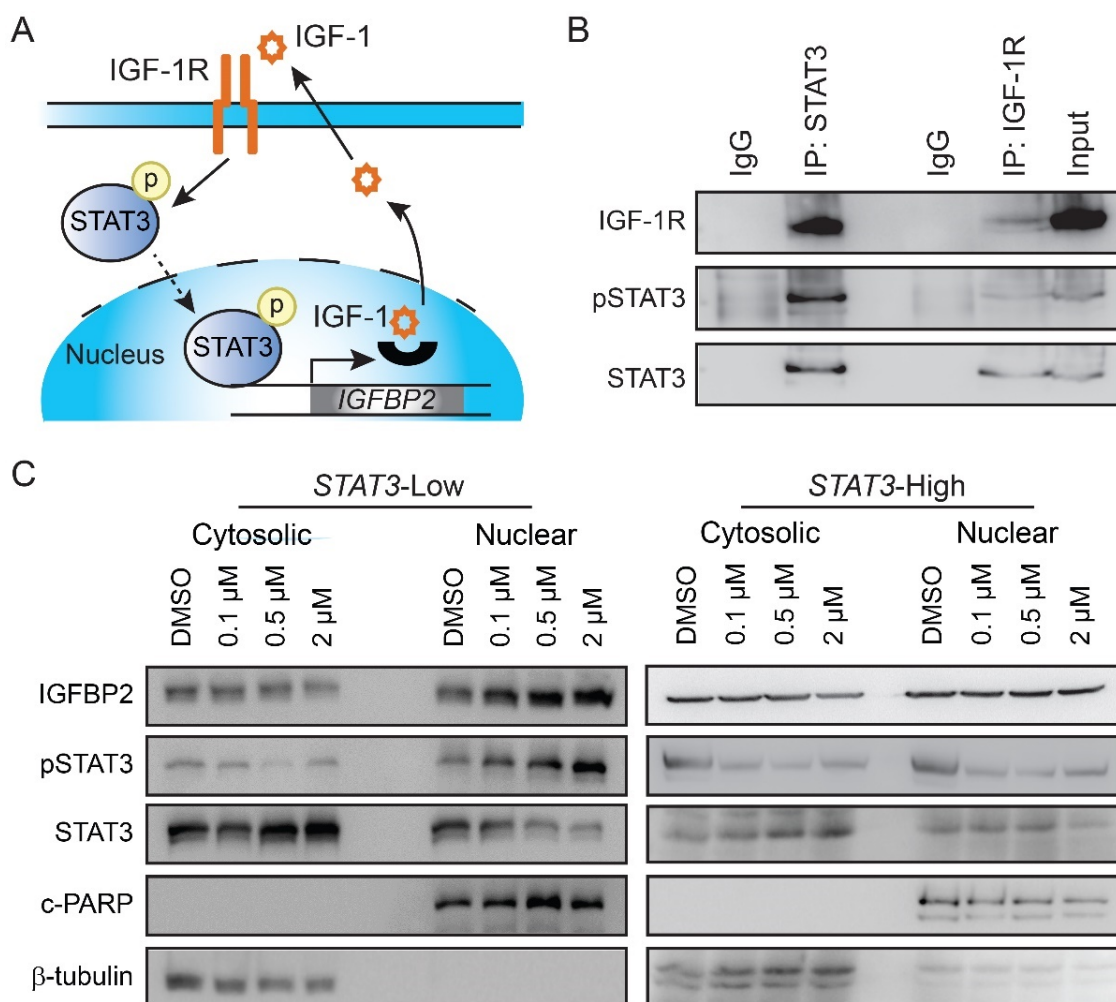


**Figure 13. Proposed mechanism in *STAT3*-low (therapeutic resistant) GBM cells.** (A) We proposed that in *STAT3*-low cells, phosphorylated STAT3 (pSTAT3) activates the transcription of *IGFBP2*, which increases the production of IGF-1. Increased production of IGF-1 triggers the activation of IGF-1R pathway, contributing to a feed-forward mechanism. (B) Immunoprecipitation assays demonstrated the physical interaction of IGF-1R with STAT3. (C) Treatment effect of cells with STAT3 inhibitor (AZD1480) demonstrated an increase in pSTAT3 and IGFBP2 expression levels in the nuclear fraction of *STAT3*-low cells but not in *STAT3*-high.  $\beta$ -tubulin and c-PARP were used as loading controls for the cytosolic and nuclear fractions respectively.

Kinases represent dominant therapeutic targets in major pharmaceutical pipelines; therefore, we established an approach of using biological evidence to substantiate our computational predictions, by measuring phosphorylation levels of 144 kinases in *STAT3*-signature-stratified GBM cells using the PamChip kinome screen (methodology described in Figure 4). In addition, our proposed method of analysis facilitates the mapping of the complete kinase-transcription factor-target gene network in the proneural-mesenchymal transition represented by *STAT3* activation (Segerman *et al.*, 2016). Accordingly, we included biochemical and functional modules in the kinome analysis pipeline that addressed the following: (i) Assigned clinical and cellular phenotypes to kinase candidates that are therapeutically targetable, (ii) Identify kinases upstream of *STAT3* inhibition mediated by AZD1480 treatment, through indirect mapping using molecular databases where the *STAT3* module is enriched, (iii) Identify downstream transcription factors and target genes using the similar database by association. Thus, through this computational pipeline, we are able to define the entire kinase signalling network mediating the PMT process, allowing a critical decision to be made regarding therapeutically targetable kinase candidates. We treated *STAT3*-high and -low cells with AZD1480 and carried out a PamChip screen. Our approach using the kinome screen confirmed IGF-1R as a top-ranking tyrosine kinase uniquely and biochemically elevated in *STAT3*-low tumours upon treatment with AZD1480 (Figure 14A and Appendix E). Together with our kinome data, we used protein analyses to substantiate our results. We verified a dose-dependent increase of secreted IGFBP2 and IGF-1 proteins in NNI-20 cells (*STAT3*-low GBM cell line) upon treatment with AZD1480 (Figure 14B). Furthermore, we observed a significant increase of IGFBP2 and IGF-1R proteins in *STAT3*-low cells (NNI-20, -23) upon AZD1480 treatment, compared to *STAT3*-high cells (NNI-21, -24) (Figure 14C). In summary, our data provides a basis to explore the IGF-1R pathway in *STAT3*-low cells. These unique changes were quantified, and provide preliminary evidence for our hypothesis that the IGF-1R pathway could potentially be mediating the resistant profile of *STAT3*-low cells.

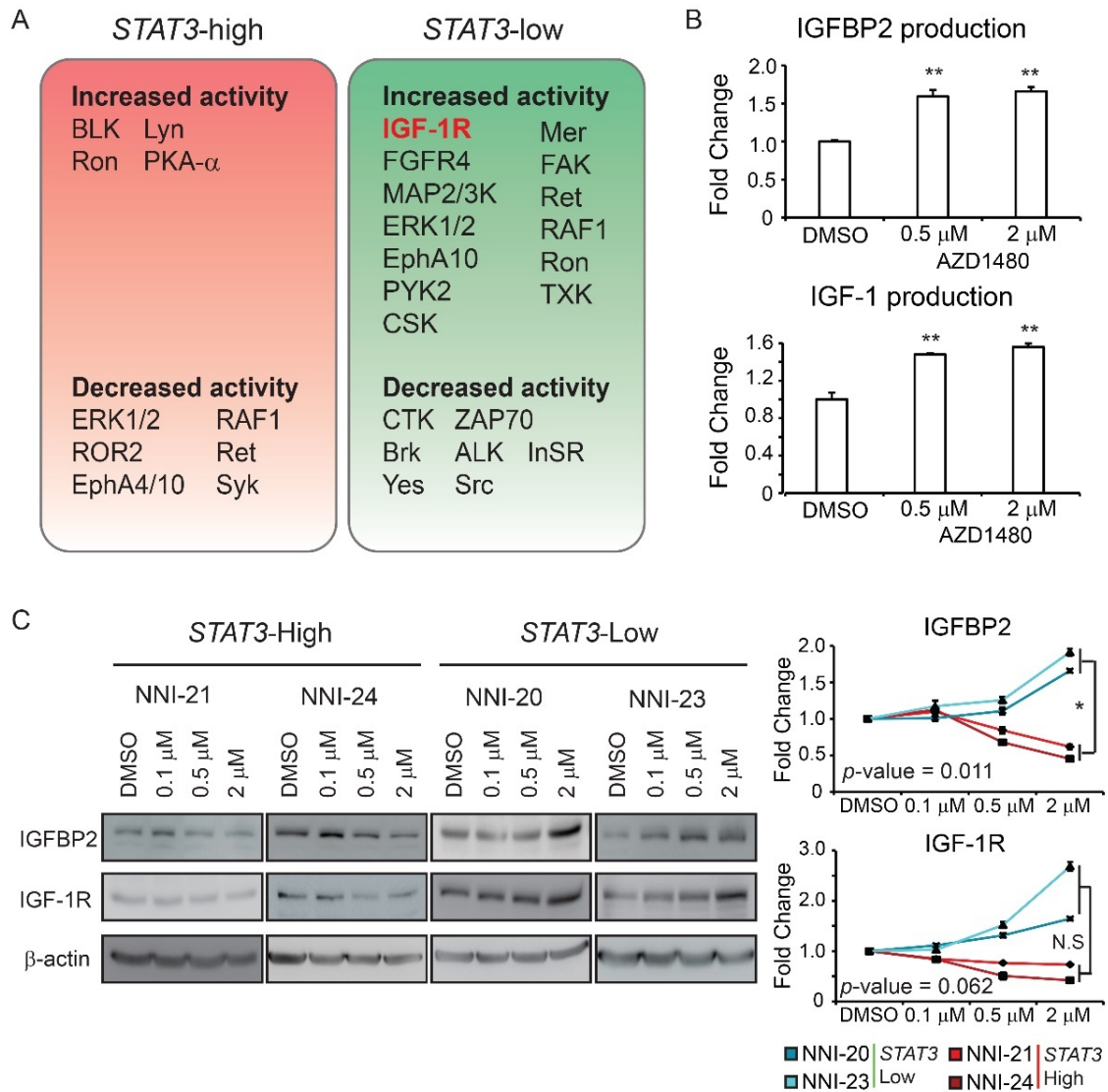


**Figure 14. Mechanistic gene candidates identified by NNI-STAT3 gene signature representing resistance to STAT3 inhibitor. (A)** Graphical illustration of responsive and resistant protein tyrosine kinase candidates in *STAT3*-high and -low cell lines treated with AZD1480 using computational workflow described in Appendix B. **(B)** Fold-change differences in secreted proteins demonstrated increased IGFBP2 and IGF-1R in resistant cells post-treatment with STAT3 inhibitor. **(C)** *STAT3*-high GBM cells displayed modest reduction in *IGF-1R* and *IGFBP2* expression levels. In contrast, IGF-1R and IGFBP2 protein expression in *STAT3*-low cells increased dose-dependently upon AZD1480 treatment, albeit IGF-1R was marginally insignificant. Fold-change differences in protein expression of IGFBP2 and IGF-1R were compared between *STAT3*-high and -low GBM cells. \*,  $p$ -value $<0.05$ ; \*\*,  $p$ -value $<0.01$ ; \*\*\*,  $p$ -value $<0.001$ ; *STAT3*-high vs *STAT3*-low. For statistical analysis, two-sided Student's t-test was used. Error bars represent standard deviation of the mean.

### 3.5. Depletion of IGFBP2 and C-terminal IGF-1R Restores Sensitivity

To provide firm evidence, we attenuated IGF-1R signalling pathway by targeting its effector, IGFBP2, using lentiviral-mediated shRNA knockdown (Figure 15Ai and Bi). Depletion of IGFBP2 significantly sensitized *STAT3*-low cells to STAT3 inhibitor treatment. Compared to the non-targeting control (NTC), using 2 different *IGFBP2* knockdown clones, we observed in both *STAT3*-low cell lines a decrease in viability and clonogenic potential (Figure 15Aii-iii and Bii-iii).

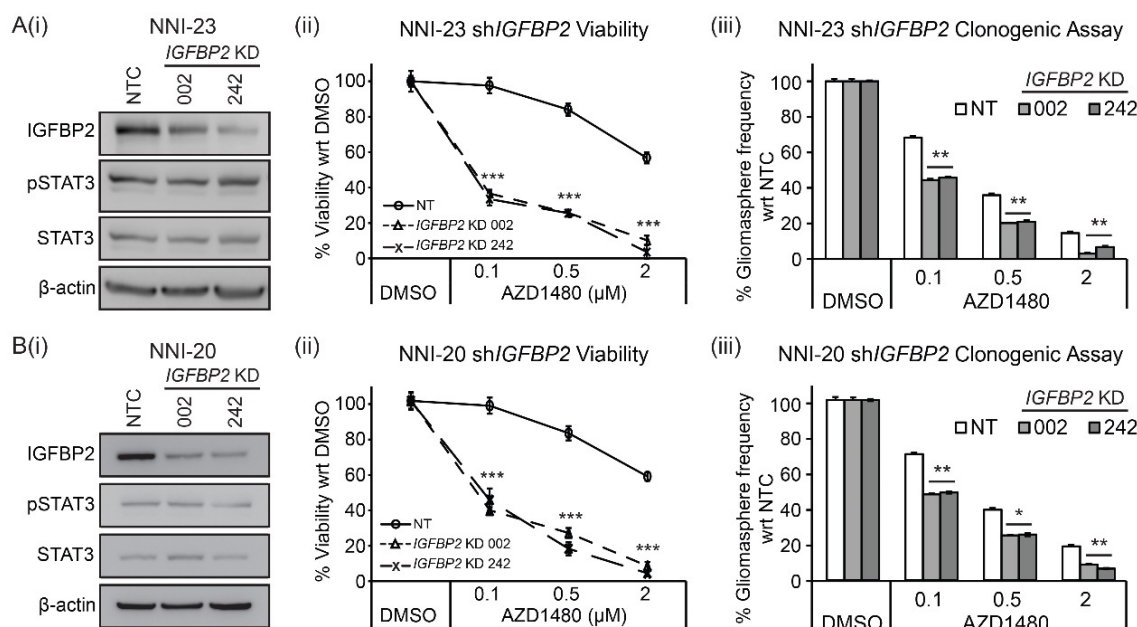


**Figure 15. Depletion of mechanistic gene *IGFBP2* restores sensitivity in *STAT3*-low GBM cells.** Depletion of mechanistic gene *IGFBP2* demonstrated induced sensitivity to STAT3 inhibitor. Compared to the non-targeting control (NTC), sh*IGFBP2* clones displayed increased sensitivity to STAT3 inhibitor, as observed by (i) decreased viability and (ii) reduced gliomasphere frequency in *STAT3*-low cell lines (A) NNI-23 and (B) NNI-20. \*\*,  $p$ -value<0.01; \*\*\*,  $p$ -value<0.001; KD clones vs NTC. For statistical analysis, two-sided Student's t-test was used. Error bars represent standard deviation of the mean.

We previously demonstrated that IGF-1R directly binds to STAT3 (Figure 13B), and it has been shown that the C-terminal of IGF-1R is crucial for its interaction with STAT3 (Zhang *et al.*, 2006b). To further explore the mechanistic role of IGF-1R in *STAT3*-low GBM cells, we abolished the binding of STAT3 to IGF-1R (Figure 16). We deleted the C-terminal domain of IGF-1R in *STAT3*-low

cell lines. This resulted in the sensitization of GBM cells to STAT3 inhibitor, represented by the reduction of pSTAT3 (Figure 16A), followed by a significant reduction in GPC viability, self-renewal frequency and proliferation (Figure 15B).

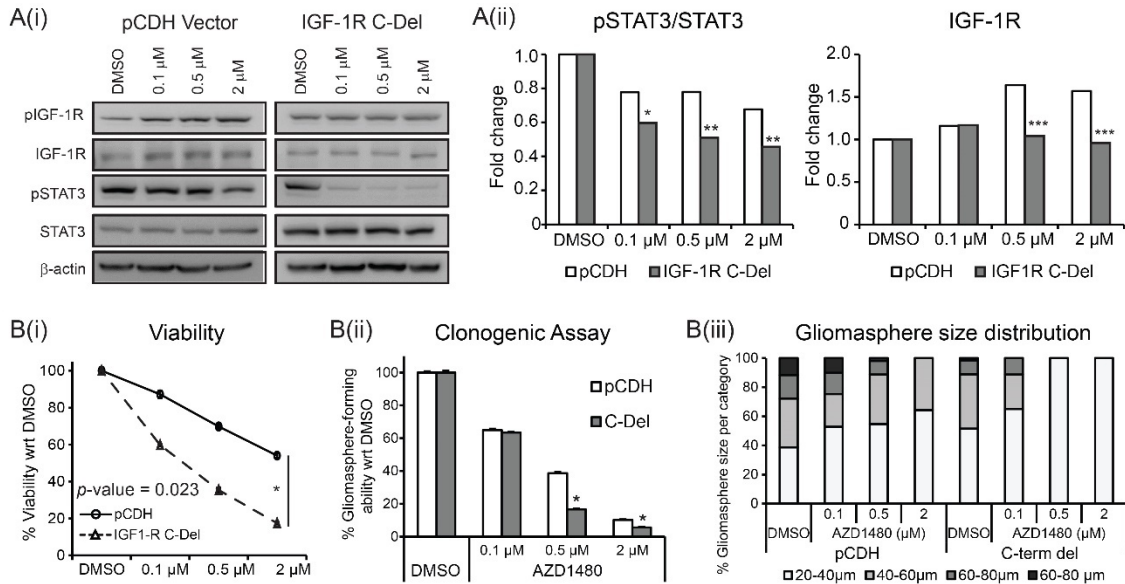


**Figure 16. Depletion of IGF-1R C-terminal domain restores sensitivity in *STAT3*-low GBM cells.** (A) In the pCDH vector control, phospho-IGF-1R increased with elevated dose of STAT3 inhibitor, demonstrating that IGF-1R is implicated in the resistance mechanism. (i) Immunoblot of pCDH vector control and IGF-1R C-terminal deletion post-treatment with AZD1480. (ii) Protein quantification of the ratio of pSTAT3/STAT3. (iii) A reduction in the secretion of IGF-1 upon deletion of IGF-1R C-terminal deletion demonstrated that the IGF-1R pathway contributes to a feed forward loop in therapeutic resistance. Compared to pCDH vector control, there was greater reduction in pSTAT3/STAT3 ratio in the C-terminal deletion clone, demonstrating greater sensitivity to the STAT3 inhibitor. (B) Therapeutic sensitivity to STAT3 inhibitors was observed in the IGF-1R C-terminal-deleted clone as seen by (i) decreased viability (Day 10), (ii) reduced gliomasphere-forming ability and (iii) reduced self-renewal property as shown by smaller sphere size distribution. \*,  $p$ -value < 0.05; pCDH control vector vs C-terminal deleted IGF-1R clone (C-Del). For statistical analysis, two-sided Student's t-test was used. Error bars represent standard deviation of the mean.

To substantiate the importance of a feed-forward mechanism in the *STAT3*-low cell lines, we conducted dual inhibition of both STAT3 and IGF-1R pathways



in our GPCs. Dual inhibitor treatment targeting STAT3 and IGF-1R demonstrated synergistic effect in *STAT3*-low cells *in vitro* and *in vivo* (Figure 17 and 18). Single inhibitor treatment (AZD1480 or Linsitinib) alone could not sensitize the *STAT3*-low group of cells as compared to the significant reduction of viability and clonogenic potential when *STAT3*-low cells were subjected to dual inhibitors (Figure 17A and B). The CI for the dual treatment (AZD1480 1  $\mu$ M and Linsitinib 0.5  $\mu$ M) was 0.23 and 0.209 for NNI-23 and -20 respectively, suggesting that drugs were synergistic. Mice bearing *STAT3*-low tumours treated with dual inhibition molecules demonstrated significantly prolonged survival compared to single inhibitor treatment (AZD1480 or Linsitinib alone). Dual-treated NNI-20 bearing mice displayed extended survival of up to 200 days as compared to the single inhibitor treatment with AZD1480 (154 days) or Linsitinib (137 days). Of note, in NNI-24 *STAT3*-high tumour-bearing mice, dual inhibitor treatment (192 days) conferred no significant additional advantage against single inhibitor treatment with AZD1480 alone (181 days) (Figure 17C and Table 3).

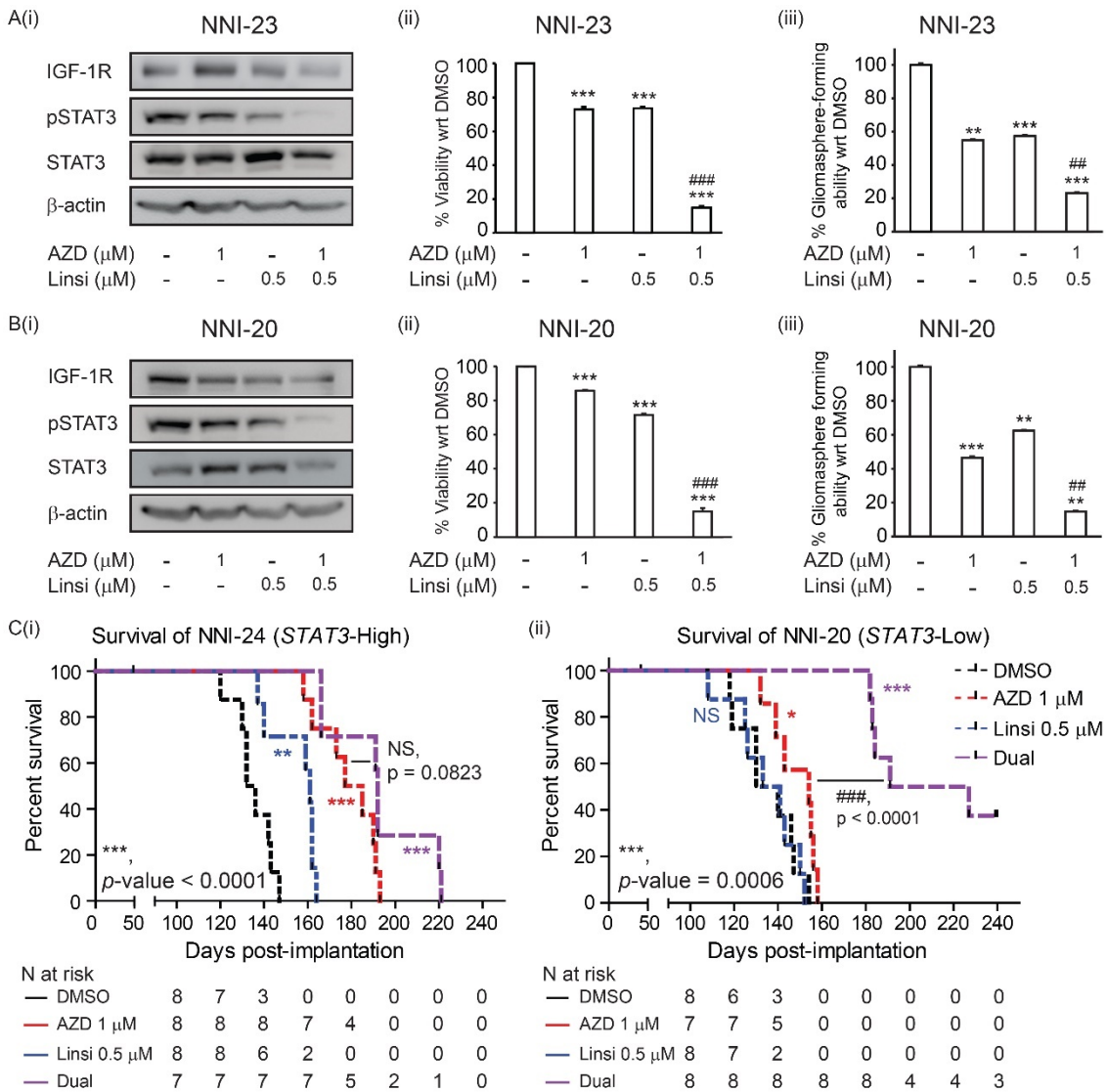


**Figure 17. Sensitisation of resistant *STAT3*-low GBM cells with dual inhibition.** Dual inhibition of *STAT3* and IGF-1R serves as a putative therapeutic strategy for *STAT3*-low GBM patients. Single inhibitor treatment alone was not as effective in sensitizing the *STAT3*-low cells (A) NNI-23 and (B) NNI-20 when compared to dual inhibitor treatment. Using (i) immunoblot analysis (ii) viability and (iii) gliosphere frequency assay, a dual treatment strategy demonstrated reduction of IGF-1R and p*STAT3*. CI of AZD1480 (1 μM) and Linsitinib (0.5 μM) was 0.23 (NNI-23) and 0.209 (NNI-20), suggesting the drugs act in synergism. \*\*, *p*-value<0.01; \*\*\*, *p*-value<0.001; treatment groups vs DMSO control. ##, *p*-value<0.01; ###, *p*-value<0.001; dual inhibitors (*STAT3* and IGF-1R) vs individual inhibitors (*STAT3* or IGF-1R). For statistical analysis, two-sided Student’s t-test was used. Error bars represent standard deviation of the mean. (Ci) NNI-24 *STAT3*-high xenograft model displayed prolonged survival upon treatment with AZD1480 alone, while (ii) NNI-20 *STAT3*-low xenograft model

received less survival benefit with single treatment. In contrast, dual treatment targeting both STAT3 and IGF-1R significantly prolonged survival and extended tumour latency of *STAT3*-low xenograft mice (groups of 8 in 4 arms). \*,  $p$ -value<0.05; \*\*,  $p$ -value<0.01; \*\*\*,  $p$ -value<0.001 treatment group versus DMSO; ##,  $p$ -value<0.01; ###,  $p$ -value<0.001 dual inhibitors (STAT3 and IGF-1R) vs single inhibitors (STAT3 or IGF-1R). Censored points are indicated by the black tick marks which represent terminated mice without evidence of brain tumours.

**Table 3. Kaplan-Meier Statistics**

Cell Line	Treatment Groups	Median Survival (Days)	Hazard ratio	Logrank $p$ -value vs DMSO
NNI-24 <i>STAT3</i> -High	DMSO (N=8)	134	1.00	-
	AZD1480 0.5 $\mu$ M (N=8)	171	25.17	***, 0.0001
	AZD1480 1 $\mu$ M (N=8)	181	25.17	***, <0.0001
	Linsitinib 0.5 $\mu$ M (N=8)	161	6.83	**, 0.0044
	Dual (N=8)	192	20.07	***, <0.0001
NNI-20 <i>STAT3</i> -Low	DMSO (N=8)	135	1.00	-
	AZD1480 0.5 $\mu$ M (N=8)	143	1.14	NS, 0.8118
	AZD1480 1 $\mu$ M (N=8)	154	3.53	*, 0.041
	Linsitinib 0.5 $\mu$ M (N=8)	137	0.90	NS, 0.8373
	Dual (N=7)	200	25.17	***, <0.0001

Upon presentation of neurological deficits, we terminated our mice and harvested the brain tumour tissue for validation. We subjected our PDX tumours to immunoblot and immunohistochemical analyses to assess the expression of pSTAT3 and IGF-1R in their respective treatment groups. Similar to our *in vitro* results, NNI-20 (*STAT3*-low) PDX tumours demonstrated an increase in IGF-1R upon treatment with STAT3 inhibitor AZD1480 alone in a dose-dependent manner (Figure 18A and Ci), while we observed a reduction of IGF-1R expression in the dual-treated tumours. In contrast, pSTAT3 expression in NNI-24 (*STAT3*-high) PDX tumours displayed a reduction upon exposure to AZD1480 treatment, and there was no change in IGF-1 expression (Figure 18A and Cii). Immunoreactivity scores (IRS) of the PDX tissues were evaluated for pSTAT3 and IGF-1R expression (Figure 18Bi and ii). These results highlight the role of the IGF-1R pathway at conferring STAT3 resistance, thus suggesting a potential therapeutic strategy utilizing a dual inhibitor approach to sensitize the *STAT3*-low GBM patient

subgroup. A critical element of precision medicine studies does not solely focus on responders alone (*STAT3*-high), but also evaluates therapeutic options to bring about a curative outcome for non-responders (*STAT3*-low).

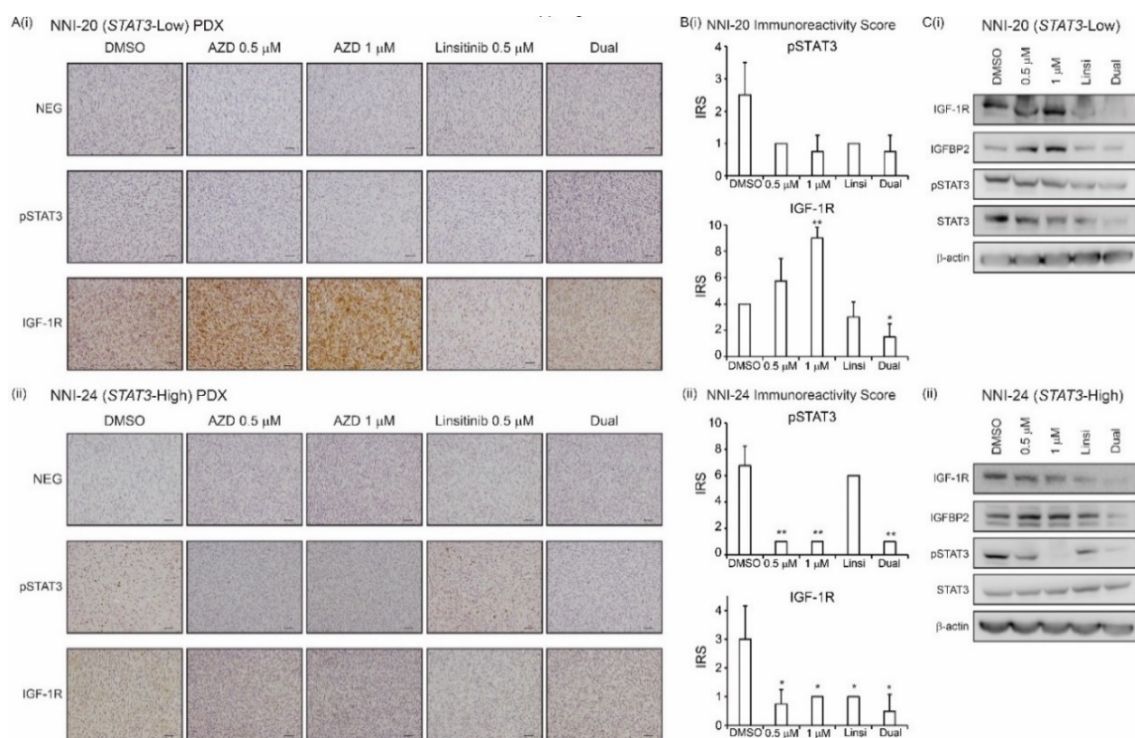


**Figure 18. Immunohistochemical (IHC) staining and quantification of pSTAT3 and IGF-1R on patient-derived xenograft (PDX) tumours.** (A) Representative images of PDX tumours stained for pSTAT3 and IGF-1R. (i) PDX-derived tumours from *STAT3* inhibitor-treated cells demonstrated a reduction of pSTAT3 expression in NNI-24 (*STAT3*-high). In contrast, (ii) NNI-20 (*STAT3*-low) PDX tumours demonstrated a significant increase in IGF-1R expression. Scale bar denotes 50  $\mu$ m. (B) Immunoreactivity scores (IRS) of PDX tissues were assessed for pSTAT3 and IGF-1R expression. For statistical analysis, two-sided Student's *t* test was used. Error bars represent standard deviation of the mean. (C) Immunoblot analysis of PDX tumours demonstrated that mice implanted with (i) NNI-24 (*STAT3*-high) treated with *STAT3* inhibitor, showed a reduction in pSTAT3 expression, while (ii) NNI-20 (*STAT3*-low) showed an evident increase in IGF-1R expression. This strongly suggests that cells pre-treated with dual *STAT3* and IGF-1R inhibitors was effective at sensitizing the *STAT3*-low cells.

As additional proof-of-concept validation, we treated *STAT3*-low (NNI-20, 23) and *STAT3*-high (NNI-21, 24) GBM cells with NT157, a selective inhibitor of insulin receptor substrate (IRS-1/2) that has the potential to inhibit both IGF-1R and STAT3 signalling pathways in cancer and stromal cells of the tumour microenvironment (Ibuki *et al.*, 2014). Similar to our dual inhibition results shown in Figures 17 and 18, we observed significant mitigation of viability and self-renewal capability of *STAT3*-low cells (NNI-20 and -23), at levels comparable to dual inhibition using AZD1480 and Linsitinib together (Figure 19A and B). In contrast, *STAT3*-high cells (NNI-21 and -24) treated with NT157 demonstrated marginal difference from AZD1480 treatment alone (Figure 19C and D), suggesting that IGF-1R targeting constitutes no additional, significant benefit in this subgroup.

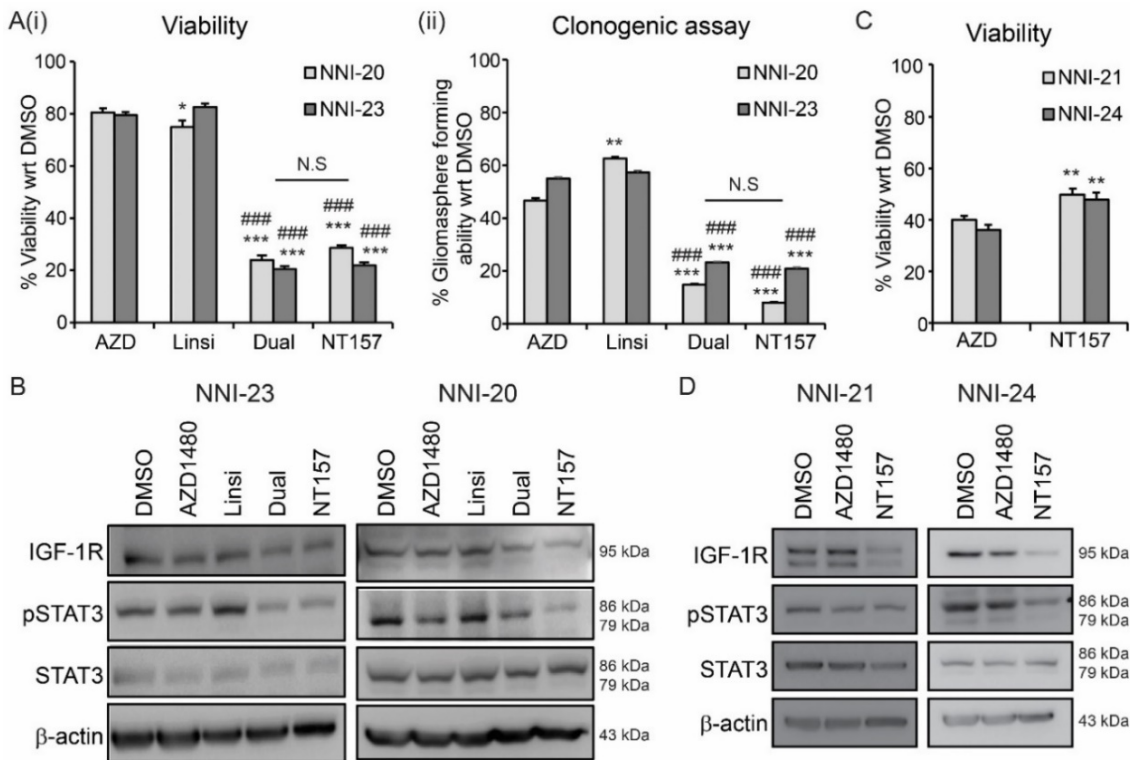


**Figure 19. Response to NT157, a selective inhibitor targeting IGF-1R and STAT3 signalling pathways. (Ai) Viability, (ii) clonogenic assay and (B) immunoblot of *STAT3*-low cells (NNI-20 and NNI-23) to single inhibitors AZD1480, Linsitinib, a combination of AZD1480 and Linsitinib (Dual) and NT157. There was no significant difference between treatment with NT157 versus a dual inhibitor treatment (AZD1480 and Linsitinib). On the other hand, NT157 did not confer additional therapeutic benefit to *STAT3*-high cells (NNI-21 and NNI-24) demonstrated by (C) viability and (D) immunoblot. \*\*,  $p$ -value<0.01; \*\*\*,  $p$ -**

value<0.001 versus AZD1480; ###,  $p$ -value<0.001 versus single inhibitor treatment (AZD1480 and Linsitinib).

### 3.6. Utility of *STAT3* Functionally-tuned Gene Signature

Conventional methods to detect STAT3 pathway activation are often carried out by immunohistochemistry where pSTAT3-specific antibodies are used on frozen or paraffin-embedded tumour sections. Interestingly, we show data that our *STAT3* functionally-tuned gene signature outperforms pSTAT3 status alone; in describing sensitivity of cells to drugs, the absolute levels of drug doses cannot be measured accurately by pSTAT3. We demonstrated that pSTAT3 immunohistochemical staining on our NNI-patient tumours was inadequate to stratify the *STAT3*-high from -low patient groups, for which we previously demonstrated significant correlation with IC<sub>50</sub> values (Figure 9Ci, 20A). Briefly, comparing various methods of H-score (Appendix F, I.), IC<sub>50</sub> values (Appendix F, II.) and our signature score (nearest template prediction, NTP-score), we showed that there was no significant correlation of H-score to either the NTP-score or IC<sub>50</sub> values (Figure 20Bi, ii and Appendix F). However, when we compared the IC<sub>50</sub> values to the NTP-score, we derived a significant negative correlation (Figure 20Biii), suggesting that the *STAT3* functionally-tuned gene signature is able to accurately profile sensitive and resistant patient cohorts. This implies that to precisely explain variations in sensitivity to drugs, only the gene signature could match those differences in concentrations.

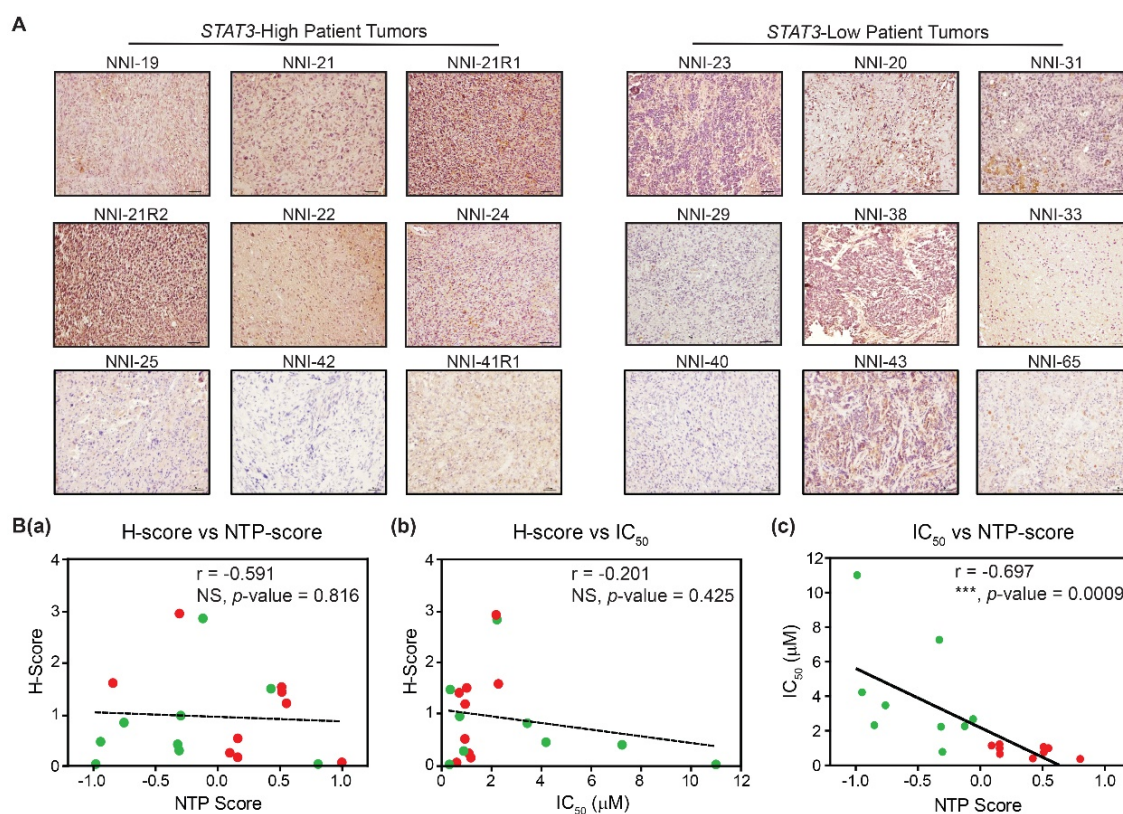


**Figure 20. NNI-*STAT3* signature better identifies responsive patient cohorts compared to p*STAT3* using immunohistochemistry staining. (A)** Immunohistochemical staining of NNI patient tumours with phospho-*STAT3*. Representative images are shown, scale bar denotes 50  $\mu$ m. Based on immunohistochemistry (IHC) staining method, patient samples could not be accurately stratified by their p*STAT3* status. **(B)** Using 3 different analyses, there was no significant correlation of **(i)** H-score vs Nearest Template Prediction (NTP) score derived from NNI-*STAT3* signature, or **(ii)** H-score vs  $IC_{50}$ . **(iii)** Significant negative correlation was only established when  $IC_{50}$  was plotted against NTP-score. \*\*,  $p$ -value<0.01. This emphasizes the importance of our gene signature to accurately identify responsive cohorts. H-scores and  $IC_{50}$  values are listed in Appendix F. *STAT3*-high is denoted by the red dots, while *STAT3*-low is denoted by the green dots. For statistical analysis, Pearson correlation coefficient was used.

### 3.7. Chemosensitisation of *STAT3*-stratified cells Synergises with Standard of Care Temozolomide

Over the past decade, the standard of care for GBM patients remained unchanged, with temozolomide and radiation as the frontline therapy. Despite this,

GBM patients have almost always demonstrated recurrence with no curative outcome. To assess the efficacy of our proposed therapeutic strategies in our *STAT3*-stratified patient cohorts, we first treated the cells with either DMSO solvent, 0.5  $\mu\text{M}$  AZD1480 with/without temozolomide (TMZ) at range of 20-200  $\mu\text{M}$ . We compared to current standard of care temozolomide, we observed significant dose-dependent mitigation of GBM cell viability in the presence of AZD1480 and 50-200  $\mu\text{M}$  TMZ (Figure 21Ai). In contrast, *STAT3*-low cells demonstrated a marginal (less than 20%) decrease in viability with AZD1480 20-200  $\mu\text{M}$  TMZ. Using Chou-Talalay method for synergy quantification (Chou, 2010), we evaluated the combination index (CI) to determine synergism of AZD1480 with TMZ, where increased synergism with TMZ correlated with  $\text{CI} < 1$  (Figure 21Aii). The CI values were calculated using the CompuSyn software for evaluation of drug combinations (Chou, 2006, 2010). CI-fraction affected (Fa, indicating fraction of cell viability affected) plots of our patient-derived GBM cell lines treated with increasing doses of TMZ (20, 50, 100 and 200  $\mu\text{M}$ ) with AZD1480 0.5  $\mu\text{M}$  demonstrated that *STAT3*-high cell lines (NNI-21 and NNI-24) displayed a synergistic cytotoxic effect ( $\text{CI} < 1$ ) with larger fraction affected (Fa), while *STAT3*-low cell lines (NNI-20 and NNI-23) had smaller Fa values (lesser fraction of cell viability affected).

We previously identified *STAT3*-low stratified cohorts required a dual inhibition strategy (Figure 17). We assessed the fraction affected (reduced viability) in *STAT3*-low cell lines (NNI-20 and NNI-23) after treatment with AZD1480, Linsitinib or both (Figure 21Bi). Similarly, our CI plot showed increasing synergism with TMZ (increasingly negative ratio) for dual treatments (Figure 21Bii). Collectively, our *in vitro* data provides strong evidence for both *STAT3* inhibition and dual *STAT3*/IGF-1R inhibition in *STAT3*-high and -low cells respectively; and synergize with TMZ, thus suggesting the advancement of both therapeutic approaches in a clinical setting.



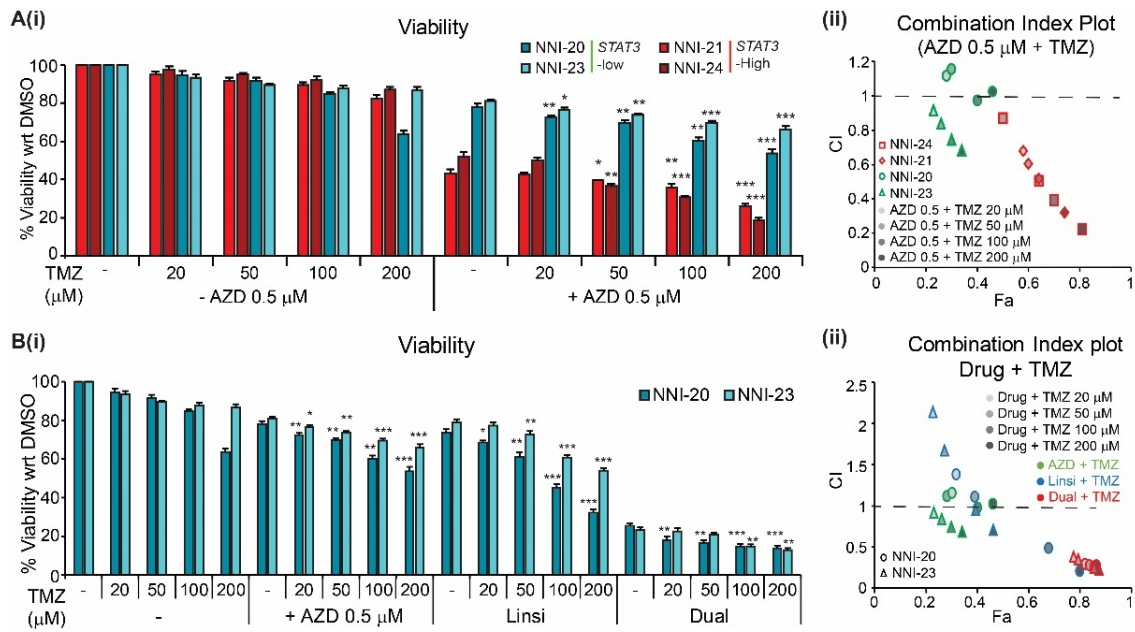


**Figure 21. Chemosensitisation of patient-derived GPCs with standard of care temozolomide treatment.** (A) Patient cell lines were treated to increasing doses of temozolomide (TMZ). (i) The addition of STAT3 inhibitor AZD1480 to temozolomide treatment demonstrated greater chemosensitivity effect observed with the greater reduction in viability. Consistent with bioinformatics prediction, *STAT3*-high cell lines (NNI-21 and NNI-24) displayed greater chemosensitivity to AZD1480 treatment with TMZ as compared to *STAT3*-low cell lines (NNI-20 and NNI-23). Results are mean of triplicate experiments. \*,  $p$ -value<0.05; \*\*,  $p$ -value<0.01; \*\*\*,  $p$ -value<0.001 compared to absence of TMZ. (ii) Combination Index (CI)-fraction affected (Fa, indicating fraction of cell viability affected) plots of GBM cell lines treated with increasing doses of TMZ with 0.5 μM AZD1480. *STAT3*-high cell lines (NNI-21 and NNI-24) displayed a synergistic, cytotoxic effect (CI<1) with larger fraction affected (Fa), while *STAT3*-low cell lines (NNI-20 and NNI-23) showed marginally reduced Fa values. (B) Chemosensitisation for *STAT3*-low cell lines (NNI-20 and NNI-23) was observed for combination treatments of Temozolomide as demonstrated in the (i) viability plots and (ii) Combination Index plots with dual treatment (AZD1480 and Linsitinib). In the CI plots, dashed line at CI=1 indicates an additive effect between two compounds, values above and below indicate antagonism or synergism respectively.

To provide further support of our *in vitro* data above, we focused on demonstrating that STAT3 inhibitors can selectively target *STAT3*-high

glioblastoma tumours. The premise of our approach lies in TCGA studies elucidating that gene expression drives GBM disease progression and prognostic outcome. We therefore tapped into a recent article where drug and disease signature integration identifies synergistic combinations in GBM (Stathias *et al.*, 2018). This study utilized the Library of Integrated Network-Based Cellular Signatures (LINCS) database where several commercial cancer cell lines were treated with FDA-approved and experimental small molecule drugs, and the transcriptomic profile of each treated cell line was acquired (Keenan *et al.*, 2018). The LINCS perturbagen-response transcriptional profiles are generated using the L1000 assay, which is a high-throughput bead-based assay that measures the expression of 978 representative landmark transcripts (Subramanian *et al.*, 2017). The authors similarly treated primary GBM cells with these drugs including TMZ with radiation, and further mapped the association of transcriptomic patterns to prognostic information in TCGA. They thus identified clinically relevant drug combinations capable of reversing the disease transcriptomic profile. In our scenario, we defined the disease pattern by our *STAT3* functionally-tuned gene signature. Using an orthogonal plot, we identified drugs that demonstrated low concordance with TMZ, and high discordance with the *STAT3*-high tumour phenotype (Figure 22). Interestingly, Ruxolitinib, a Jak2 inhibitor, and AZD1480 emerged as the top ranked drugs (Table 4). Ruxolitinib is currently in clinical trial for GBM. These drugs thus have the potential to reverse the *STAT3*-high disease profile, and supports their use in targeting PMT that typifies highly aggressive and recurrent tumours.

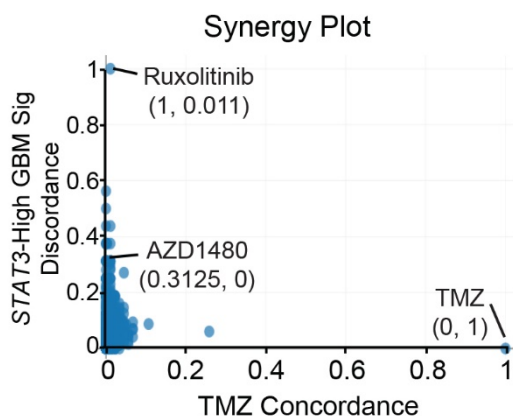


**Figure 22. Ranking of LINC compounds based on their concordance to temozolomide consensus signature.** Compounds with a high x-axis have a signature concordant to temozolomide, and compounds with a high y-axis value have a signature discordant to the *STAT3*-high GBM disease signature. *STAT3* inhibitors Ruxolitinib and AZD1480 demonstrated low concordance to temozolomide (0.011 and 0 respectively) and a high discordance to the *STAT3*-high GBM disease signature (1 and 0.3125 respectively).

**Table 4. List of top synergistic compounds able to reverse *STAT3*-high GBM disease signature (temozolomide as reference compound).**

Drug	LINC ID	<i>STAT3</i> -high GBM Sig Discordance	TMZ Orthogonality
Ruxolitinib	LSM-1139	1	0.011236
LCQ-908	LSM-45255	0.5626	0
Procaine	LSM-5396	0.5	0
Chlorthalidone	LSM-1417	0.4375	0.011236
Nilotinib	LSM-1099	0.4375	0
Alectinib	LSM-1202	0.375	0
BRD-K68548958	LSM-43281	0.375	0.003745
Indapamide	LSM-1936	0.375	0.011236
Taltirelin	LSM-45418	0.375	0
Timolol	LSM-15524	0.375	0
Anamorelin	LSM-45737	0.3125	0
AZD1480	LSM-1140 LSM-45764	0.3125	0

## 4.0 DISCUSSION

The utility of STAT3 inhibitors has largely been confined to myeloproliferative disorders, in part due to their poor blood-brain barrier (BBB) penetration. In polycythemia vera, the STAT3 pathway correlates with poorer prognosis and is constitutively active due to the presence of the *JAK2* V617F mutation (Jamieson *et al.*, 2006). However, no such mutation exists in GBM tumours, although STAT3 has been implicated in the proliferation and self-renewal of GBM stem-like cells. We have also observed that increased *STAT3*-wild-type expression correlates with poor prognostic outcome. This suggests that other mechanisms of STAT3 pathway activation remains, and current STAT3 inhibitor molecules with efficient BBB penetration capability in clinical trials may find utility in GBM treatment. To add to the complexity of solid tumours such as GBM, various studies have suggested the presence of molecular heterogeneity (Verhaak *et al.*, 2010). This may account for the frequently observed inter-patient variability to treatment response. Indeed, the mesenchymal profile has been associated with the poorest prognosis, while the proneural subtype typifies the more chemosensitive and treatable cohort (Wang *et al.*, 2018). Currently, routine pathological diagnosis uses morphological features to define the grades of tumour tissue. We now know that such histological approaches are woefully inadequate to influence treatment decisions. Precision oncology applies these concepts of molecular markers and stratification to determine targeted therapeutic strategies. This in turn reduces the chemotherapeutic side effects and financial costs.

### 4.1. *STAT3* Functionally-tuned Gene Signature as a Prognostic Indicator

STAT3 plays an established role in GBM tumourigenesis and tumour suppression, portraying it to be a practical candidate for prognostic indication. In patients with various malignancies including glioblastoma, pSTAT3 has been demonstrated to be a negative prognostic marker (Ferguson *et al.*, 2015). In a study conducted by Lin *et al.*, they showed that patients with high pSTAT3 tumours had shorter median survival, and activation at both tyrosine 705 (tyr705) or serine 727 (ser727) promotes tumourigenesis (Lin *et al.*, 2014a; Lin *et al.*, 2014b). Additionally, Tu *et al.* studied JAK/STAT3 signalling in GBM patient samples and observed a diminished prognosis in GBM patients expressing components of this

signalling axis (Tu *et al.*, 2011). Although these studies suggest the utility of pSTAT3 as a prognostic marker, our work reveals the limitation of sole focus on pSTAT3 since it does not entirely correlate with TCGA's molecular subtypes and subsequent clinical outcome.

We hypothesized that most signalling pathways, such as the IL-6/STAT3 axis, could be represented by a set of genes defining key regulatory modules. TCGA efforts have provided a firm basis to how gene expression data drives brain tumour disease progression and clinical outcome. In addition, such efforts identified key signalling modules represented by the receptor tyrosine kinase (RTK), p53 and Retinoblastoma master regulators. The premise of our hypothesis rests on being able to map these modules in clinical databases comprising molecular information and indicators used by the physician, using a ranked, non-parametric approach (Lamb, 2007; Lamb *et al.*, 2006). Such a strategy facilitates the quantitative analysis of multi-dimensional data represented as molecular information, magnetic resonance imaging (MRI) scans, and clinical indicators used to assess the patient's disease and functional status. We previously successfully demonstrated the utility of such a strategy in determining tumour cell resistance and invasiveness.

#### **4.2. Understanding Mechanisms underlying *STAT3*-stratified Patients**

In this study, we identified *STAT3*-high to describe a cohort of patients who had poorer prognosis. This subgroup comprised of genes previously implicated in ATP-binding cassette (ABC) drug transporters, RTK signalling and tumour cell invasiveness. Our method to winnow down the gene list associated with *STAT3* combined functional validation with co-expressed genes in clinical databases. This reduced our scope to only clinically relevant genes with phenotypic changes in *STAT3*-perturbed primary GBM cells and PDX mice models. Our *STAT3* functionally-tuned gene signature is not confounded by current clinical and molecular classification, thereby emphasizing the molecular heterogeneity contributed by this mechanistic pathway. While we showed significant survival benefit after treating *STAT3*-high mouse tumours, we also identified the top-ranking causative mechanism responsible for conferring increased resistance after STAT3 inhibition therapy in *STAT3*-low patients, and validated its biochemical activity using a kinome screen. GBM tumour cell resistance to targeted therapy is often

attributed to the compensatory activation of RTKs (Chakravarti *et al.*, 2002; Ma *et al.*, 2016a; Stommel *et al.*, 2007). Studies have described the frequent activation of insulin receptor (InsR) and IGF-1R in glioblastoma specimens and PDX cells at conferring resistance to EGFR inhibitors (Gong *et al.*, 2016; Ma *et al.*, 2016b; Stommel *et al.*, 2007); both frequently activated in GBM but rarely amplified or mutated in glioblastoma according to TCGA (<2%) (Cerami *et al.*, 2012). IGFBP2 is the second most abundant IGF binding protein (after IGFBP3), and functions as a carrier for IGF-1 and likely promotes tumour progression through IGF-1R pathway (Holmes *et al.*, 2012). In gliomas, IGFBP2 is also often overexpressed (Dunlap *et al.*, 2007); moreover, increased expression of IGFBP2 has been implicated in reduced survival and resistance to chemotherapy (Colman *et al.*, 2010). Therefore, our data supports that the InsR/IGF-1R pathway may possibly be activated through an autocrine mechanism in a subgroup of glioblastoma tumours. Previous studies have shown that IGF-1 and its receptor are able to induce STAT3 activation. A novel pipeline for analysis of the kinome screen data was implemented in this study, which involved assigning a “biological threshold” to the otherwise voluminous and numerical values typical of such screens. The successful application of this method was subsequently confirmed *in vitro* and in mouse models treated with Linsitinib, a drug targeting IGF-1R. We thus propose a model where STAT3 activation results in binding to nuclear IGFBP2, with resultant secretion of IGF-1 cytokine that contributes in a novel feed-forward loop leading to IGF-1R activation. We envisage that this autocrine mechanism can contribute in part to STAT3 activation, since both AZD1480 and Linsitinib dual targeting conferred a significant mitigation of tumour cell growth and proliferation.

### 4.3. Tumour Recurrence

Tumour recurrence is a major obstacle in the therapeutic management of GBM patients. Often recurrent GBM tumours undergo significant genomic changes, largely through clonal selection of mutations. Recent literature published by Ozawa *et al* emphasized the role of STAT3 in proneural to mesenchymal molecular subtype transition (Ozawa *et al.*, 2014). In the evaluation of the suitability of STAT3 inhibition therapy in GBM patients, we considered the likely scenario of tumour recurrence, typical of the disease’s highly aggressive and infiltrative nature. Using

the recurrent tumour databases from Samsung Medical Centre and Genentech, we evaluated the distribution of matched recurrent patients with subtype switching (Kim *et al.*, 2015; Phillips *et al.*, 2006). Consistent with our earlier data, the responsive cohort predominantly remained as *STAT3*-high mesenchymal tumours upon recurrence. Our analysis included profiling tumours at first diagnosis and at recurrence, with the finding that mesenchymal *STAT3*-high tumours largely maintained their molecular profile (Table 5). In contrast, non-mesenchymal (classical, proneural) tumours underwent molecular switching upon recurrence. In particular, classical tumours at first diagnosis (64%) switched subtypes at recurrence (*STAT3*-high, 57%; *STAT3*-low, 43%).

**Table 5. Distribution of matched recurrent patients with subtype switching**

Molecular classes	1st presentation	Recurrence
Mesenchymal (N=11; 35%)	<i>STAT3</i> -High (N=7; 64%)	<i>STAT3</i> -High (N=6; 86%)
		<i>STAT3</i> -Low (N=1; 14%)
	<i>STAT3</i> -Low (N=4; 36%)	<i>STAT3</i> -High (N=4; 100%)
Classical (N=11; 35%)	<i>STAT3</i> -High (N=7; 64%)	<i>STAT3</i> -High (N=4; 57%)
		<i>STAT3</i> -Low (N=3; 43%)
	<i>STAT3</i> -Low (N=4; 36%)	<i>STAT3</i> -High (N=3; 75%)
		<i>STAT3</i> -Low (N=1; 25%)
Proneural (N=13; 30%)	<i>STAT3</i> -High (N=4; 31%)	<i>STAT3</i> -High (N=3; 75%)
		<i>STAT3</i> -Low (N=1; 25%)
	<i>STAT3</i> -Low (N=9; 69%)	<i>STAT3</i> -High (N=2; 22%)
		<i>STAT3</i> -Low (N=7; 78%)

This finding has three implications: First, it is imperative that serial molecular profiling be carried out on tumours at all stages to provide a clear decision to the use of *STAT3* inhibitory molecules. The failure to stratify patients can potentially result in an unfavourable outcome caused by increased resistance in the *STAT3*-low cohort. Second, as *STAT3* is the key switch effecting a proneural-mesenchymal transition, its early implementation when the tumour is *STAT3*-high and non-

mesenchymal could possibly mitigate its subtype switching. Lastly, our analysis strongly suggests that other mechanisms beside epidermal growth factor receptor (EGFR) activation can contribute to STAT3 signalling. Recent work by Bonni and colleagues suggested that *EGFRvIII*-GBM tumours are constitutively active for STAT3, through co-receptor binding of EGFR and Oncostatin-M (OSM) (Jahani-Asl *et al.*, 2016). They further postulated that *EGFR*-wild-type-GBM tumours require EGF and OSM cytokines, beside co-receptor binding, to maintain active STAT3 signalling. The classical subtype of GBM tumours is represented by *EGFR* gain-of-function mutations such as *EGFRvIII* (Verhaak *et al.*, 2010). Our earlier observation of subtype switching in classical tumours which were *STAT3*-high thus suggests that additional mechanisms can contribute to STAT3 activation, and that combinational therapies may be prescribed.

#### 4.4. Clinical Significance

Clinically, glial tumours with chromosomal 1p/19q co-deletion typifies patients who are amenable to conventional procarbazine, lomustine, vincristine (PCV) therapy, compared to patients lacking the co-deletion status (Cairncross *et al.*, 1998). Our results demonstrated that all *STAT3*-high patients lack the chromosomal 1p/19q co-deletion, an indication that this cohort can now potentially receive treatment benefit from STAT3 inhibition therapy. Many studies including ours, continue to describe the role of STAT3 as a constitutively active component in glioblastoma. STAT3 activation has been associated with tumour establishment due to the upregulation of stem cell traits, anti-apoptotic factors, angiogenic elements and pro-invasive components. Furthermore, STAT3 is involved in the orchestration of immune evasion and has been shown to be a useful tumour marker for prognosis (Kim *et al.*, 2014). Conversely, investigations have also demonstrated the paradox of STAT3 in facilitating tumour suppression through growth inhibitory signalling and cell differentiation (Zhang and Lai, 2014). More in-depth research is required to capitalise on STAT3's potential role as a prognostic indicator and target for molecular therapy, in light of TCGA findings which strongly support the need to stratify patient cohorts. In our study, we demonstrated the importance of such stratification methodologies prior to administration of STAT3 inhibitors. Our transcriptomic signature reveals potential responders, as well as identify mechanistic



gene candidates leading to the development of a dual targeting strategy to sensitize non-responders. This has direct relevance to ongoing clinical trials as well as drug-development initiatives. Importantly, we provided evidence that AD1480 in *STAT3*-high GBM cells, and AZD1480/Linsitinib in *STAT3*-low GBM cells synergised with TMZ to mitigate in vitro tumour cell viability. Using transcriptomic information gleaned from clinical and small molecule-treated cell databases, we further identified Ruxolitinib and AZD1480 among the top ranked small molecules capable of reversing the *STAT3*-high disease profile.

## 5.0 FUTURE DIRECTIONS

Our study is described in a pending manuscript of which I am the co-first author with fellow PhD candidate Mr Edwin Sandanaraj (G1403220A), who contributed largely to the bioinformatics component. Our current work addressed the importance of patient stratification prior to treatment decision, illustrating the principles of precision medicine in facilitating targeted therapy to improve patient survival outcome. We demonstrate that the application of the *STAT3* functionally-tuned gene signature stratification approach not only identifies potential responders, but also uncovers methods to sensitise non-responders to therapeutic intervention. We recognize from the clinical setting that our work suggests that *STAT3*-low stratified patients already display better prognosis with current standard of care treatment regimen (Figure 7A). However, in recurrent GBM, there are no standard of care treatment protocols established despite many ongoing clinical trials. Moreover, as we have provided evidence that subtype switching occurs when tumours recur, the group that presents as *STAT3*-high at first diagnosis, but recur as resistant *STAT3*-low, now lends itself amenable to the dual STAT3/IGF-1R treatment strategy to overcome drug resistance. Future work should aim to demonstrate the efficacy of the dual inhibitor treatment, compared against standard of care TMZ/radiotherapy treatment. This highlights the importance of patient stratification and the utility of targeted therapy instead of employing a “one-size-fits-all” strategy. An alternative to the dual inhibitor treatment for *STAT3*-low patients would be to identify targetable kinases that are upregulated. Kinases are well-known druggable targets, and can modify up to 30% of all human proteins. By identifying upregulated kinases in *STAT3*-low stratified patients, we can potentially reduce the combined toxic side effects from administration of dual inhibitors instead of a single agent.

Additionally, the high costs and lengthy gene expression analyses preclude the direct application of the *STAT3* functionally-tuned gene signature in the clinic to diagnose and treat patients. We will thus characterize the spectrum of somatic mutations unique to the *STAT3*-stratified patient cohort, which will then facilitate rapid identification of individuals most likely to receive treatment benefit. In addition, such somatic mutations potentially reveal driver/passenger events implicated in STAT3 regulation of brain tumours, specifically GBM.

Finally, we aim to understand how the master regulator of STAT3 orchestrate its transcriptional activity. Zhang *et al.* showed that epigenetic gene silencing could be promoted by oncogenic STAT3 by inducing DNA methyltransferase 1 (DNMT1) expression to foster epigenetic silencing of tumour suppressor genes (Zhang *et al.*, 2005; Zhang *et al.*, 2006a). In addition, efforts by Lee *et al.* demonstrated that acetylated STAT3 could facilitate STAT3-DNMT1 interaction, essential for methylation of tumour suppressor gene promoters (Lee *et al.*, 2012b). Recent efforts by the US National Institutes of Health Roadmap Epigenomics consortium demonstrated clear evidence for various histone marks implicated in normal cell biology (Roadmap Epigenomics *et al.*, 2015). Accompanying this study, various groups have since shown alterations of such histone marks in several cancers including GBM (Polak *et al.*, 2015). It is thus conceivable that the identification of histone marks associated with *STAT3*-stratified patient tumours, distinct from normal cells and tissue, will open up new avenues for epigenetic drug targeting, many of which are in current pharmaceutical small molecule pipelines. Moving forward, we will engage in chromatin immunoprecipitation with sequencing (ChIP-seq) experiments to profile *STAT3*-stratified tumours for various histone marks such as the promoters (H3K4me3), enhancers (H3K4me1), regulatory regions (H3K27ac) and repressive mark (H3K27me3). We have also recently demonstrated that the study of the GBM chromatin landscape identified specific super-enhancer driven genes and novel bromodomain inhibitors targeting the invasive phenotype of brain tumours (Xu *et al.*, 2018).

## 6.0 CONCLUSION

Glioblastoma is the most lethal form of primary malignant brain tumour, frequently associated with resistance to standard therapy, in part due to invasion of tumour cells into healthy brain tissue parenchyma. Studies have reported that activated STAT3 plays a key molecular event in mesenchymal transformation of primary GBM (Carro *et al.*, 2010). The function of STAT3 in GBM subtypes remains to be explored; and warrants subsequent development of patient stratification methodologies (Gray *et al.*, 2014; Jackson *et al.*, 2012; Yue and Turkson, 2009). Our study provides a firm basis for the use of STAT3 inhibition therapy in GBM tumours, and highlights the importance of molecular subtyping prior to treatment decision. We show that the STAT3 pathway contributes to the molecular heterogeneity of GBM tumours, in a manner that cannot be accounted for by current clinical indicators. In view of the prominent role of STAT3 signalling in the worst prognosis mesenchymal subtype, patients with activated STAT3 could prospectively gain from a STAT3-targeted therapy. We recommend that serial molecular subtyping be carried out on tumours at all stages (i.e. first diagnosis and recurrence) to facilitate therapeutic decisions. However, in the other spectrum of patients with low STAT3 activation, targeting a single signalling pathway may not be beneficial. Instead, this group of patients would potentially benefit from a dual inhibition strategy using STAT3 and IGF-1R inhibitors.

Currently, routine pathological diagnosis uses morphological features to define the grades of tumour tissue. We now know, in light of TCGA findings, that such histological approaches are inadequate to influence treatment decisions. Precision oncology applies these concepts of molecular markers and stratification to determine targeted therapeutic strategies. This in turn reduces the chemotherapeutic side effects and financial costs to non-responders. Ultimately, the use of precision medicine-based therapeutic approaches will refine each patient's needs, and consequently improve the individual's survival outcome and quality of life.

## 7.0 REFERENCES

1. Agamanolis, D.P., 2005. TUMORS OF THE CENTRAL NERVOUS SYSTEM, Neuropathology. Northeast Ohio Medical University (NEOMED), pp. An illustrated interactive course for medical students and residents.
2. Alcantara Llaguno, S., Chen, J., Kwon, C.-H., Jackson, E.L., Li, Y., Burns, D.K., Alvarez-Buylla, A., Parada, L.F., 2009. Malignant Astrocytomas Originate from Neural Stem/Progenitor Cells in a Somatic Tumor Suppressor Mouse Model. *Cancer cell* 15, 45-56.
3. Allan, J.M., Travis, L.B., 2005. Mechanisms of therapy-related carcinogenesis. *Nature Reviews Cancer* 5, 943-955.
4. Alvarez, J.V., Mukherjee, N., Chakravarti, A., Robe, P., Zhai, G., Chakladar, A., Loeffler, J., Black, P., Frank, D.A., 2007. A STAT3 Gene Expression Signature in Gliomas is Associated with a Poor Prognosis. *Transl Oncogenomics* 2, 99-105.
5. Anido, J., Saez-Borderias, A., Gonzalez-Junca, A., Rodon, L., Folch, G., Carmona, M.A., Prieto-Sanchez, R.M., Barba, I., Martinez-Saez, E., Prudkin, L., Cuartas, I., Raventos, C., Martinez-Ricarte, F., Poca, M.A., Garcia-Dorado, D., Lahn, M.M., Yingling, J.M., Rodon, J., Sahuquillo, J., Baselga, J., Seoane, J., 2010. TGF-beta Receptor Inhibitors Target the CD44(high)/Id1(high) Glioma-Initiating Cell Population in Human Glioblastoma. *Cancer cell* 18, 655-668.
6. Asgari, K., Sesterhenn, I.A., McLeod, D.G., Cowan, K., Moul, J.W., Seth, P., Srivastava, S., 1997. Inhibition of the growth of pre-established subcutaneous tumor nodules of human prostate cancer cells by single injection of the recombinant adenovirus p53 expression vector. *Int J Cancer* 71, 377-382.
7. Atlas, T.C.G., 2008. Comprehensive genomic characterization defines human glioblastoma genes and core pathways. *Nature* 455, 1061-1068.
8. Azar, W.J., Azar, S.H., Higgins, S., Hu, J.F., Hoffman, A.R., Newgreen, D.F., Werther, G.A., Russo, V.C., 2011. IGFBP-2 enhances VEGF gene promoter activity and consequent promotion of angiogenesis by neuroblastoma cells. *Endocrinology* 152, 3332-3342.
9. Bachoo, R.M., Maher, E.A., Ligon, K.L., Sharpless, N.E., Chan, S.S., You, M.J., Tang, Y., DeFrances, J., Stover, E., Weissleder, R., Rowitch, D.H., Louis, D.N., DePinho, R.A., 2002. Epidermal growth factor receptor and Ink4a/Arf: convergent mechanisms governing terminal differentiation and transformation along the neural stem cell to astrocyte axis. *Cancer cell* 1, 269-277.
10. Bajenaru, M.L., Hernandez, M.R., Perry, A., Zhu, Y., Parada, L.F., Garbow, J.R., Gutmann, D.H., 2003. Optic nerve glioma in mice requires astrocyte Nfl gene inactivation and Nfl brain heterozygosity. *Cancer research* 63, 8573-8577.
11. Bao, S., Wu, Q., McLendon, R.E., Hao, Y., Shi, Q., Hjelmeland, A.B., Dewhirst, M.W., Bigner, D.D., Rich, J.N., 2006a. Glioma stem cells promote

- radioresistance by preferential activation of the DNA damage response. *Nature* 444, 756-760.
12. Bao, S., Wu, Q., Sathornsumetee, S., Hao, Y., Li, Z., Hjelmeland, A.B., Shi, Q., McLendon, R.E., Bigner, D.D., Rich, J.N., 2006b. Stem Cell-like Glioma Cells Promote Tumor Angiogenesis through Vascular Endothelial Growth Factor. *Cancer Research* 66, 7843.
  13. Bar, E.E., Chaudhry, A., Lin, A., Fan, X., Schreck, K., Matsui, W., Piccirillo, S., Vescovi, A.L., DiMeco, F., Olivi, A., Eberhart, C.G., 2007. Cyclopamine-mediated hedgehog pathway inhibition depletes stem-like cancer cells in glioblastoma. *Stem Cells* 25, 2524-2533.
  14. Barbie, D.A., Tamayo, P., Boehm, J.S., Kim, S.Y., Moody, S.E., Dunn, I.F., Schinzel, A.C., Sandy, P., Meylan, E., Scholl, C., Frohling, S., Chan, E.M., Sos, M.L., Michel, K., Mermel, C., Silver, S.J., Weir, B.A., Reiling, J.H., Sheng, Q., Gupta, P.B., Wadlow, R.C., Le, H., Hoersch, S., Wittner, B.S., Ramaswamy, S., Livingston, D.M., Sabatini, D.M., Meyerson, M., Thomas, R.K., Lander, E.S., Mesirov, J.P., Root, D.E., Gilliland, D.G., Jacks, T., Hahn, W.C., 2009. Systematic RNA interference reveals that oncogenic KRAS-driven cancers require TBK1. *Nature* 462, 108-112.
  15. Becker, S., Groner, B., Müller, C.W., 1998. Three-dimensional structure of the Stat3 $\beta$  homodimer bound to DNA. *Nature* 394, 145-151.
  16. Behnan, J., Stangeland, B., Hosainey, S.A., Joel, M., Olsen, T.K., Micci, F., Glover, J.C., Isakson, P., Brinchmann, J.E., 2017. Differential propagation of stroma and cancer stem cells dictates tumorigenesis and multipotency. *Oncogene* 36, 570-584.
  17. Berishaj, M., Gao, S.P., Ahmed, S., Leslie, K., Al-Ahmadie, H., Gerald, W.L., Bornmann, W., Bromberg, J.F., 2007. Stat3 is tyrosine-phosphorylated through the interleukin-6/glycoprotein 130/Janus kinase pathway in breast cancer. *Breast Cancer Res* 9, R32.
  18. Bonni, A., Sun, Y., Nadal-Vicens, M., Bhatt, A., Frank, D.A., Rozovsky, I., Stahl, N., Yancopoulos, G.D., Greenberg, M.E., 1997. Regulation of gliogenesis in the central nervous system by the JAK-STAT signaling pathway. *Science* 278, 477-483.
  19. Bowman, T., Garcia, R., Turkson, J., Jove, R., 2000. STATs in oncogenesis. *Oncogene* 19, 2474-2488.
  20. Brennan, C., Momota, H., Hambardzumyan, D., Ozawa, T., Tandon, A., Pedraza, A., Holland, E., 2009. Glioblastoma subclasses can be defined by activity among signal transduction pathways and associated genomic alterations. *PLoS One* 4, e7752.
  21. Bromberg, J., Darnell, J.E., Jr., 2000. The role of STATs in transcriptional control and their impact on cellular function. *Oncogene* 19, 2468-2473.
  22. Bromberg, J.F., Wrzeszczynska, M.H., Devgan, G., Zhao, Y., Pestell, R.G., Albanese, C., Darnell, J.E., Jr., 1999. Stat3 as an oncogene. *Cell* 98, 295-303.
  23. Buck, E., Gokhale, P.C., Koujak, S., Brown, E., Eyzaguirre, A., Tao, N., Rosenfeld-Franklin, M., Lerner, L., Chiu, M.I., Wild, R., Epstein, D., Pachter, J.A., Miglarese, M.R., 2010. Compensatory insulin receptor (IR) activation

- on inhibition of insulin-like growth factor-1 receptor (IGF-1R): rationale for cotargeting IGF-1R and IR in cancer. *Mol Cancer Ther* 9, 2652-2664.
24. Buettner, R., Mora, L.B., Jove, R., 2002. Activated STAT signaling in human tumors provides novel molecular targets for therapeutic intervention. *Clinical cancer research : an official journal of the American Association for Cancer Research* 8, 945-954.
  25. Cahill, D.P., Levine, K.K., Betensky, R.A., Codd, P.J., Romany, C.A., Reavie, L.B., Batchelor, T.T., Futreal, P.A., Stratton, M.R., Curry, W.T., Iafrate, A.J., Louis, D.N., 2007. Loss of the mismatch repair protein MSH6 in human glioblastomas is associated with tumor progression during temozolomide treatment. *Clinical cancer research : an official journal of the American Association for Cancer Research* 13, 2038-2045.
  26. Cairncross, J.G., Ueki, K., Zlatescu, M.C., Lisle, D.K., Finkelstein, D.M., Hammond, R.R., Silver, J.S., Stark, P.C., Macdonald, D.R., Ino, Y., Ramsay, D.A., Louis, D.N., 1998. Specific genetic predictors of chemotherapeutic response and survival in patients with anaplastic oligodendrogliomas. *J Natl Cancer Inst* 90, 1473-1479.
  27. Carro, M.S., Lim, W.K., Alvarez, M.J., Bollo, R.J., Zhao, X., Snyder, E.Y., Sulman, E.P., Anne, S.L., Doetsch, F., Colman, H., Lasorella, A., Aldape, K., Califano, A., Iavarone, A., 2010. The transcriptional network for mesenchymal transformation of brain tumours. *Nature* 463, 318-325.
  28. Ceccarelli, M., Barthel, F.P., Malta, T.M., Sabedot, T.S., Salama, S.R., Murray, B.A., Morozova, O., Newton, Y., Radenbaugh, A., Pagnotta, S.M., Anjum, S., Wang, J., Manyam, G., Zoppoli, P., Ling, S., Rao, A.A., Grifford, M., Cherniack, A.D., Zhang, H., Poisson, L., Carlotti, C.G., Jr., Tirapelli, D.P., Rao, A., Mikkelsen, T., Lau, C.C., Yung, W.K., Rabadan, R., Huse, J., Brat, D.J., Lehman, N.L., Barnholtz-Sloan, J.S., Zheng, S., Hess, K., Rao, G., Meyerson, M., Beroukhi, R., Cooper, L., Akbani, R., Wrensch, M., Haussler, D., Aldape, K.D., Laird, P.W., Gutmann, D.H., Network, T.R., Nounshahr, H., Iavarone, A., Verhaak, R.G., 2016. Molecular Profiling Reveals Biologically Discrete Subsets and Pathways of Progression in Diffuse Glioma. *Cell* 164, 550-563.
  29. Cerami, E., Gao, J., Dogrusoz, U., Gross, B.E., Sumer, S.O., Aksoy, B.A., Jacobsen, A., Byrne, C.J., Heuer, M.L., Larsson, E., Antipin, Y., Reva, B., Goldberg, A.P., Sander, C., Schultz, N., 2012. The cBio cancer genomics portal: an open platform for exploring multidimensional cancer genomics data. *Cancer Discov* 2, 401-404.
  30. Chakrabarty, S., Kondratick, L., 2006. Insulin-like growth factor binding protein-2 stimulates proliferation and activates multiple cascades of the mitogen-activated protein kinase pathways in NIH-OVCAR3 human epithelial ovarian cancer cells. *Cancer Biol Ther* 5, 189-197.
  31. Chakravarti, A., Loeffler, J.S., Dyson, N.J., 2002. Insulin-like growth factor receptor I mediates resistance to anti-epidermal growth factor receptor therapy in primary human glioblastoma cells through continued activation of phosphoinositide 3-kinase signaling. *Cancer Res* 62, 200-207.

32. Chatterjee, S., Park, E.S., Soloff, M.S., 2004. Proliferation of DU145 prostate cancer cells is inhibited by suppressing insulin-like growth factor binding protein-2. *Int J Urol* 11, 876-884.
33. Chen, F., Xu, Y., Luo, Y., Zheng, D., Song, Y., Yu, K., Li, H., Zhang, L., Zhong, W., Ji, Y., 2010. Down-regulation of Stat3 decreases invasion activity and induces apoptosis of human glioma cells. *J Mol Neurosci* 40, 353-359.
34. Chen, H.X., Sharon, E., 2013. IGF-1R as an anti-cancer target--trials and tribulations. *Chinese journal of cancer* 32, 242-252.
35. Chen, Y., Wang, J., Wang, X., Liu, X., Li, H., Lv, Q., Zhu, J., Wei, B., Tang, Y., 2013. STAT3, a Poor Survival Predictor, Is Associated with Lymph Node Metastasis from Breast Cancer. *J Breast Cancer* 16, 40-49.
36. Chong, Y.K., Toh, T.B., Zaiden, N., Poonepalli, A., Leong, S.H., Ong, C.E., Yu, Y., Tan, P.B., See, S.J., Ng, W.H., Ng, I., Hande, M.P., Kon, O.L., Ang, B.T., Tang, C., 2009. Cryopreservation of neurospheres derived from human glioblastoma multiforme. *Stem Cells* 27, 29-39.
37. Chong, Y.K., Sandanaraj, E., Koh, L.W., Thangaveloo, M., Tan, M.S., Koh, G.R., Toh, T.B., Lim, G.G., Holbrook, J.D., Kon, O.L., Nadarajah, M., Ng, I., Ng, W.H., Tan, N.S., Lim, K.L., Tang, C., Ang, B.T., 2016. ST3GAL1-Associated Transcriptomic Program in Glioblastoma Tumor Growth, Invasion, and Prognosis. *J Natl Cancer Inst* 108.
38. Chou, T.-C., 2006. Theoretical Basis, Experimental Design, and Computerized Simulation of Synergism and Antagonism in Drug Combination Studies. *Pharmacological Reviews* 58, 621.
39. Chou, T.-C., 2010. Drug Combination Studies and Their Synergy Quantification Using the Chou-Talalay Method. *Cancer Research* 70, 440.
40. Coffey, P.J., van Puijenbroek, A., Burgering, B.M., Klop-de Jonge, M., Koenderman, L., Bos, J.L., Kruijer, W., 1997. Insulin activates Stat3 independently of p21ras-ERK and PI-3K signal transduction. *Oncogene* 15, 2529-2539.
41. Colman, H., Zhang, L., Sulman, E.P., McDonald, J.M., Shooshtari, N.L., Rivera, A., Popoff, S., Nutt, C.L., Louis, D.N., Cairncross, J.G., Gilbert, M.R., Phillips, H.S., Mehta, M.P., Chakravarti, A., Pelloski, C.E., Bhat, K., Feuerstein, B.G., Jenkins, R.B., Aldape, K., 2010. A multigene predictor of outcome in glioblastoma. *Neuro Oncol* 12, 49-57.
42. Daniel, P., Sabri, S., Chaddad, A., Meehan, B., Jean-Claude, B., Rak, J., Abdulkarim, B.S., 2019. Temozolomide Induced Hypermutation in Glioma: Evolutionary Mechanisms and Therapeutic Opportunities. *Frontiers in oncology* 9, 41-41.
43. Darnell, J.E., Jr., Kerr, I.M., Stark, G.R., 1994. Jak-STAT pathways and transcriptional activation in response to IFNs and other extracellular signaling proteins. *Science* 264, 1415-1421.
44. de Groot, J., Liang, J., Kong, L.-Y., Wei, J., Piao, Y., Fuller, G., Qiao, W., Heimberger, A.B., 2012. Modulating antiangiogenic resistance by inhibiting the signal transducer and activator of transcription 3 pathway in glioblastoma. *Oncotarget* 3, 1036-1048.



45. de Groot, J.F., Fuller, G., Kumar, A.J., Piao, Y., Eterovic, K., Ji, Y., Conrad, C.A., 2010. Tumor invasion after treatment of glioblastoma with bevacizumab: radiographic and pathologic correlation in humans and mice. *Neuro-oncology* 12, 233-242.
46. de la Iglesia, N., Konopka, G., Lim, K.L., Nutt, C.L., Bromberg, J.F., Frank, D.A., Mischel, P.S., Louis, D.N., Bonni, A., 2008. Deregulation of a STAT3-interleukin 8 signaling pathway promotes human glioblastoma cell proliferation and invasiveness. *J Neurosci* 28, 5870-5878.
47. Derenzini, E., Lemoine, M., Buglio, D., Katayama, H., Ji, Y., Davis, R.E., Sen, S., Younes, A., 2011. The JAK inhibitor AZD1480 regulates proliferation and immunity in Hodgkin lymphoma. *Blood cancer journal* 1, e46-e46.
48. Dolan, M.E., Moschel, R.C., Pegg, A.E., 1990. Depletion of mammalian O6-alkylguanine-DNA alkyltransferase activity by O6-benzylguanine provides a means to evaluate the role of this protein in protection against carcinogenic and therapeutic alkylating agents. *Proc Natl Acad Sci U S A* 87, 5368-5372.
49. Dunlap, S.M., Celestino, J., Wang, H., Jiang, R., Holland, E.C., Fuller, G.N., Zhang, W., 2007. Insulin-like growth factor binding protein 2 promotes glioma development and progression. *Proc Natl Acad Sci U S A* 104, 11736-11741.
50. Eide, P.W., Bruun, J., Lothe, R.A., Sveen, A., 2017. CMScaller: an R package for consensus molecular subtyping of colorectal cancer pre-clinical models. *Sci Rep* 7, 16618.
51. Eyler, C.E., Foo, W.C., LaFiura, K.M., McLendon, R.E., Hjelmeland, A.B., Rich, J.N., 2008. Brain cancer stem cells display preferential sensitivity to Akt inhibition. *Stem Cells* 26, 3027-3036.
52. Ferguson, S.D., Srinivasan, V.M., Heimberger, A.B., 2015. The role of STAT3 in tumor-mediated immune suppression. *J Neurooncol* 123, 385-394.
53. Foong, C.S., Sandanaraj, E., Brooks, H.B., Campbell, R.M., Ang, B.T., Chong, Y.K., Tang, C., 2012. Glioma-propagating cells as an in vitro screening platform: PLK1 as a case study. *J Biomol Screen* 17, 1136-1150.
54. Foong, C.S., Ng, F.S., Phong, M., Toh, T.B., Chong, Y.K., Tucker-Kellogg, G., Campbell, R.M., Ang, B.T., Tang, C., 2011. Cryopreservation of cancer-initiating cells derived from glioblastoma. *Frontiers in bioscience* 3, 698-708.
55. Friedman, H.S., Kokkinakis, D.M., Pluda, J., Friedman, A.H., Cokgor, I., Haglund, M.M., Ashley, D.M., Rich, J., Dolan, M.E., Pegg, A.E., Moschel, R.C., McLendon, R.E., Kerby, T., Herndon, J.E., Bigner, D.D., Schold, S.C., Jr., 1998a. Phase I trial of O6-benzylguanine for patients undergoing surgery for malignant glioma. *J Clin Oncol* 16, 3570-3575.
56. Friedman, H.S., McLendon, R.E., Kerby, T., Dugan, M., Bigner, S.H., Henry, A.J., Ashley, D.M., Krischer, J., Lovell, S., Rasheed, K., Marchev, F., Seman, A.J., Cokgor, I., Rich, J., Stewart, E., Colvin, O.M., Provenzale, J.M., Bigner, D.D., Haglund, M.M., Friedman, A.H., Modrich, P.L., 1998b. DNA mismatch repair and O6-alkylguanine-DNA alkyltransferase analysis and

- response to Temodal in newly diagnosed malignant glioma. *J Clin Oncol* 16, 3851-3857.
57. Fukushima, T., Tezuka, T., Shimomura, T., Nakano, S., Kataoka, H., 2007. Silencing of insulin-like growth factor-binding protein-2 in human glioblastoma cells reduces both invasiveness and expression of progression-associated gene CD24. *J Biol Chem* 282, 18634-18644.
  58. Furqan, M., Akinleye, A., Mukhi, N., Mittal, V., Chen, Y., Liu, D., 2013. STAT inhibitors for cancer therapy. *Journal of hematology & oncology* 6, 90-90.
  59. Furstenberger, G., Senn, H.J., 2002. Insulin-like growth factors and cancer. *Lancet Oncol* 3, 298-302.
  60. Gabrilovich, D.I., Chen, H.L., Girgis, K.R., Cunningham, H.T., Meny, G.M., Nadaf, S., Kavanaugh, D., Carbone, D.P., 1996. Production of vascular endothelial growth factor by human tumors inhibits the functional maturation of dendritic cells. *Nat Med* 2, 1096-1103.
  61. Galli, R., Binda, E., Orfanelli, U., Cipelletti, B., Gritti, A., De Vitis, S., Fiocco, R., Foroni, C., Dimeco, F., Vescovi, A., 2004. Isolation and characterization of tumorigenic, stem-like neural precursors from human glioblastoma. *Cancer Res* 64, 7011-7021.
  62. Gangemi, R.M., Griffero, F., Marubbi, D., Perera, M., Capra, M.C., Malatesta, P., Ravetti, G.L., Zona, G.L., Daga, A., Corte, G., 2009. SOX2 silencing in glioblastoma tumor-initiating cells causes stop of proliferation and loss of tumorigenicity. *Stem Cells* 27, 40-48.
  63. Gao, S.P., Mark, K.G., Leslie, K., Pao, W., Motoi, N., Gerald, W.L., Travis, W.D., Bornmann, W., Veach, D., Clarkson, B., Bromberg, J.F., 2007. Mutations in the EGFR kinase domain mediate STAT3 activation via IL-6 production in human lung adenocarcinomas. *J Clin Invest* 117, 3846-3856.
  64. Gautier, L., Cope, L., Bolstad, B.M., Irizarry, R.A., 2004. affy--analysis of Affymetrix GeneChip data at the probe level. *Bioinformatics* 20, 307-315.
  65. Geron, I., Abrahamsson, A.E., Barroga, C.F., Kavalerchik, E., Gotlib, J., Hood, J.D., Durocher, J., Mak, C.C., Noronha, G., Soll, R.M., Tefferi, A., Kaushansky, K., Jamieson, C.H., 2008. Selective inhibition of JAK2-driven erythroid differentiation of polycythemia vera progenitors. *Cancer cell* 13, 321-330.
  66. Gomez-Manzano, C., Fueyo, J., Kyritsis, A.P., McDonnell, T.J., Steck, P.A., Levin, V.A., Yung, W.K., 1997. Characterization of p53 and p21 functional interactions in glioma cells en route to apoptosis. *J Natl Cancer Inst* 89, 1036-1044.
  67. Gong, Y., Ma, Y., Sinyuk, M., Loganathan, S., Thompson, R.C., Sarkaria, J.N., Chen, W., Lathia, J.D., Mobley, B.C., Clark, S.W., Wang, J., 2016. Insulin-mediated signaling promotes proliferation and survival of glioblastoma through Akt activation. *Neuro Oncol* 18, 48-57.
  68. Gravendeel, L.A., Kouwenhoven, M.C., Gevaert, O., de Rooij, J.J., Stubbs, A.P., Duijm, J.E., Daemen, A., Bleeker, F.E., Bralten, L.B., Kloosterhof, N.K., De Moor, B., Eilers, P.H., van der Spek, P.J., Kros, J.M., Sillevius Smitt,

- P.A., van den Bent, M.J., French, P.J., 2009. Intrinsic gene expression profiles of gliomas are a better predictor of survival than histology. *Cancer Res* 69, 9065-9072.
69. Gray, G.K., McFarland, B.C., Nozell, S.E., Benveniste, E.N., 2014. NF-kappaB and STAT3 in glioblastoma: therapeutic targets coming of age. *Expert Rev Neurother* 14, 1293-1306.
70. Gritti, A., Parati, E.A., Cova, L., Frolichsthal, P., Galli, R., Wanke, E., Faravelli, L., Morassutti, D.J., Roisen, F., Nickel, D.D., Vescovi, A.L., 1996. Multipotential stem cells from the adult mouse brain proliferate and self-renew in response to basic fibroblast growth factor. *J Neurosci* 16, 1091-1100.
71. Guryanova, O.A., Wu, Q., Cheng, L., Lathia, J.D., Huang, Z., Yang, J., MacSwords, J., Eyler, C.E., McLendon, R.E., Heddleston, J.M., Shou, W., Hambardzumyan, D., Lee, J., Hjelmeland, A.B., Sloan, A.E., Bredel, M., Stark, G.R., Rich, J.N., Bao, S., 2011. Nonreceptor tyrosine kinase BMX maintains self-renewal and tumorigenic potential of glioblastoma stem cells by activating STAT3. *Cancer Cell* 19, 498-511.
72. Guschin, D., Rogers, N., Briscoe, J., Witthuhn, B., Watling, D., Horn, F., Pellegrini, S., Yasukawa, K., Heinrich, P., Stark, G.R., 1995. A major role for the protein tyrosine kinase JAK1 in the JAK/STAT signal transduction pathway in response to interleukin-6. *The EMBO journal* 14, 1421-1429.
73. Halliday, J., Helmy, K., Pattwell, S.S., Pitter, K.L., LaPlant, Q., Ozawa, T., Holland, E.C., 2014. In vivo radiation response of proneural glioma characterized by protective p53 transcriptional program and proneural-mesenchymal shift. *Proc Natl Acad Sci U S A* 111, 5248-5253.
74. Hatiboglu, M.A., Kong, L.Y., Wei, J., Wang, Y., McEnery, K.A., Fuller, G.N., Qiao, W., Davies, M.A., Priebe, W., Heimberger, A.B., 2012. The tumor microenvironment expression of p-STAT3 influences the efficacy of cyclophosphamide with WP1066 in murine melanoma models. *Int J Cancer* 131, 8-17.
75. Haura, E.B., Turkson, J., Jove, R., 2005. Mechanisms of disease: Insights into the emerging role of signal transducers and activators of transcription in cancer. *Nat Clin Pract Oncol* 2, 315-324.
76. Hedvat, M., Huszar, D., Herrmann, A., Gozgit, J.M., Schroeder, A., Sheehy, A., Buettner, R., Proia, D., Kowolik, C.M., Xin, H., Armstrong, B., Beberitz, G., Weng, S., Wang, L., Ye, M., McEachern, K., Chen, H., Morosini, D., Bell, K., Alimzhanov, M., Ioannidis, S., McCoon, P., Cao, Z.A., Yu, H., Jove, R., Zinda, M., 2009. The JAK2 Inhibitor, AZD1480, Potently Blocks Stat3 Signaling and Oncogenesis in Solid Tumors. *Cancer cell* 16, 487-497.
77. Herrmann, A., Kortylewski, M., Kujawski, M., Zhang, C., Reckamp, K., Armstrong, B., Wang, L., Kowolik, C., Deng, J., Figlin, R., Yu, H., 2010. Targeting Stat3 in the myeloid compartment drastically improves the in vivo antitumor functions of adoptively transferred T cells. *Cancer research* 70, 7455-7464.
78. Hodge, D.R., Hurt, E.M., Farrar, W.L., 2005. The role of IL-6 and STAT3 in inflammation and cancer. *European Journal of Cancer* 41, 2502-2512.

79. Hodgson, J.G., Yeh, R.F., Ray, A., Wang, N.J., Smirnov, I., Yu, M., Hariono, S., Silber, J., Feiler, H.S., Gray, J.W., Spellman, P.T., Vandenberg, S.R., Berger, M.S., James, C.D., 2009. Comparative analyses of gene copy number and mRNA expression in glioblastoma multiforme tumors and xenografts. *Neuro Oncol* 11, 477-487.
80. Holmes, K.M., Annala, M., Chua, C.Y., Dunlap, S.M., Liu, Y., Hugen, N., Moore, L.M., Cogdell, D., Hu, L., Nykter, M., Hess, K., Fuller, G.N., Zhang, W., 2012. Insulin-like growth factor-binding protein 2-driven glioma progression is prevented by blocking a clinically significant integrin, integrin-linked kinase, and NF-kappaB network. *Proc Natl Acad Sci U S A* 109, 3475-3480.
81. Hornbeck, P.V., Kornhauser, J.M., Tkachev, S., Zhang, B., Skrzypek, E., Murray, B., Latham, V., Sullivan, M., 2012. PhosphoSitePlus: a comprehensive resource for investigating the structure and function of experimentally determined post-translational modifications in man and mouse. *Nucleic Acids Res* 40, D261-270.
82. Horten, B.C., Basler, G.A., Shapiro, W.R., 1981. Xenograft of human malignant glial tumors into brains of nude mice. A histopathological study. *J Neuropathol Exp Neurol* 40, 493-511.
83. Hoshida, Y., 2010. Nearest template prediction: a single-sample-based flexible class prediction with confidence assessment. *PloS one* 5, e15543.
84. Hwa, V., Oh, Y., Rosenfeld, R.G., 1999. The insulin-like growth factor-binding protein (IGFBP) superfamily. *Endocr Rev* 20, 761-787.
85. Ibuki, N., Ghaffari, M., Reuveni, H., Pandey, M., Fazli, L., Azuma, H., Gleave, M.E., Levitzki, A., Cox, M.E., 2014. The tyrphostin NT157 suppresses insulin receptor substrates and augments therapeutic response of prostate cancer. *Mol Cancer Ther* 13, 2827-2839.
86. Iwamaru, A., Szymanski, S., Iwado, E., Aoki, H., Yokoyama, T., Fokt, I., Hess, K., Conrad, C., Madden, T., Sawaya, R., Kondo, S., Priebe, W., Kondo, Y., 2006. A novel inhibitor of the STAT3 pathway induces apoptosis in malignant glioma cells both in vitro and in vivo. *Oncogene* 26, 2435-2444.
87. Jackson, C., Ruzevick, J., Amin, A.G., Lim, M., 2012. Potential role for STAT3 inhibitors in glioblastoma. *Neurosurg Clin N Am* 23, 379-389.
88. Jacques, T.S., Swales, A., Brzozowski, M.J., Henriquez, N.V., Linehan, J.M., Mirzadeh, Z., C, O.M., Naumann, H., Alvarez-Buylla, A., Brandner, S., 2010. Combinations of genetic mutations in the adult neural stem cell compartment determine brain tumour phenotypes. *Embo J* 29, 222-235.
89. Jahani-Asl, A., Yin, H., Soleimani, V.D., Haque, T., Luchman, H.A., Chang, N.C., Sincennes, M.C., Puram, S.V., Scott, A.M., Lorimer, I.A., Perkins, T.J., Ligon, K.L., Weiss, S., Rudnicki, M.A., Bonni, A., 2016. Control of glioblastoma tumorigenesis by feed-forward cytokine signaling. *Nat Neurosci* 19, 798-806.
90. Jamieson, C.H., Gotlib, J., Durocher, J.A., Chao, M.P., Mariappan, M.R., Lay, M., Jones, C., Zehnder, J.L., Lilleberg, S.L., Weissman, I.L., 2006. The JAK2 V617F mutation occurs in hematopoietic stem cells in polycythemia vera and

- predisposes toward erythroid differentiation. *Proc Natl Acad Sci U S A* 103, 6224-6229.
91. Joo, K.M., Kim, J., Jin, J., Kim, M., Seol, H.J., Muradov, J., Yang, H., Choi, Y.L., Park, W.Y., Kong, D.S., Lee, J.I., Ko, Y.H., Woo, H.G., Lee, J., Kim, S., Nam, D.H., 2013. Patient-specific orthotopic glioblastoma xenograft models recapitulate the histopathology and biology of human glioblastomas in situ. *Cell Rep* 3, 260-273.
  92. Kaleko, M., Rutter, W.J., Miller, A.D., 1990. Overexpression of the human insulinlike growth factor I receptor promotes ligand-dependent neoplastic transformation. *Molecular and Cellular Biology* 10, 464.
  93. Karran, P., Hampson, R., 1996. Genomic instability and tolerance to alkylating agents. *Cancer Surv* 28, 69-85.
  94. Kass, R.E., Raftery, A.E., 1995. Bayes Factors. *Journal of the American Statistical Association* 90, 773-795.
  95. Kaye, A.H., Morstyn, G., Gardner, I., Pyke, K., 1986. Development of a xenograft glioma model in mouse brain. *Cancer Res* 46, 1367-1373.
  96. Keenan, A.B., Jenkins, S.L., Jagodnik, K.M., Koplev, S., He, E., Torre, D., Wang, Z., Dohlman, A.B., Silverstein, M.C., Lachmann, A., Kuleshov, M.V., Ma'ayan, A., Stathias, V., Terryn, R., Cooper, D., Forlin, M., Koletti, A., Vidovic, D., Chung, C., Schürer, S.C., Vasiliauskas, J., Pilarczyk, M., Shamsaei, B., Fazel, M., Ren, Y., Niu, W., Clark, N.A., White, S., Mahi, N., Zhang, L., Kouril, M., Reichard, J.F., Sivaganesan, S., Medvedovic, M., Meller, J., Koch, R.J., Birtwistle, M.R., Iyengar, R., Sobie, E.A., Azeloglu, E.U., Kaye, J., Osterloh, J., Haston, K., Kalra, J., Finkbiener, S., Li, J., Milani, P., Adam, M., Escalante-Chong, R., Sachs, K., Lenail, A., Ramamoorthy, D., Fraenkel, E., Daigle, G., Hussain, U., Coye, A., Rothstein, J., Sareen, D., Ornelas, L., Banuelos, M., Mandefro, B., Ho, R., Svendsen, C.N., Lim, R.G., Stocksdale, J., Casale, M.S., Thompson, T.G., Wu, J., Thompson, L.M., Dardov, V., Venkatraman, V., Matlock, A., Van Eyk, J.E., Jaffe, J.D., Papanastasiou, M., Subramanian, A., Golub, T.R., Erickson, S.D., Fallahi-Sichani, M., Hafner, M., Gray, N.S., Lin, J.-R., Mills, C.E., Muhlich, J.L., Niepel, M., Shamu, C.E., Williams, E.H., Wrobel, D., Sorger, P.K., Heiser, L.M., Gray, J.W., Korkola, J.E., Mills, G.B., LaBarge, M., Feiler, H.S., Dane, M.A., Bucher, E., Nederlof, M., Sudar, D., Gross, S., Kilburn, D.F., Smith, R., Devlin, K., Margolis, R., Derr, L., Lee, A., Pillai, A., 2018. The Library of Integrated Network-Based Cellular Signatures NIH Program: System-Level Cataloging of Human Cells Response to Perturbations. *Cell systems* 6, 13-24.
  97. Kim, E., Kim, M., Woo, D.H., Shin, Y., Shin, J., Chang, N., Oh, Y.T., Kim, H., Rhee, J., Nakano, I., Lee, C., Joo, K.M., Rich, J.N., Nam, D.H., Lee, J., 2013. Phosphorylation of EZH2 activates STAT3 signaling via STAT3 methylation and promotes tumorigenicity of glioblastoma stem-like cells. *Cancer cell* 23, 839-852.
  98. Kim, J., Lee, I.H., Cho, H.J., Park, C.K., Jung, Y.S., Kim, Y., Nam, S.H., Kim, B.S., Johnson, M.D., Kong, D.S., Seol, H.J., Lee, J.I., Joo, K.M., Yoon,

- Y., Park, W.Y., Lee, J., Park, P.J., Nam, D.H., 2015. Spatiotemporal Evolution of the Primary Glioblastoma Genome. *Cancer Cell* 28, 318-328.
99. Kim, J.E., Patel, M., Ruzevick, J., Jackson, C.M., Lim, M., 2014. STAT3 Activation in Glioblastoma: Biochemical and Therapeutic Implications. *Cancers* 6, 376-395.
100. Kleihues, P., Louis, D.N., Scheithauer, B.W., Rorke, L.B., Reifenberger, G., Burger, P.C., Cavenee, W.K., 2002. The WHO classification of tumors of the nervous system. *J Neuropathol Exp Neurol* 61, 215-225; discussion 226-219.
101. Koh, L.W., Koh, G.R., Ng, F.S., Toh, T.B., Sandanaraj, E., Chong, Y.K., Phong, M., Tucker-Kellogg, G., Kon, O.L., Ng, W.H., Ng, I.H., Clement, M.V., Pervaiz, S., Ang, B.T., Tang, C.S., 2013. A distinct reactive oxygen species profile confers chemoresistance in glioma-propagating cells and associates with patient survival outcome. *Antioxid Redox Signal* 19, 2261-2279.
102. Kohsaka, S., Wang, L., Yachi, K., Mahabir, R., Narita, T., Itoh, T., Tanino, M., Kimura, T., Nishihara, H., Tanaka, S., 2012. STAT3 inhibition overcomes temozolomide resistance in glioblastoma by downregulating MGMT expression. *Mol Cancer Ther* 11, 1289-1299.
103. Kotliarova, S., Pastorino, S., Kovell, L.C., Kotliarov, Y., Song, H., Zhang, W., Bailey, R., Maric, D., Zenklusen, J.C., Lee, J., Fine, H.A., 2008. Glycogen synthase kinase-3 inhibition induces glioma cell death through c-MYC, nuclear factor-kappaB, and glucose regulation. *Cancer research* 68, 6643-6651.
104. Kumari, N., Dwarakanath, B.S., Das, A., Bhatt, A.N., 2016. Role of interleukin-6 in cancer progression and therapeutic resistance. *Tumour Biol* 37, 11553-11572.
105. Kuriyan, J., Cowburn, D., 1997. MODULAR PEPTIDE RECOGNITION DOMAINS IN EUKARYOTIC SIGNALING. *Annual Review of Biophysics and Biomolecular Structure* 26, 259-288.
106. Kusaba, T., Nakayama, T., Yamazumi, K., Yakata, Y., Yoshizaki, A., Inoue, K., Nagayasu, T., Sekine, I., 2006. Activation of STAT3 is a marker of poor prognosis in human colorectal cancer. *Oncol Rep* 15, 1445-1451.
107. Kwon, C.H., Zhao, D., Chen, J., Alcantara, S., Li, Y., Burns, D.K., Mason, R.P., Lee, E.Y., Wu, H., Parada, L.F., 2008. Pten haploinsufficiency accelerates formation of high-grade astrocytomas. *Cancer research* 68, 3286-3294.
108. Lam, L.T., Wright, G., Davis, R.E., Lenz, G., Farinha, P., Dang, L., Chan, J.W., Rosenwald, A., Gascoyne, R.D., Staudt, L.M., 2008. Cooperative signaling through the signal transducer and activator of transcription 3 and nuclear factor- $\kappa$ B pathways in subtypes of diffuse large B-cell lymphoma. *Blood* 111, 3701-3713.
109. Lamb, J., 2007. The Connectivity Map: a new tool for biomedical research. *Nat Rev Cancer* 7, 54-60.
110. Lamb, J., Crawford, E.D., Peck, D., Modell, J.W., Blat, I.C., Wrobel, M.J., Lerner, J., Brunet, J.P., Subramanian, A., Ross, K.N., Reich, M., Hieronymus,

- H., Wei, G., Armstrong, S.A., Haggarty, S.J., Clemons, P.A., Wei, R., Carr, S.A., Lander, E.S., Golub, T.R., 2006. The Connectivity Map: using gene-expression signatures to connect small molecules, genes, and disease. *Science* 313, 1929-1935.
111. Larochelle, A., Vormoor, J., Hanenberg, H., Wang, J.C.Y., Bhatia, M., Lapidot, T., Moritz, T., Murdoch, B., Xiao, X.L., Kato, I., Williams, D.A., Dick, J.E., 1996. Identification of primitive human hematopoietic cells capable of repopulating NOD/SCID mouse bone marrow: Implications for gene therapy. *Nat Med* 2, 1329-1337.
112. Lathia, J.D., Gallagher, J., Heddleston, J.M., Wang, J., Eyler, C.E., Macswords, J., Wu, Q., Vasanji, A., McLendon, R.E., Hjelmeland, A.B., Rich, J.N., 2010. Integrin alpha 6 regulates glioblastoma stem cells. *Cell Stem Cell* 6, 421-432.
113. Lee, C., Fotovati, A., Triscott, J., Chen, J., Venugopal, C., Singhal, A., Dunham, C., Kerr, J.M., Verreault, M., Yip, S., Wakimoto, H., Jones, C., Jayanthan, A., Narendran, A., Singh, S.K., Dunn, S.E., 2012a. Polo-like kinase 1 inhibition kills glioblastoma multiforme brain tumor cells in part through loss of SOX2 and delays tumor progression in mice. *Stem Cells* 30, 1064-1075.
114. Lee, E.-S., Ko, K.-K., Joe, Y.A., Kang, S.-G., Hong, Y.-K., 2011. Inhibition of STAT3 reverses drug resistance acquired in temozolomide-resistant human glioma cells. *Oncology letters* 2, 115-121.
115. Lee, H., Zhang, P., Herrmann, A., Yang, C., Xin, H., Wang, Z., Hoon, D.S.B., Forman, S.J., Jove, R., Riggs, A.D., Yu, H., 2012b. Acetylated STAT3 is crucial for methylation of tumor-suppressor gene promoters and inhibition by resveratrol results in demethylation. *Proceedings of the National Academy of Sciences of the United States of America* 109, 7765-7769.
116. Lee, J., Kotliarova, S., Kotliarov, Y., Li, A., Su, Q., Donin, N.M., Pastorino, S., Purow, B.W., Christopher, N., Zhang, W., Park, J.K., Fine, H.A., 2006. Tumor stem cells derived from glioblastomas cultured in bFGF and EGF more closely mirror the phenotype and genotype of primary tumors than do serum-cultured cell lines. *Cancer Cell* 9, 391-403.
117. Lee, J.M., Bernstein, A., 1993. p53 mutations increase resistance to ionizing radiation. *Proc Natl Acad Sci U S A* 90, 5742-5746.
118. Lee, J.S., Kang, J.H., Boo, H.J., Hwang, S.J., Hong, S., Lee, S.C., Park, Y.J., Chung, T.M., Youn, H., Lee, S.M., Kim, B.J., Chung, J.K., Chung, Y., William, W.N., Jr., Shin, Y.K., Lee, H.J., Oh, S.H., Lee, H.Y., 2015. STAT3-mediated IGF-2 secretion in the tumour microenvironment elicits innate resistance to anti-IGF-1R antibody. *Nat Commun* 6, 8499.
119. Leung, S.Y., Yuen, S.T., Chan, T.L., Chan, A.S., Ho, J.W., Kwan, K., Fan, Y.W., Hung, K.N., Chung, L.P., Wyllie, A.H., 2000. Chromosomal instability and p53 inactivation are required for genesis of glioblastoma but not for colorectal cancer in patients with germline mismatch repair gene mutation. *Oncogene* 19, 4079-4083.

120. Levine, R.L., Gilliland, D.G., 2008. Myeloproliferative disorders. *Blood* 112, 2190-2198.
121. Li, S., Wang, C., Sandanaraj, E., Aw, S.S., Koe, C.T., Wong, J.J., Yu, F., Ang, B.T., Tang, C., Wang, H., 2014. The SCFSlimb E3 ligase complex regulates asymmetric division to inhibit neuroblast overgrowth. *EMBO Rep* 15, 165-174.
122. Lin, G.S., Chen, Y.P., Lin, Z.X., Wang, X.F., Zheng, Z.Q., Chen, L., 2014a. STAT3 serine 727 phosphorylation influences clinical outcome in glioblastoma. *Int J Clin Exp Pathol* 7, 3141-3149.
123. Lin, G.S., Yang, L.J., Wang, X.F., Chen, Y.P., Tang, W.L., Chen, L., Lin, Z.X., 2014b. STAT3 Tyr705 phosphorylation affects clinical outcome in patients with newly diagnosed supratentorial glioblastoma. *Med Oncol* 31, 924.
124. Liu, C., Zhang, Z., Tang, H., Jiang, Z., You, L., Liao, Y., 2014. Crosstalk between IGF-1R and other tumor promoting pathways. *Curr Pharm Des* 20, 2912-2921.
125. Liu, J., Xu, X., Feng, X., Zhang, B., Wang, J., 2011. Adenovirus-mediated delivery of bFGF small interfering RNA reduces STAT3 phosphorylation and induces the depolarization of mitochondria and apoptosis in glioma cells U251. *J Exp Clin Cancer Res* 30, 80.
126. Louis, D.N., 2006. Molecular pathology of malignant gliomas. *Annu Rev Pathol* 1, 97-117.
127. Louis, D.N., Ohgaki, H., Wiestler, O.D., Cavenee, W.K., Burger, P.C., Jouvet, A., Scheithauer, B.W., Kleihues, P., 2007. The 2007 WHO classification of tumours of the central nervous system. *Acta Neuropathol* 114, 97-109.
128. Louis, D.N., Perry, A., Reifenberger, G., von Deimling, A., Figarella-Branger, D., Cavenee, W.K., Ohgaki, H., Wiestler, O.D., Kleihues, P., Ellison, D.W., 2016. The 2016 World Health Organization Classification of Tumors of the Central Nervous System: a summary. *Acta neuropathologica* 131, 803-820.
129. Ludwig, H., Nachbaur, D.M., Fritz, E., Krainer, M., Huber, H., 1991. Interleukin-6 is a prognostic factor in multiple myeloma. *Blood* 77, 2794-2795.
130. Ma, N.K., Lim, J.K., Leong, M.F., Sandanaraj, E., Ang, B.T., Tang, C., Wan, A.C., 2016a. Collaboration of 3D context and extracellular matrix in the development of glioma stemness in a 3D model. *Biomaterials* 78, 62-73.
131. Ma, Y., Tang, N., Thompson, R.C., Mobley, B.C., Clark, S.W., Sarkaria, J.N., Wang, J., 2016b. InsR/IGF1R Pathway Mediates Resistance to EGFR Inhibitors in Glioblastoma. *Clin Cancer Res* 22, 1767-1776.
132. Macha, M.A., Matta, A., Kaur, J., Chauhan, S.S., Thakar, A., Shukla, N.K., Gupta, S.D., Ralhan, R., 2011. Prognostic significance of nuclear pSTAT3 in oral cancer. *Head Neck* 33, 482-489.
133. Madhavan, S., Zenklusen, J.-C., Kotliarov, Y., Sahni, H., Fine, H.A., Buetow, K., 2009. Rembrandt: Helping Personalized Medicine Become a Reality through Integrative Translational Research. *Molecular Cancer Research* 7, 157-167.



134. Marbach, D., Lamparter, D., Quon, G., Kellis, M., Kutalik, Z., Bergmann, S., 2016. Tissue-specific regulatory circuits reveal variable modular perturbations across complex diseases. *Nat Methods* 13, 366-370.
135. McCaffery, I., Tudor, Y., Deng, H., Tang, R., Suzuki, S., Badola, S., Kindler, H.L., Fuchs, C.S., Loh, E., Patterson, S.D., Chen, L., Gansert, J.L., 2013. Putative predictive biomarkers of survival in patients with metastatic pancreatic adenocarcinoma treated with gemcitabine and ganitumab, an IGF1R inhibitor. *Clin Cancer Res* 19, 4282-4289.
136. McFarland, B.C., Ma, J.Y., Langford, C.P., Gillespie, G.Y., Yu, H., Zheng, Y., Nozell, S.E., Huszar, D., Benveniste, E.N., 2011. Therapeutic potential of AZD1480 for the treatment of human glioblastoma. *Mol Cancer Ther* 10, 2384-2393.
137. Milacic, M., Haw, R., Rothfels, K., Wu, G., Croft, D., Hermjakob, H., D'Eustachio, P., Stein, L., 2012. Annotating cancer variants and anti-cancer therapeutics in reactome. *Cancers (Basel)* 4, 1180-1211.
138. Miyai, M., Tomita, H., Soeda, A., Yano, H., Iwama, T., Hara, A., 2017. Current trends in mouse models of glioblastoma. *Journal of neuro-oncology* 135, 423-432.
139. Miyake, H., Hara, I., Yamanaka, K., Muramaki, M., Gleave, M., Eto, H., 2005. Introduction of insulin-like growth factor binding protein-2 gene into human bladder cancer cells enhances their metastatic potential. *Oncol Rep* 13, 341-345.
140. Monzo, P., Chong, Y.K., Guetta-Terrier, C., Krishnasamy, A., Sathe, S.R., Yim, E.K., Ng, W.H., Ang, B.T., Tang, C., Ladoux, B., Gauthier, N.C., Sheetz, M.P., 2016. Mechanical confinement triggers glioma linear migration dependent on formin FHOD3. *Mol Biol Cell* 27, 1246-1261.
141. Morgan, K.J., Gilliland, D.G., 2008. A role for JAK2 mutations in myeloproliferative diseases. *Annu Rev Med* 59, 213-222.
142. Murray, R., Lee, F., Chiu, C.P., 1990. The genes for leukemia inhibitory factor and interleukin-6 are expressed in mouse blastocysts prior to the onset of hemopoiesis. *Mol Cell Biol* 10, 4953-4956.
143. Nagane, M., Coufal, F., Lin, H., Bogler, O., Cavenee, W.K., Huang, H.J., 1996. A common mutant epidermal growth factor receptor confers enhanced tumorigenicity on human glioblastoma cells by increasing proliferation and reducing apoptosis. *Cancer Res* 56, 5079-5086.
144. Nair, P.N., De Armond, D.T., Adamo, M.L., Strodel, W.E., Freeman, J.W., 2001. Aberrant expression and activation of insulin-like growth factor-1 receptor (IGF-1R) are mediated by an induction of IGF-1R promoter activity and stabilization of IGF-1R mRNA and contributes to growth factor independence and increased survival of the pancreatic cancer cell line MIA PaCa-2. *Oncogene* 20, 8203-8214.
145. Nakada, M., Nakada, S., Demuth, T., Tran, N.L., Hoelzinger, D.B., Berens, M.E., 2007. Molecular targets of glioma invasion. *Cell Mol Life Sci* 64, 458-478.

146. Network, T.C., 2013. Corrigendum: Comprehensive genomic characterization defines human glioblastoma genes and core pathways. *Nature* 494, 506.
147. Newcomb, E.W., Cohen, H., Lee, S.R., Bhalla, S.K., Bloom, J., Hayes, R.L., Miller, D.C., 1998. Survival of patients with glioblastoma multiforme is not influenced by altered expression of p16, p53, EGFR, MDM2 or Bcl-2 genes. *Brain Pathol* 8, 655-667.
148. Ng, F.S., Toh, T.B., Ting, E.H., Koh, G.R., Sandanaraj, E., Phong, M., Wong, S.S., Leong, S.H., Kon, O.L., Tucker-Kellogg, G., Ng, W.H., Ng, I., Tang, C., Ang, B.T., 2012. Progenitor-like traits contribute to patient survival and prognosis in oligodendroglial tumors. *Clin Cancer Res* 18, 4122-4135.
149. Noushmehr, H., Weisenberger, D.J., Diefes, K., Phillips, H.S., Pujara, K., Berman, B.P., Pan, F., Pelloski, C.E., Sulman, E.P., Bhat, K.P., Verhaak, R.G., Hoadley, K.A., Hayes, D.N., Perou, C.M., Schmidt, H.K., Ding, L., Wilson, R.K., Van Den Berg, D., Shen, H., Bengtsson, H., Neuvial, P., Cope, L.M., Buckley, J., Herman, J.G., Baylin, S.B., Laird, P.W., Aldape, K., Cancer Genome Atlas Research, N., 2010. Identification of a CpG island methylator phenotype that defines a distinct subgroup of glioma. *Cancer cell* 17, 510-522.
150. Olow, A., Chen, Z., Niedner, R.H., Wolf, D.M., Yau, C., Pankov, A., Lee, E.P., Brown-Swigart, L., van 't Veer, L.J., Coppe, J.P., 2016. An Atlas of the Human Kinome Reveals the Mutational Landscape Underlying Dysregulated Phosphorylation Cascades in Cancer. *Cancer Res* 76, 1733-1745.
151. Ozawa, T., Riester, M., Cheng, Y.K., Huse, J.T., Squatrito, M., Helmy, K., Charles, N., Michor, F., Holland, E.C., 2014. Most human non-GCIMP glioblastoma subtypes evolve from a common proneural-like precursor glioma. *Cancer Cell* 26, 288-300.
152. Pan, Y., Zhou, F., Zhang, R., Claret, F.X., 2013. Stat3 inhibitor Stattic exhibits potent antitumor activity and induces chemo- and radio-sensitivity in nasopharyngeal carcinoma. *PLoS One* 8, e54565.
153. Park, J.H., Choi, Y.J., Kim, S.Y., Lee, J.E., Sung, K.J., Park, S., Kim, W.S., Song, J.S., Choi, C.M., Sung, Y.H., Rho, J.K., Lee, J.C., 2016. Activation of the IGF1R pathway potentially mediates acquired resistance to mutant-selective 3rd-generation EGF receptor tyrosine kinase inhibitors in advanced non-small cell lung cancer. *Oncotarget* 7, 22005-22015.
154. Pažanin, L., Vučić, M., Čupić, H., Plavec, D., Krušlin, B., 2011. IGFBP-2 expression, angiogenesis and pseudopalisades in glioblastoma. *Translational Neuroscience* 2, 219-224.
155. Phillips, H.S., Kharbanda, S., Chen, R., Forrest, W.F., Soriano, R.H., Wu, T.D., Misra, A., Nigro, J.M., Colman, H., Soroceanu, L., Williams, P.M., Modrusan, Z., Feuerstein, B.G., Aldape, K., 2006. Molecular subclasses of high-grade glioma predict prognosis, delineate a pattern of disease progression, and resemble stages in neurogenesis. *Cancer Cell* 9, 157-173.
156. Polak, P., Karlič, R., Koren, A., Thurman, R., Sandstrom, R., Lawrence, M.S., Reynolds, A., Rynes, E., Vlahoviček, K., Stamatoyannopoulos, J.A., Sunyaev,

- S.R., 2015. Cell-of-origin chromatin organization shapes the mutational landscape of cancer. *Nature* 518, 360.
157. Pollak, M.N., Schernhammer, E.S., Hankinson, S.E., 2004. Insulin-like growth factors and neoplasia. *Nature Reviews Cancer* 4, 505.
158. Prasad, T.S., Kandasamy, K., Pandey, A., 2009. Human Protein Reference Database and Human Proteinpedia as discovery tools for systems biology. *Methods Mol Biol* 577, 67-79.
159. Puchalski, R.B., Shah, N., Miller, J., Dalley, R., Nomura, S.R., Yoon, J.G., Smith, K.A., Lankerovich, M., Bertagnolli, D., Bickley, K., Boe, A.F., Brouner, K., Butler, S., Caldejon, S., Chapin, M., Datta, S., Dee, N., Desta, T., Dolbeare, T., Dotson, N., Ebbert, A., Feng, D., Feng, X., Fisher, M., Gee, G., Goldy, J., Gourley, L., Gregor, B.W., Gu, G., Hejazinia, N., Hohmann, J., Hothi, P., Howard, R., Joines, K., Kriedberg, A., Kuan, L., Lau, C., Lee, F., Lee, H., Lemon, T., Long, F., Mastan, N., Mott, E., Murthy, C., Ngo, K., Olson, E., Reding, M., Riley, Z., Rosen, D., Sandman, D., Shapovalova, N., Slaughterbeck, C.R., Sodt, A., Stockdale, G., Szafer, A., Wakeman, W., Wohnoutka, P.E., White, S.J., Marsh, D., Rostomily, R.C., Ng, L., Dang, C., Jones, A., Keogh, B., Gittleman, H.R., Barnholtz-Sloan, J.S., Cimino, P.J., Uppin, M.S., Keene, C.D., Farrokhi, F.R., Lathia, J.D., Berens, M.E., Iavarone, A., Bernard, A., Lein, E., Phillips, J.W., Rostad, S.W., Cobbs, C., Hawrylycz, M.J., Foltz, G.D., 2018. An anatomic transcriptional atlas of human glioblastoma. *Science* 360, 660-663.
160. Rajan, P., McKay, R.D., 1998. Multiple routes to astrocytic differentiation in the CNS. *J Neurosci* 18, 3620-3629.
161. Rao, J.S., 2003. Molecular mechanisms of glioma invasiveness: the role of proteases. *Nat Rev Cancer* 3, 489-501.
162. Reya, T., Morrison, S.J., Clarke, M.F., Weissman, I.L., 2001. Stem cells, cancer, and cancer stem cells. *Nature* 414, 105-111.
163. Reynolds, B., Weiss, S., 1992. Generation of neurons and astrocytes from isolated cells of the adult mammalian central nervous system. *Science* 255, 1707-1710.
164. Reynolds, B.A., Weiss, S., 1996. Clonal and Population Analyses Demonstrate That an EGF-Responsive Mammalian Embryonic CNS Precursor Is a Stem Cell. *Developmental Biology* 175, 1-13.
165. Reynolds, B.A., Rietze, R.L., 2005. Neural stem cells and neurospheres--re-evaluating the relationship. *Nat Methods* 2, 333-336.
166. Ricci-Vitiani, L., Pallini, R., Biffoni, M., Todaro, M., Invernici, G., Cenci, T., Maira, G., Parati, E.A., Stassi, G., Larocca, L.M., De Maria, R., 2010. Tumour vascularization via endothelial differentiation of glioblastoma stem-like cells. *Nature* 468, 824.
167. Rietze, R.L., Valcanis, H., Brooker, G.F., Thomas, T., Voss, A.K., Bartlett, P.F., 2001. Purification of a pluripotent neural stem cell from the adult mouse brain. *Nature* 412, 736-739.

168. Ritchie, M.E., Phipson, B., Wu, D., Hu, Y., Law, C.W., Shi, W., Smyth, G.K., 2015. limma powers differential expression analyses for RNA-sequencing and microarray studies. *Nucleic Acids Res* 43, e47.
169. Roadmap Epigenomics, C., Kundaje, A., Meuleman, W., Ernst, J., Bilenky, M., Yen, A., Heravi-Moussavi, A., Kheradpour, P., Zhang, Z., Wang, J., Ziller, M.J., Amin, V., Whitaker, J.W., Schultz, M.D., Ward, L.D., Sarkar, A., Quon, G., Sandstrom, R.S., Eaton, M.L., Wu, Y.C., Pfening, A.R., Wang, X., Claussnitzer, M., Liu, Y., Coarfa, C., Harris, R.A., Shores, N., Epstein, C.B., Gjonneska, E., Leung, D., Xie, W., Hawkins, R.D., Lister, R., Hong, C., Gascard, P., Mungall, A.J., Moore, R., Chuah, E., Tam, A., Canfield, T.K., Hansen, R.S., Kaul, R., Sabo, P.J., Bansal, M.S., Carles, A., Dixon, J.R., Farh, K.H., Feizi, S., Karlic, R., Kim, A.R., Kulkarni, A., Li, D., Lowdon, R., Elliott, G., Mercer, T.R., Neph, S.J., Onuchic, V., Polak, P., Rajagopal, N., Ray, P., Sallari, R.C., Siebenthal, K.T., Sinnott-Armstrong, N.A., Stevens, M., Thurman, R.E., Wu, J., Zhang, B., Zhou, X., Beaudet, A.E., Boyer, L.A., De Jager, P.L., Farnham, P.J., Fisher, S.J., Haussler, D., Jones, S.J., Li, W., Marra, M.A., McManus, M.T., Sunyaev, S., Thomson, J.A., Tlsty, T.D., Tsai, L.H., Wang, W., Waterland, R.A., Zhang, M.Q., Chadwick, L.H., Bernstein, B.E., Costello, J.F., Ecker, J.R., Hirst, M., Meissner, A., Milosavljevic, A., Ren, B., Stamatoyannopoulos, J.A., Wang, T., Kellis, M., 2015. Integrative analysis of 111 reference human epigenomes. *Nature* 518, 317-330.
170. Rosenthal, N., Brown, S., 2007. The mouse ascending: perspectives for human-disease models. *Nat Cell Biol* 9, 993-999.
171. Sariban, E., Kohn, K.W., Zlotogorski, C., Laurent, G., D'Incalci, M., Day, R., 3rd, Smith, B.H., Kornblith, P.L., Erickson, L.C., 1987. DNA cross-linking responses of human malignant glioma cell strains to chloroethylnitrosoureas, cisplatin, and diaziquone. *Cancer Res* 47, 3988-3994.
172. Schaefer, L.K., Ren, Z., Fuller, G.N., Schaefer, T.S., 2002. Constitutive activation of Stat3alpha in brain tumors: localization to tumor endothelial cells and activation by the endothelial tyrosine kinase receptor (VEGFR-2). *Oncogene* 21, 2058-2065.
173. Schindler, C., Darnell, J.E., Jr., 1995. Transcriptional responses to polypeptide ligands: the JAK-STAT pathway. *Annu Rev Biochem* 64, 621-651.
174. Schlegel, J., Merdes, A., Stumm, G., Albert, F.K., Forsting, M., Hynes, N., Kiessling, M., 1994. Amplification of the epidermal-growth-factor-receptor gene correlates with different growth behaviour in human glioblastoma. *Int J Cancer* 56, 72-77.
175. Schust, J., Sperl, B., Hollis, A., Mayer, T.U., Berg, T., 2006. Stattic: a small-molecule inhibitor of STAT3 activation and dimerization. *Chem Biol* 13, 1235-1242.
176. Scotlandi, K., Avnet, S., Benini, S., Manara, M.C., Serra, M., Cerisano, V., Perdichizzi, S., Lollini, P.-L., De Giovanni, C., Landuzzi, L., Picci, P., 2002. Expression of an IGF-I receptor dominant negative mutant induces apoptosis,

- inhibits tumorigenesis and enhances chemosensitivity in Ewing's sarcoma cells. *International Journal of Cancer* 101, 11-16.
177. See, A.P., Han, J.E., Phallen, J., Binder, Z., Gallia, G., Pan, F., Jinasena, D., Jackson, C., Belcaid, Z., Jeong, S.J., Gottschalk, C., Zeng, J., Ruzevick, J., Nicholas, S., Kim, Y., Albesiano, E., Pardoll, D.M., Lim, M., 2012. The role of STAT3 activation in modulating the immune microenvironment of GBM. *J Neurooncol* 110, 359-368.
178. Segerman, A., Niklasson, M., Haglund, C., Bergstrom, T., Jarvius, M., Xie, Y., Westermark, A., Sonmez, D., Hermansson, A., Kastemar, M., Naimaie-Ali, Z., Nyberg, F., Berglund, M., Sundstrom, M., Hesselager, G., Uhrbom, L., Gustafsson, M., Larsson, R., Fryknas, M., Segerman, B., Westermark, B., 2016. Clonal Variation in Drug and Radiation Response among Glioma-Initiating Cells Is Linked to Proneural-Mesenchymal Transition. *Cell Rep* 17, 2994-3009.
179. Senft, C., Priester, M., Polacin, M., Schroder, K., Seifert, V., Kogel, D., Weissenberger, J., 2011. Inhibition of the JAK-2/STAT3 signaling pathway impedes the migratory and invasive potential of human glioblastoma cells. *J Neurooncol* 101, 393-403.
180. Shapiro, W.R., Basler, G.A., Chernik, N.L., Posner, J.B., 1979. Human brain tumor transplantation into nude mice. *J Natl Cancer Inst* 62, 447-453.
181. Sherry, M.M., Reeves, A., Wu, J.K., Cochran, B.H., 2009. STAT3 is required for proliferation and maintenance of multipotency in glioblastoma stem cells. *Stem Cells* 27, 2383-2392.
182. Singh, S.K., Clarke, I.D., Terasaki, M., Bonn, V.E., Hawkins, C., Squire, J., Dirks, P.B., 2003. Identification of a cancer stem cell in human brain tumors. *Cancer research* 63, 5821-5828.
183. Smith, A.G., Heath, J.K., Donaldson, D.D., Wong, G.G., Moreau, J., Stahl, M., Rogers, D., 1988. Inhibition of pluripotential embryonic stem cell differentiation by purified polypeptides. *Nature* 336, 688-690.
184. Soda, Y., Marumoto, T., Friedmann-Morvinski, D., Soda, M., Liu, F., Michiue, H., Pastorino, S., Yang, M., Hoffman, R.M., Kesari, S., Verma, I.M., 2011. Transdifferentiation of glioblastoma cells into vascular endothelial cells. *Proceedings of the National Academy of Sciences* 108, 4274-4280.
185. Son, M.J., Woolard, K., Nam, D.H., Lee, J., Fine, H.A., 2009. SSEA-1 is an enrichment marker for tumor-initiating cells in human glioblastoma. *Cell Stem Cell* 4, 440-452.
186. Stathias, V., Jermakowicz, A.M., Maloof, M.E., Forlin, M., Walters, W., Suter, R.K., Durante, M.A., Williams, S.L., Harbour, J.W., Volmar, C.H., Lyons, N.J., Wahlestedt, C., Graham, R.M., Ivan, M.E., Komotar, R.J., Sarkaria, J.N., Subramanian, A., Golub, T.R., Schurer, S.C., Ayad, N.G., 2018. Drug and disease signature integration identifies synergistic combinations in glioblastoma. *Nat Commun* 9, 5315.
187. Stommel, J.M., Kimmelman, A.C., Ying, H., Nabioullin, R., Ponugoti, A.H., Wiedemeyer, R., Stegh, A.H., Bradner, J.E., Ligon, K.L., Brennan, C., Chin,

- L., DePinho, R.A., 2007. Coactivation of receptor tyrosine kinases affects the response of tumor cells to targeted therapies. *Science* 318, 287-290.
188. Subramanian, A., Narayan, R., Corsello, S.M., Peck, D.D., Natoli, T.E., Lu, X., Gould, J., Davis, J.F., Tubelli, A.A., Asiedu, J.K., Lahr, D.L., Hirschman, J.E., Liu, Z., Donahue, M., Julian, B., Khan, M., Wadden, D., Smith, I.C., Lam, D., Liberzon, A., Toder, C., Bagul, M., Orzechowski, M., Enache, O.M., Piccioni, F., Johnson, S.A., Lyons, N.J., Berger, A.H., Shamji, A.F., Brooks, A.N., Vrcic, A., Flynn, C., Rosains, J., Takeda, D.Y., Hu, R., Davison, D., Lamb, J., Ardlie, K., Hogstrom, L., Greenside, P., Gray, N.S., Clemons, P.A., Silver, S., Wu, X., Zhao, W.-N., Read-Button, W., Wu, X., Haggarty, S.J., Ronco, L.V., Boehm, J.S., Schreiber, S.L., Doench, J.G., Bittker, J.A., Root, D.E., Wong, B., Golub, T.R., 2017. A Next Generation Connectivity Map: L1000 Platform and the First 1,000,000 Profiles. *Cell* 171, 1437-1452.e1417.
189. Svendsen, C.N., ter Borg, M.G., Armstrong, R.J., Rosser, A.E., Chandran, S., Ostenfeld, T., Caldwell, M.A., 1998. A new method for the rapid and long term growth of human neural precursor cells. *J Neurosci Methods* 85, 141-152.
190. Taga, T., Hibi, M., Hirata, Y., Yamasaki, K., Yasukawa, K., Matsuda, T., Hirano, T., Kishimoto, T., 1989. Interleukin-6 triggers the association of its receptor with a possible signal transducer, gp130. *Cell* 58, 573-581.
191. Tu, Y., Zhong, Y., Fu, J., Cao, Y., Fu, G., Tian, X., Wang, B., 2011. Activation of JAK/STAT signal pathway predicts poor prognosis of patients with gliomas. *Med Oncol* 28, 15-23.
192. Uchida, N., Buck, D.W., He, D., Reitsma, M.J., Masek, M., Phan, T.V., Tsukamoto, A.S., Gage, F.H., Weissman, I.L., 2000. Direct isolation of human central nervous system stem cells. *Proceedings of the National Academy of Sciences of the United States of America* 97, 14720-14725.
193. Ueki, K., Ono, Y., Henson, J.W., Efrid, J.T., von Deimling, A., Louis, D.N., 1996. CDKN2/p16 or RB alterations occur in the majority of glioblastomas and are inversely correlated. *Cancer Res* 56, 150-153.
194. Verhaak, R.G.W., Hoadley, K.A., Purdom, E., Wang, V., Qi, Y., Wilkerson, M.D., Miller, C.R., Ding, L., Golub, T., Mesirov, J.P., Alexe, G., Lawrence, M., O'Kelly, M., Tamayo, P., Weir, B.A., Gabrie, S., Winckler, W., Gupta, S., Jakkula, L., Feiler, H.S., Hodgson, J.G., James, C.D., Sarkaria, J.N., Brennan, C., Kahn, A., Spellman, P.T., Wilson, R.K., Speed, T.P., Gray, J.W., Meyerson, M., Getz, G., Perou, C.M., Hayes, D.N., The Cancer Genome Atlas Research, N., 2010. An integrated genomic analysis identifies clinically relevant subtypes of glioblastoma characterized by abnormalities in PDGFRA, IDH1, EGFR and NF1. *Cancer Cell* 17, 98-110.
195. Villanueva, J., Vultur, A., Lee, J.T., Somasundaram, R., Fukunaga-Kalabis, M., Cipolla, A.K., Wubbenhorst, B., Xu, X., Gimotty, P.A., Kee, D., Santiago-Walker, A.E., Letrero, R., D'Andrea, K., Pushparajan, A., Hayden, J.E., Brown, K.D., Laquerre, S., McArthur, G.A., Sosman, J.A., Nathanson, K.L., Herlyn, M., 2010. Acquired resistance to BRAF inhibitors mediated by

- a RAF kinase switch in melanoma can be overcome by cotargeting MEK and IGF-1R/PI3K. *Cancer cell* 18, 683-695.
196. Wald, N.J., Hackshaw, A.K., Frost, C.D., 1999. When can a risk factor be used as a worthwhile screening test? *BMJ* 319, 1562-1565.
  197. Wan, X., Harkavy, B., Shen, N., Grohar, P., Helman, L.J., 2007. Rapamycin induces feedback activation of Akt signaling through an IGF-1R-dependent mechanism. *Oncogene* 26, 1932-1940.
  198. Wang, H., Lathia, J.D., Wu, Q., Wang, J., Li, Z., Heddleston, J.M., Eyler, C.E., Elderbroom, J., Gallagher, J., Schusch, J., MacSwords, J., Cao, Y., McLendon, R.E., Wang, X.F., Hjelmeland, A.B., Rich, J.N., 2009. Targeting interleukin 6 signaling suppresses glioma stem cell survival and tumor growth. *Stem Cells* 27, 2393-2404.
  199. Wang, Q., Hu, B., Hu, X., Kim, H., Squatrito, M., Scarpace, L., deCarvalho, A.C., Lyu, S., Li, P., Li, Y., Barthel, F., Cho, H.J., Lin, Y.H., Satani, N., Martinez-Ledesma, E., Zheng, S., Chang, E., Gabriel Saive, C.E., Olar, A., Lan, Z.D., Finocchiaro, G., Phillips, J.J., Berger, M.S., Gabrusiewicz, K.R., Wang, G., Eskilsson, E., Hu, J., Mikkelsen, T., DePinho, R.A., Muller, F., Heimberger, A.B., Sulman, E.P., Nam, D.H., Verhaak, R.G.W., 2018. Tumor Evolution of Glioma-Intrinsic Gene Expression Subtypes Associates with Immunological Changes in the Microenvironment. *Cancer Cell* 33, 152.
  200. Weathers, S.P., de Groot, J., 2015. VEGF Manipulation in Glioblastoma. *Oncology (Williston Park)* 29, 720-727.
  201. Wee, B., Charles, N., Holland, E.C., 2011. Animal models to study cancer-initiating cells from glioblastoma. *Front Biosci (Landmark Ed)* 16, 2243-2258.
  202. Wei, J., Wu, A., Kong, L.Y., Wang, Y., Fuller, G., Fokt, I., Melillo, G., Priebe, W., Heimberger, A.B., 2011. Hypoxia potentiates glioma-mediated immunosuppression. *PLoS one* 6, e16195.
  203. Weller, M., Malipiero, U., Aguzzi, A., Reed, J.C., Fontana, A., 1995. Protooncogene bcl-2 gene transfer abrogates Fas/APO-1 antibody-mediated apoptosis of human malignant glioma cells and confers resistance to chemotherapeutic drugs and therapeutic irradiation. *J Clin Invest* 95, 2633-2643.
  204. Wen, P.Y., Kesari, S., 2008. Malignant gliomas in adults. *N Engl J Med* 359, 492-507.
  205. Wieduwilt, M.J., Moasser, M.M., 2008. The epidermal growth factor receptor family: biology driving targeted therapeutics. *Cell Mol Life Sci* 65, 1566-1584.
  206. Wong, A.L., Soo, R.A., Tan, D.S., Lee, S.C., Lim, J.S., Marban, P.C., Kong, L.R., Lee, Y.J., Wang, L.Z., Thuya, W.L., Soong, R., Yee, M.Q., Chin, T.M., Cordero, M.T., Asuncion, B.R., Pang, B., Pervaiz, S., Hirpara, J.L., Sinha, A., Xu, W.W., Yuasa, M., Tsunoda, T., Motoyama, M., Yamauchi, T., Goh, B.C., 2015. Phase I and biomarker study of OPB-51602, a novel signal transducer and activator of transcription (STAT) 3 inhibitor, in patients with refractory solid malignancies. *Annals of Oncology* 26, 998-1005.

207. Xu, L., Chen, Y., Mayakonda, A., Koh, L., Chong, Y.K., Buckley, D.L., Sandanaraj, E., Lim, S.W., Lin, R.Y., Ke, X.Y., Huang, M.L., Chen, J., Sun, W., Wang, L.Z., Goh, B.C., Dinh, H.Q., Kappei, D., Winter, G.E., Ding, L.W., Ang, B.T., Berman, B.P., Bradner, J.E., Tang, C., Koeffler, H.P., 2018. Targetable BET proteins- and E2F1-dependent transcriptional program maintains the malignancy of glioblastoma. *Proc Natl Acad Sci U S A* 115, E5086-E5095.
208. Yang, C., Cirielli, C., Capogrossi, M.C., Passaniti, A., 1995. Adenovirus-mediated wild-type p53 expression induces apoptosis and suppresses tumorigenesis of prostatic tumor cells. *Cancer Res* 55, 4210-4213.
209. Yang, X.O., Panopoulos, A.D., Nurieva, R., Chang, S.H., Wang, D., Watowich, S.S., Dong, C., 2007. STAT3 regulates cytokine-mediated generation of inflammatory helper T cells. *J Biol Chem* 282, 9358-9363.
210. Yip, S., Miao, J., Cahill, D.P., Iafrate, A.J., Aldape, K., Nutt, C.L., Louis, D.N., 2009. MSH6 mutations arise in glioblastomas during temozolomide therapy and mediate temozolomide resistance. *Clinical cancer research : an official journal of the American Association for Cancer Research* 15, 4622-4629.
211. Yoshimatsu, T., Kawaguchi, D., Oishi, K., Takeda, K., Akira, S., Masuyama, N., Gotoh, Y., 2006. Non-cell-autonomous action of STAT3 in maintenance of neural precursor cells in the mouse neocortex. *Development* 133, 2553-2563.
212. Yu, H., Jove, R., 2004. The STATs of cancer--new molecular targets come of age. *Nat Rev Cancer* 4, 97-105.
213. Yu, H., Pardoll, D., Jove, R., 2009. STATs in cancer inflammation and immunity: a leading role for STAT3. *Nat Rev Cancer* 9, 798-809.
214. Yue, P., Turkson, J., 2009. Targeting STAT3 in cancer: how successful are we? *Expert Opin Investig Drugs* 18, 45-56.
215. Zhang, H.-F., Lai, R., 2014. STAT3 in Cancer-Friend or Foe? *Cancers* 6, 1408-1440.
216. Zhang, Q., Wang, H.Y., Marzec, M., Raghunath, P.N., Nagasawa, T., Wasik, M.A., 2005. STAT3- and DNA methyltransferase 1-mediated epigenetic silencing of SHP-1 tyrosine phosphatase tumor suppressor gene in malignant T lymphocytes. *Proceedings of the National Academy of Sciences of the United States of America* 102, 6948-6953.
217. Zhang, Q., Wang, H.Y., Woetmann, A., Raghunath, P.N., Odum, N., Wasik, M.A., 2006a. STAT3 induces transcription of the DNA methyltransferase 1 gene (DNMT1) in malignant T lymphocytes. *Blood* 108, 1058-1064.
218. Zhang, W., Zong, C.S., Hermanto, U., Lopez-Bergami, P., Ronai, Z.e., Wang, L.-H., 2006b. RACK1 Recruits STAT3 Specifically to Insulin and Insulin-Like Growth Factor 1 Receptors for Activation, Which Is Important for Regulating Anchorage-Independent Growth. *Molecular and Cellular Biology* 26, 413-424.
219. Zheng, H., Ying, H., Yan, H., Kimmelman, A.C., Hiller, D.J., Chen, A.J., Perry, S.R., Tonon, G., Chu, G.C., Ding, Z., Stommel, J.M., Dunn, K.L.,



- Wiedemeyer, R., You, M.J., Brennan, C., Wang, Y.A., Ligon, K.L., Wong, W.H., Chin, L., DePinho, R.A., 2008. p53 and Pten control neural and glioma stem/progenitor cell renewal and differentiation. *Nature* 455, 1129-1133.
220. Zhou, H., Miki, R., Eeva, M., Fike, F.M., Seligson, D., Yang, L., Yoshimura, A., Teitell, M.A., Jamieson, C.A., Cacalano, N.A., 2007. Reciprocal regulation of SOCS 1 and SOCS3 enhances resistance to ionizing radiation in glioblastoma multiforme. *Clin Cancer Res* 13, 2344-2353.
221. Zong, C.S., Chan, J., Levy, D.E., Horvath, C., Sadowski, H.B., Wang, L.H., 2000. Mechanism of STAT3 activation by insulin-like growth factor I receptor. *J Biol Chem* 275, 15099-15105.

## 8.0 APPENDICES

### A. List of Genes Comprising the *STAT3* Functionally-tuned Gene Signature

Probe ID	SYMBOL	Log fold change (KD vs NT)	<i>p</i> -value	Adj <i>p</i> -value
205353 s at	PEBP1P2	0.433296765	1.67E-05	0.001743919
210825 s at	PEBP1	0.442394112	6.26E-06	0.000868573
205353 s at	PEBP1	0.433296765	1.67E-05	0.001743919
217491 x at	COX7CP1	1.047442341	6.63E-13	7.24E-09
212964 at	HIC2	0.782347662	2.99E-07	9.23E-05
227064 at	ANKRD40	1.071426888	6.14E-06	0.000860402
213234 at	KIAA1467	0.909560041	1.90E-08	1.25E-05
205353 s at	RETSAT	0.433296765	1.67E-05	0.001743919
203387 s at	TBC1D4	0.495299346	9.38E-06	0.001146284
210201 x at	BIN1	1.259061855	1.31E-09	1.79E-06
214643 x at	BIN1	0.578410723	4.45E-06	0.000670277
210202 s at	BIN1	0.574198906	1.35E-07	5.10E-05
202931 x at	BIN1	0.905217007	4.96E-08	2.40E-05
214439 x at	BIN1	1.237094138	4.21E-10	8.83E-07
221810 at	RAB15	0.570770067	7.32E-07	0.000179691
59697 at	RAB15	0.6078659	1.53E-05	0.001627199
201674 s at	AKAP1	0.427032672	1.80E-05	0.001813
209380 s at	ABCC5	0.488877013	5.46E-05	0.004102576
228454 at	LCOR	0.716439336	3.64E-07	0.000108373
226520 at	LCOR	0.711460444	5.19E-07	0.000143898
238974 at	C2orf69	0.354853672	0.000105882	0.006623759
238890 at	BRWD1	0.529133088	1.40E-05	0.001519851
230296 at	C16orf52	0.527585515	1.59E-09	1.98E-06
222880 at	AKT3	0.442970745	0.000118808	0.007191216
212607 at	AKT3	0.663056326	8.07E-06	0.001034896
209845 at	MKRN1	0.878168821	1.02E-05	0.00121941
213304 at	FAM179B	0.445533968	2.99E-05	0.00262377
211383 s at	WDR37	0.321256758	8.55E-05	0.005709813
212050 at	WIPF2	0.293485722	2.26E-05	0.002129344
226033 at	USP31	0.348069858	2.71E-06	0.000468537
218862 at	ASB13	0.302990815	4.47E-05	0.003499296
223184 s at	AGPAT3	0.655549583	4.15E-05	0.003330501
212114 at	ATXN7L3B	0.753989001	3.39E-08	1.78E-05
225957 at	CREBRF	0.557724594	0.000184028	0.009963001
217491 x at	COX7C	1.047442341	6.63E-13	7.24E-09
201134 x at	COX7C	1.210242166	1.14E-13	2.40E-09
219175 s at	SLC41A3	0.510114508	1.15E-06	0.000248324
224931 at	SLC41A3	0.477907138	3.49E-08	1.82E-05
222494 at	FOXN3	0.283877313	1.27E-05	0.001408797
231969 at	STOX2	0.502052836	1.70E-05	0.001757107
205052 at	AUH	0.99041228	1.48E-07	5.45E-05
219093 at	PID1	0.803943854	5.30E-05	0.003997974

212655 at	ZCCHC14	0.532781896	0.000174755	0.009630579
225511 at	GPRC5B	0.379615887	1.73E-05	0.001769406
211475 s at	BAG1	0.527496975	5.79E-06	0.00082353
226680 at	IKZF5	0.461945003	1.37E-06	0.000289101
37566 at	KIAA1045	0.365948316	0.000104529	0.006576747
226310 at	RICTOR	0.517924196	1.23E-05	0.001386839
226312 at	RICTOR	0.62017486	2.27E-08	1.40E-05
228248 at	RICTOR	0.517367522	1.02E-05	0.00121941
224495 at	SNORD118	-0.568950232	7.91E-06	0.001015928
231896 s at	DENR	-0.496587511	1.80E-07	6.24E-05
218622 at	NUP37	-0.412470015	0.000139572	0.008134963
220239 at	KLHL7	-0.953057006	3.16E-12	2.16E-08
203664 s at	POLR2D	-0.362518088	8.94E-05	0.005866287
202663 at	WIPF1	-0.72324048	7.34E-05	0.005078614
1554451 s at	DNAJC14	-0.298195513	1.40E-05	0.001519851
225837 at	RHNO1	-0.852648658	2.59E-05	0.002354766
220358 at	BATF3	-0.268712986	3.31E-05	0.002816552
224783 at	UBALD2	-0.562831502	1.23E-05	0.001386839
225872 at	SLC35F5	-0.702897734	2.79E-05	0.00248779
222519 s at	IFT57	-0.485287361	3.47E-05	0.002915154
205061 s at	EXOSC9	-0.357316048	8.93E-05	0.005866287
222602 at	UBA6	-0.630284325	6.29E-08	2.89E-05
222601 at	UBA6	-0.479435608	1.24E-06	0.000265086
239413 at	CEP152	-0.470898387	1.11E-05	0.001298372
202253 s at	DNM2	-0.321716645	3.46E-05	0.002909123
224714 at	MKI67IP	-0.221325861	0.000175689	0.009650242
217738 at	NAMPT	-0.516889292	8.49E-06	0.001077299
220199 s at	AIDA	-1.00372432	6.37E-06	0.000876941
224617 at	PTBP3	-0.267390012	3.28E-06	0.000529742
225592 at	PPP1R18	-0.422623732	1.90E-05	0.001886765
219083 at	SHQ1	-0.262055432	5.82E-05	0.004286846
203024 s at	C5orf15	-0.624591476	3.10E-06	0.000517693
225080 at	MYO1C	-0.744080211	1.81E-08	1.22E-05
225592 at	NRM	-0.422623732	1.90E-05	0.001886765
218131 s at	GATAD2A	-0.431793696	0.000160996	0.009045734
202716 at	PTPN1	-0.482761247	1.44E-05	0.00155989
218474 s at	KCTD5	-0.346923516	2.20E-06	0.000402599
1552470 a at	ABHD11	-0.334488179	2.79E-05	0.00248779
1553678 a at	ITGB1P1	-0.498832565	7.03E-05	0.004949843
225308 s at	TANC1	-0.370186201	1.83E-06	0.000358235
209130 at	SNAP23	-0.566059891	0.00015134	0.008672756
202076 at	BIRC2	-0.466272661	5.89E-05	0.004327914
210844 x at	CTNNA1	-0.408342655	3.55E-06	0.000560909
200764 s at	CTNNA1	-0.373769988	8.58E-06	0.001082429
200765 x at	CTNNA1	-0.420775093	1.05E-05	0.001245242
232231 at	RUNX2	-0.585408616	1.89E-06	0.000366498

238590 x at	TMEM107	-0.457089117	8.56E-05	0.005709813
239824 s at	TMEM107	-0.467439181	0.000113984	0.00700223
224495 at	TMEM107	-0.568950232	7.91E-06	0.001015928
213012 at	NEDD4	-0.815041138	8.72E-11	2.65E-07
208749 x at	FLOT1	-0.716672114	1.64E-06	0.000330039
222446 s at	BACE2	-0.452072584	7.90E-05	0.005389695
212949 at	NCAPH	-0.483401536	2.46E-05	0.002279434
225297 at	HAUS1	-0.222105321	0.000101285	0.006402158
202350 s at	MATN2	-0.678512064	4.84E-06	0.000707225
225406 at	TWSG1	-0.96002712	3.01E-05	0.002636179
204017 at	KDELR3	-0.745956098	2.25E-08	1.40E-05
207265 s at	KDELR3	-0.502976395	7.46E-07	0.000181052
203843 at	RPS6KA3	-0.872759755	6.03E-05	0.004393941
238606 at	ZNF747	-0.313718652	7.58E-05	0.005209986
204531 s at	BRCA1	-0.375033919	9.08E-05	0.00591885
228234 at	TICAM2	-0.547371653	3.23E-07	9.92E-05
213141 at	PSKH1	-0.493616067	2.61E-07	8.42E-05
212262 at	QKI	-0.513125157	1.42E-06	0.000294669
208828 at	POLE3	-0.471787456	1.03E-06	0.000229381
228234 at	TMED7-	-0.547371653	3.23E-07	9.92E-05
239231 at	ZNF101	-0.348344439	4.23E-06	0.000648808
202043 s at	SMS	-0.700475345	3.25E-05	0.002780939
202695 s at	STK17A	-0.350944507	4.29E-05	0.003399304
203823 at	RGS3	-0.655681581	0.000150751	0.008648043
212900 at	SEC24A	-0.336548654	2.81E-05	0.002497189
219838 at	TTC23	-0.340813525	4.59E-05	0.003571744
212415 at	SEPT6	-0.711330002	9.00E-05	0.00588946
208689 s at	RPN2	-0.329444537	5.52E-05	0.004132446
213399 x at	RPN2	-0.311282628	0.000183774	0.009963001
201776 s at	EFCAB14	-0.63282897	1.57E-07	5.57E-05
228273 at	PRR11	-0.22943255	8.96E-05	0.005866287
218718 at	PDGFC	-0.521990685	6.06E-05	0.004404599
213113 s at	SLC43A3	-0.499561147	5.74E-06	0.000817851
210692 s at	SLC43A3	-0.407818545	8.94E-06	0.00110968
225538 at	ZCCHC9	-0.525692121	6.93E-05	0.004890429
209307 at	SWAP70	-0.924465151	7.32E-07	0.000179691
209306 s at	SWAP70	-0.740490966	6.88E-07	0.000177278
235489 at	RHOJ	-0.545250331	1.46E-05	0.001580498
209344 at	TPM4	-0.605468838	1.58E-05	0.001672422
235177 at	METTL21A	-0.353911844	2.37E-05	0.002209913
203967 at	CDC6	-0.39014975	5.81E-05	0.004286846
217926 at	MRI1	-0.50991417	3.15E-06	0.000522419
217926 at	C19orf53	-0.50991417	3.15E-06	0.000522419
223065 s at	STARD3NL	-0.685511323	8.53E-08	3.46E-05
1053 at	RFC2	-0.300698133	2.47E-05	0.002289575
201125 s at	ITGB5	-0.710229499	6.01E-05	0.004382592

1553978 at	MEF2BNB-	-0.568404669	7.07E-06	0.000948173
209198 s at	SYT11	-0.83003113	3.38E-11	1.23E-07
224858 at	ZDHHC5	-0.534040372	1.63E-05	0.001713985
1553978 at	MEF2BNB	-0.568404669	7.07E-06	0.000948173
224749 at	ITFG3	-0.444375221	5.36E-05	0.004034133
231823 s at	SH3PXD2B	-0.720720947	2.19E-08	1.40E-05
223024 at	AP1M1	-0.447245519	8.01E-07	0.00019022
209387 s at	TM4SF1	-0.714078244	7.63E-05	0.005237147
200907 s at	PALLD	-0.425345733	0.000105071	0.006595677
200897 s at	PALLD	-0.449899798	6.38E-05	0.004588076
227493 s at	KIAA1143	-0.567336092	8.64E-05	0.005729516
200001 at	CAPNS1	-0.85259993	3.06E-06	0.000513471
201924 at	AFF1	-0.531039743	5.53E-05	0.004134901
201114 x at	PSMA7	-0.657910857	8.69E-07	0.000202878
216088 s at	PSMA7	-0.755081417	3.71E-06	0.000580328
201095 at	DAP	-0.604241	4.21E-05	0.003365398
235609 at	BRIP1	-0.546501014	1.19E-08	9.65E-06
203344 s at	RBBP8	-0.65704224	8.62E-05	0.005729516
212115 at	HN1L	-0.218924918	9.22E-05	0.005986392
211945 s at	ITGB1	-0.450259304	5.56E-05	0.00414682
1553678 a at	ITGB1	-0.498832565	7.03E-05	0.004949843
200004 at	EIF4G2	-0.256327971	1.69E-06	0.000337765
218815 s at	TMEM51	-0.374214572	1.61E-05	0.001699196
204027 s at	METTL1	-0.432260327	3.14E-06	0.000522419
212294 at	GNG12	-0.42807063	2.65E-07	8.42E-05
202944 at	NAGA	-0.866544715	9.85E-07	0.000223648
1555041 a at	NAGA	-0.309702492	5.99E-05	0.004376945
202943 s at	NAGA	-0.326773537	8.21E-05	0.005547013
224675 at	MESDC2	-0.582250851	7.53E-07	0.000181052
226519 s at	AGXT2L2	-0.441047662	0.000103461	0.006517994
203445 s at	CTDSP2	-0.987781015	1.20E-06	0.000258176
208735 s at	CTDSP2	-0.562503754	8.50E-06	0.001077299
221773 at	ELK3	-1.957343884	1.35E-10	3.50E-07
212005 at	SZRD1	-0.283819637	0.000113567	0.006989855
219119 at	NAA38	-0.246383118	1.50E-05	0.001609269
212923 s at	PXDC1	-0.366157539	3.16E-06	0.000522419
218070 s at	GMPPA	-0.379481284	0.000118505	0.007191019
210719 s at	HMG20B	-0.534857994	9.16E-10	1.47E-06
218025 s at	ECI2	-0.424193994	2.58E-05	0.002354766
209709 s at	HMMR	-0.743896588	3.86E-08	1.97E-05
207165 at	HMMR	-0.742132798	2.06E-09	2.37E-06
218092 s at	AGFG1	-0.383646807	2.18E-05	0.002060779
225415 at	DTX3L	-1.03771168	8.11E-05	0.005497901
201128 s at	ACLY	-0.436348759	7.09E-08	3.08E-05
201127 s at	ACLY	-0.291642941	7.13E-05	0.005004752
211561 x at	MAPK14	-0.303502273	9.34E-05	0.006040609

218847 at	IGF2BP2	-0.412588523	2.53E-05	0.002331414
205573 s at	SNX7	-1.115182619	1.24E-05	0.001387865
202006 at	PTPN12	-0.271249741	6.32E-05	0.004552959
219863 at	HERC5	-0.65950278	7.05E-05	0.004955015
218076 s at	ARHGAP17	-0.388457923	2.34E-06	0.000424747
227038 at	SGMS2	-0.396559122	1.49E-06	0.000306174
204451 at	FZD1	-0.281400201	9.43E-05	0.006085641
208992 s at	STAT3	-2.29344946	1.32E-13	2.40E-09
225289 at	STAT3	-2.241324845	1.01E-11	4.58E-08
208991 at	STAT3	-2.414521098	2.03E-14	1.11E-09
226925 at	ACPL2	-0.699390584	7.28E-05	0.005052033
208829 at	TAPBP	-0.326491451	0.00011513	0.00704676
209476 at	TMX1	-0.285869969	1.68E-05	0.001747912
208948 s at	STAU1	-0.46951292	7.66E-06	0.00099212
219924 s at	ZMYM6	-0.60779049	9.07E-05	0.005917134
219924 s at	ZMYM6NB	-0.60779049	9.07E-05	0.005917134
226122 at	PLEKHG1	-0.688659964	1.16E-05	0.001333511
229893 at	FRMD3	-0.469241058	5.71E-05	0.004238124
224752 at	C7orf73	-0.280896418	5.84E-05	0.004300475
224751 at	C7orf73	-0.605150532	5.12E-10	9.99E-07
222871 at	KLHDC8A	-0.98319795	4.09E-09	3.99E-06
207467 x at	CAST	-1.040908778	2.57E-08	1.49E-05
208908 s at	CAST	-1.06842078	2.26E-08	1.40E-05
202149 at	NEDD9	-0.985723556	1.74E-07	6.04E-05
60471 at	RIN3	-0.291845305	1.71E-05	0.001757107
219457 s at	RIN3	-0.257013893	4.84E-05	0.003715644
201342 at	SNRPC	-0.390825429	4.50E-07	0.0001286

**B. Contingency Table, Univariate and Multivariate Analyses****I. Contingency analysis accounting for:****Molecular Classes**

<i>STAT3</i> /Mol classes	All Glioma			GBM		
	<i>STAT3</i> -High N (%)	<i>STAT3</i> -Low N (%)	Fisher's Exact <i>p</i> -val	<i>STAT3</i> -High N (%)	<i>STAT3</i> -Low N (%)	Fisher's Exact <i>p</i> -val
Proneural	15 (16%)	79 (84%)	< 2.2e-16	0 (0%)	30 (100%)	< 2.2e-16
Classical	13 (18.8%)	56 (81.2%)		17 (62.96%)	10 (37.04%)	
Mesenchymal	1 (1.5%)	68 (98.5%)		46 (92%)	4 (8%)	

**WHO Classes**

<i>STAT3</i> /W.H.O	All Glioma			GBM		
	<i>STAT3</i> -High N (%)	<i>STAT3</i> -Low N (%)	Fisher's Exact <i>p</i> -val	<i>STAT3</i> -High N (%)	<i>STAT3</i> -Low N (%)	Fisher's Exact <i>p</i> -val
<i>IDH1</i> -mut CDL	2 (8.7%)	21 (91.3%)	< 7.22e-11	0 (0%)	3 (100%)	0.012
<i>IDH1</i> -mut NCDL	19 (44.2%)	24 (55.9%)		10 (43.478%)	13 (56.522%)	
<i>IDH1</i> -WT	93 (76.9%)	28 (23.1%)		40 (67.797%)	19 (32.203%)	

**Grade**

<i>STAT3</i> /Grade	All Glioma		
	<i>STAT3</i> -High N (%)	<i>STAT3</i> -Low N (%)	Fisher's Exact <i>p</i> -val
Grade II	1 (3.448%)	28 (96.552%)	< 2.2e-16
Grade III	21 (28.378%)	53 (71.622%)	
Grade IV	106 (78.519%)	29 (21.481%)	

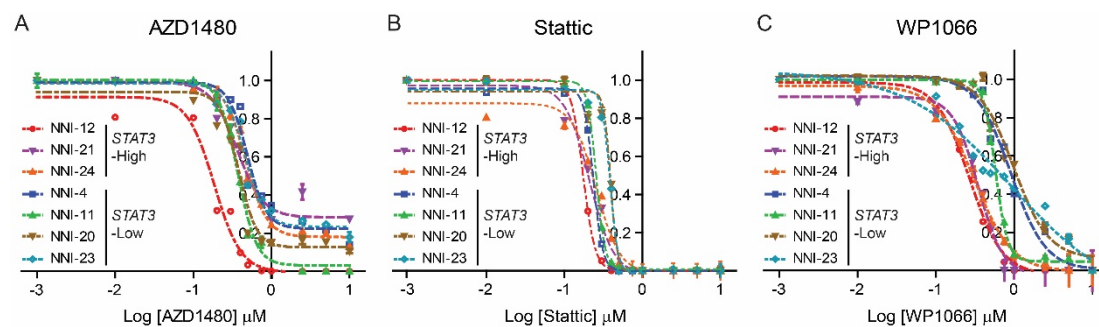
## II. Univariate and multivariate analyses accounting for molecular classes, WHO subtypes and age\*

Covariates	All Glioma						GBM					
	Univariate analysis			Multivariate analysis			Univariate analysis			Multivariate analysis		
	HR (95% CI)	SE	Pr(> z )*	HR (95% CI)	SE	Pr(> z )*	HR (95% CI)	SE	Pr(> z )*	HR (95% CI)	SE	Pr(> z )*
STAT3-High	4.587 (3.327-6.324)	0.164	<2e-16	3.366 (1.978-5.729)	0.272	7.78e-06	1.765 (1.156-2.694)	0.216	0.0085	1.343 (0.811-2.226)	0.258	0.252
WHO IDH-mut NCDL	1.932 (1.11-3.36)	0.283	0.02	2.1 (1.169-3.776)	0.299	0.013	-					
WHO IDH-WT	2.68 (1.628-3.36)	0.254	1.00e-04	1.864 (1.05-3.307)	0.293	0.033	1.801 (1.048-3.094)	0.276	0.0332	1.211 (0.676-2.171)	0.298	0.52
GI Classical	2.2 (1.559-3.105)	0.176	7.29e-06	0.891 (0.564-1.407)	0.233	0.62	1.556 (0.881-2.749)	0.29	0.127	-		
GI Mesenchymal	2.691 (1.906-3.801)	0.176	1.90e-08	0.845 (0.508-1.407)	0.26	0.518	1.35 (0.826-2.208)	0.251	0.231			
Age	1.045 (1.034-1.057)	0.006	8.49e-15	1.041 (1.027-1.055)	0.007	2.98e-9	1.036 (1.018-1.053)	0.009	4.38e-05	1.03 (1.01-1.05)	0.01	0.002

\*STAT3-low patient cohort was considered a reference category to estimate the coefficient in Cox regression model; WHO IDH-Mut CDL (codeleted for chromosome 1p/19q) patients were treated as the reference to estimate the coefficient in Cox regression model; GI (Glioma Intrinsic) Proneural patients were treated as the reference to estimate the coefficient in Cox regression model. CI = confidence interval; WHO = World Health Organization; HR = Hazard ratio; IDH = Isocitrate dehydrogenase; Mut = Mutation; NCDL = non-codeleted for chromosome 1p/19q; Pr(<|z|) = two-sided Wald test *p*-value; SE = standard error of coefficient.



### C. IC<sub>50</sub> Curves of *STAT3*-stratified GPCs Treated with Various *STAT3* Inhibitors



Appendix C. IC<sub>50</sub> curves of *STAT3*-stratified GPCs treated with various *STAT3* inhibitors (A) AZD1480, (B) Stattic and (C) WP1066.

**D. Winnowed List of Genes Contributing to Resistance in *STAT3*-low Cohorts**

ProbeID	SYMBOL	STAT3 KD Clone			REMBRANDT					Gravendeel					TCGA		
		FC Clone vs NT	<i>p</i> -val	Adj <i>p</i> -val	HR	logFC Tum vs Norm	adj <i>p</i> -val	logFC Mes vs NMes	adj <i>p</i> -val	logFC Tum vs Norm	adj <i>p</i> -val	HR	logFC Mes vs NMes	adj <i>p</i> -val	HR	logFC Mes vs NMes	adj <i>p</i> -val
208992 s at	STAT3	-2.293	0.000	0.000	1.983	1.118	0.000	0.807	0.000	1.309	0.000	1.591	0.605	0.000	2.426	0.192	0.000
221773 at	ELK3	-1.957	0.000	0.000	1.916	1.023	0.000	1.156	0.000	2.090	0.000	1.955	1.013	0.000	2.554	0.451	0.000
225415 at	DTX3L	-1.038	0.000	0.005	2.133	1.534	0.000	0.921	0.000	2.160	0.000	2.297	0.807	0.000	4.145	0.406	0.000
220199 s at	AIDA	-1.004	0.000	0.001	1.355	0.223	0.035	0.170	0.000	0.427	0.006	1.284	0.207	0.001	1.987	0.236	0.000
202149 at	NEDD9	-0.986	0.000	0.000	1.616	1.097	0.000	0.802	0.000	1.331	0.000	1.892	0.884	0.000	1.993	0.454	0.000
222871 at	KLHDC8A	-0.983	0.000	0.000	2.622	1.930	0.000	1.127	0.000	2.382	0.000	2.541	0.485	0.049	3.754	0.933	0.000
225406 at	TWSG1	-0.960	0.000	0.003	2.428	0.961	0.000	1.017	0.000	1.304	0.000	2.374	0.807	0.000	4.019	0.621	0.000
202944 at	NAGA	-0.867	0.000	0.000	1.635	0.681	0.000	0.677	0.000	0.981	0.000	1.643	0.662	0.000	3.157	0.446	0.000
225080 at	MYO1C	-0.744	0.000	0.000	1.639	0.345	0.002	0.532	0.000	0.697	0.003	1.325	0.598	0.000	3.682	0.452	0.000
231823 s at	SH3PXD2B	-0.721	0.000	0.000	1.775	1.087	0.000	0.671	0.000	1.634	0.000	2.309	0.680	0.000	1.818	0.226	0.005
225872 at	SLC35F5	-0.703	0.000	0.002	2.189	1.135	0.000	0.853	0.000	0.940	0.000	1.825	0.528	0.000	4.840	0.459	0.000
219863 at	HERC5	-0.660	0.000	0.005	1.669	0.865	0.000	0.727	0.000	1.017	0.040	1.966	0.727	0.000	2.599	0.413	0.003
203024 s at	C5orf15	-0.625	0.000	0.001	2.061	0.338	0.001	0.477	0.000	0.765	0.000	1.627	0.371	0.000	4.520	0.522	0.000
219924 s at	ZMYM6	-0.608	0.000	0.006	1.983	0.655	0.000	0.705	0.000	1.449	0.000	1.511	0.861	0.000	1.817	0.105	0.003
209344 at	TPM4	-0.605	0.000	0.002	1.881	0.509	0.032	0.840	0.000	1.060	0.003	1.955	0.925	0.000	4.554	0.922	0.000
201095 at	DAP	-0.604	0.000	0.003	1.939	1.074	0.000	0.632	0.000	1.279	0.000	1.930	0.665	0.000	5.720	0.524	0.000
209130 at	SNAP23	-0.566	0.000	0.009	1.499	0.733	0.000	0.498	0.000	0.833	0.000	1.530	0.477	0.000	2.426	0.306	0.000
235489 at	RHOJ	-0.545	0.000	0.002	2.169	0.521	0.036	0.963	0.000	1.049	0.009	2.057	0.857	0.000	4.616	0.908	0.000
210719 s at	HMG20B	-0.535	0.000	0.000	1.627	1.396	0.000	0.546	0.000	1.514	0.000	1.496	0.455	0.000	2.197	0.393	0.000
225538 at	ZCCHC9	-0.526	0.000	0.005	2.259	0.703	0.000	0.565	0.000	0.909	0.000	1.912	0.343	0.000	5.354	0.631	0.000
217738 at	NAMPT	-0.517	0.000	0.001	2.306	0.843	0.002	1.795	0.000	1.426	0.001	2.463	1.367	0.000	4.320	1.254	0.000

213113 s at	SLC43A3	-0.500	0.000	0.001	2.580	0.532	0.005	0.991	0.000	2.183	0.000	2.466	0.972	0.000	6.951	1.277	0.000
202076 at	BIRC2	-0.466	0.000	0.004	1.895	0.388	0.000	0.351	0.000	0.462	0.001	1.314	0.132	0.020	1.383	0.186	0.000
222446 s at	BACE2	-0.452	0.000	0.005	1.941	0.368	0.025	0.878	0.000	1.150	0.009	2.315	1.111	0.000	4.239	1.009	0.000
211945 s at	ITGB1	-0.450	0.000	0.004	2.034	0.825	0.000	0.815	0.000	1.192	0.000	1.772	0.791	0.000	3.070	0.673	0.000
224749 at	ITFG3	-0.444	0.000	0.004	1.527	0.548	0.000	0.322	0.000	0.662	0.000	1.592	0.294	0.000	2.839	0.198	0.000
226519 s at	AGXT2L2	-0.441	0.000	0.007	2.056	0.698	0.000	0.476	0.000	0.923	0.000	1.673	0.533	0.000	3.735	0.457	0.000
212294 at	GNG12	-0.428	0.000	0.000	2.082	0.680	0.001	0.960	0.000	1.554	0.001	2.105	0.924	0.000	5.072	0.991	0.000
200907 s at	PALLD	-0.425	0.000	0.007	1.737	1.507	0.000	0.835	0.000	1.883	0.000	1.788	0.545	0.000	3.327	0.550	0.000
218847 at	IGF2BP2	-0.413	0.000	0.002	1.649	0.740	0.001	0.636	0.000	1.790	0.001	1.796	0.959	0.000	4.273	2.056	0.000
218622 at	NUP37	-0.412	0.000	0.008	1.854	0.717	0.000	0.402	0.000	1.647	0.000	2.366	0.232	0.005	5.365	0.634	0.000
210844 x at	CTNNA1	-0.408	0.000	0.001	2.650	0.759	0.000	0.611	0.000	0.470	0.015	2.252	0.410	0.000	2.927	0.219	0.000
218070 s at	GMPPA	-0.379	0.000	0.007	1.855	0.323	0.012	0.536	0.000	0.566	0.013	2.224	0.581	0.000	3.472	0.393	0.000
204531 s at	BRCA1	-0.375	0.000	0.006	1.916	1.167	0.000	0.422	0.000	1.130	0.000	1.885	-0.226	0.036	3.131	0.330	0.000
218815 s at	TMEM51	-0.374	0.000	0.002	1.728	0.924	0.000	0.995	0.000	1.402	0.000	2.670	0.903	0.000	4.384	0.548	0.000
208689 s at	RPN2	-0.329	0.000	0.004	2.029	0.998	0.000	0.547	0.000	1.710	0.000	2.267	0.515	0.000	4.633	0.384	0.000
204451 at	FZD1	-0.281	0.000	0.006	2.366	0.409	0.014	0.750	0.000	1.501	0.000	2.804	1.024	0.000	3.876	0.537	0.000
202006 at	PTPN12	-0.271	0.000	0.005	2.174	0.836	0.000	0.710	0.000	1.206	0.000	2.497	0.520	0.000	3.415	0.412	0.000
219083 at	SHQ1	-0.262	0.000	0.004	1.811	0.329	0.004	0.432	0.000	0.310	0.043	1.899	0.146	0.023	4.778	0.476	0.000
219119 at	NAA38	-0.246	0.000	0.002	1.532	1.091	0.000	0.395	0.000	2.299	0.000	1.569	0.253	0.014	1.968	0.182	0.000

**E. List of Protein Tyrosine Kinase**

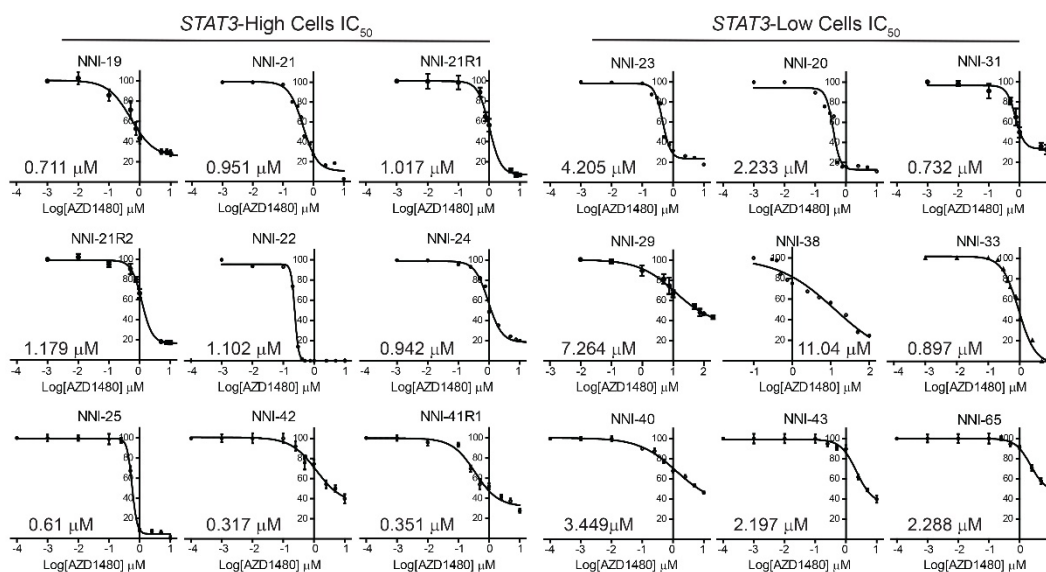
<b>STAT3-High</b>			
<b>Kinases</b>	<b>Log<sub>2</sub>Foldchange</b>	<b>p-value</b>	<b>FDR</b>
ERK1	-0.130003	0.000855	0.023359
ERK2	-0.130003	0.000855	0.023359
RAF1	-0.130003	0.000855	0.023359
BLK	0.116378	0.003183	0.065257
ROR2	-0.132880	0.009185	0.110608
JAK3	-0.072164	0.009442	0.110608
JAK3~b	-0.072164	0.009442	0.110608
Ret	-0.083986	0.014765	0.151341
Lyn	0.060460	0.020579	0.172812
Ron	0.071592	0.022478	0.172812
EphA4	-0.164597	0.023182	0.172812
EphA10	-0.075429	0.035620	0.240748
Syk	-0.140010	0.038167	0.240748
Srm	0.065889	0.049258	0.288510
PKA[alpha]	0.046967	0.096575	0.527944

<b>STAT3-Low</b>			
<b>Kinases</b>	<b>Log<sub>2</sub>Foldchange</b>	<b>p-value</b>	<b>FDR</b>
Srm	0.5972285	0.0215359	0.1818153
DDR2	0.5897400	0.0304162	0.1818153
DYRK1B	0.5807676	0.0311966	0.1818153
CTK	-0.4509096	0.0388479	0.1818153
Kit	0.6433738	0.0400803	0.1818153
IGF-1R	0.3345388	0.0421874	0.1818153
ITK	0.4015083	0.0451334	0.1818153
Mer	0.6474189	0.0468634	0.1818153
ZAP70	-0.3271584	0.0497777	0.1818153
FGFR4	0.3781613	0.0500557	0.1818153
FAK	0.6526299	0.0502942	0.1818153
EGFR	0.3924259	0.0503176	0.1818153
ASK/MAP3K5	0.4158566	0.0511232	0.1818153
MAP2K7	0.4158566	0.0511232	0.1818153
MEKK6/MAP3K6	0.4158566	0.0511232	0.1818153
SEK1/MAP2K4	0.4158566	0.0511232	0.1818153
Brk	-0.3391364	0.0533396	0.1818153
Tyro3/Sky	0.3446778	0.0536684	0.1818153

ALK	-0.4122881	0.0566978	0.1818153
FGFR1	0.4025010	0.0568583	0.1818153
Ret	0.4072459	0.0573280	0.1818153
DDR1	0.3654692	0.0586528	0.1818153
InSR	-0.3360124	0.0593668	0.1818153
Yes	-0.3953469	0.0627906	0.1818153
Src	-0.2713709	0.0631483	0.1818153
ERK1	0.3986351	0.0672459	0.1818153
ERK2	0.3986351	0.0672459	0.1818153
RAF1	0.3986351	0.0672459	0.1818153
EphA10	0.3856443	0.0687550	0.1818153
Ron	0.3677418	0.0690711	0.1818153
Fes	-0.3333383	0.0700469	0.1818153
PYK2	0.7014802	0.0709523	0.1818153
TXK	0.7321577	0.0775809	0.1927768
CSK	0.7554339	0.0845210	0.2038449
JAK3	-0.3007821	0.0922822	0.2101983
JAK3~b	-0.3007821	0.0922822	0.2101983
MEK2/MAP2K2	0.4172901	0.0963204	0.2134668

**F. H-score and IC<sub>50</sub> Values of Patient Tumours****I. H-score**

<b>STAT3</b>	<b>NNI-</b>	<b>3+</b>	<b>2+</b>	<b>1+</b>	<b>0</b>	<b>Total</b>	<b>H-score</b>	<b>Average</b>
High	19	69	80	131	89	369	134.96	1.40
	19	79	86	123	79	367	144.96	
	52/41R1	31	283	346	33	693	145.02	1.47
	52/41R1	36	298	348	24	706	149.01	
	21	95	11	5	159	270	115.56	1.18
	21	87	20	13	141	261	120.31	
	21R1	40	154	72	64	330	151.52	1.50
	21R1	59	181	50	105	395	149.11	
	21R2	0	3	10	107	120	13.33	0.14
	21R2	0	4	9	109	122	13.93	
	22	6	2	15	163	186	19.89	0.22
	22	7	3	16	158	184	23.37	
	42	0	0	0	320	320	0.00	0.00
	42	0	0	0	213	213	0.00	
	24	0	20	76	124	220	52.73	0.50
	24	0	17	82	145	244	47.54	
	25	0	0	9	164	173	5.20	0.04
	25	0	0	5	198	203	2.46	
	32	0	0	14	356	370	3.78	0.04
	32	0	0	13	367	380	3.42	
Low	31	40	81	28	197	346	89.60	0.94
	31	41	56	31	142	270	98.52	
	20	391	36	0	10	437	284.90	2.83
	20	398	35	2	15	450	281.33	
	33	0	12	37	151	200	30.50	0.27
	33	0	10	32	178	220	23.64	
	38	0	0	0	100	100	0.00	0.00
	38	0	0	0	100	100	0.00	
	40	0	12	45	813	870	7.93	0.08
	40	0	8	49	816	873	7.45	
	29	0	1	141	188	330	43.33	0.39
	29	0	2	130	258	390	34.36	
	43	484	8	9	16	517	285.69	2.90
	43	496	5	2	8	511	293.54	
	23	0	0	92	128	220	41.82	0.44
	23	0	0	95	115	210	45.24	
	65	102	34	63	88	287	152.26	1.57
	65	103	23	102	54	282	162.06	

II. IC<sub>50</sub> curves of *STAT3*-stratified GPCs treated with AZD1480Appendix F (II). IC<sub>50</sub> curves of *STAT3*-stratified GPCs treated with AZD1480.

## 9.0 PUBLICATIONS

**Melanie SY Tan**\*, Edwin Sandanaraj\*, Yuk Kien Chong, See Wee Lim, Lynnette WH Koh, Wai Hoe Ng, Nguan Soon Tan, Carol Tang, Beng Ti Ang. *STAT3*-based Glioma Patient Stratification and Application in Precision Oncology. \*co-first authors. Manuscript under revision (Nature Communications).

**Tan SY Melanie**, Sandanaraj E, Tang C, Ang BT. Biobanking: An Important Resource for Precision Medicine in Glioblastoma. *Advances in Experimental Medicine and Biology* 2016.

Yuk Kien Chong, Edwin Sandanaraj, Lynnette WH Koh, Moogaambikai Thangaveloo, **Melanie SY Tan**, Geraldene RH Koh, Tan Boon Toh, Grace GY Lim, Joanna D Holbrook, Oi Lian Kon, Mahendran Nadarajah, Ivan Ng, Wai Hoe Ng, Nguan Soon Tan, Kah Leong Lim, Carol Tang, Beng Ti Ang. *ST3GALI*-associated transcriptomic program in glioblastoma tumor growth, invasion and prognosis. *Journal of the National Cancer Institute* 2016.



**10.0 POSTERS**

**Melanie SY Tan**\*, Edwin Sandanaraj\*, See Wee Lim, Yuk Kien Chong, Lynnette WH Koh, Wai Hoe Ng, Nguan Soon Tan, Carol Tang, Beng Ti Ang. STAT3 Signalling Stratifies Glioma Patients and Identifies Cohorts Most Likely to Receive Treatment Benefit from Inhibition Therapy. Cancer Research UK – Brain Tumour Conference 2018. \*co-first authors.

**Melanie SY Tan**\*, Edwin Sandanaraj\*, Yuk Kien Chong, Lynnette WH Koh, See Wee Lim, Wai Hoe Ng, Nguan Soon Tan, Carol Tang, Beng Ti Ang. STAT3 Signalling Stratifies Glioma Patients and Identifies Cohorts Most Likely to Receive Treatment Benefit from Inhibition Therapy. Frontiers in Cancer Science 2016. \*co-first authors.

**Melanie SY Tan**\*, Edwin Sandanaraj\*, Yuk Kien Chong, Moogaambikai Thangaveloo, Lynnette WH Koh, Dipti Thakkar, Wai Hoe Ng, Nguan Soon Tan, Carol Tang, Beng Ti Ang. Patient stratification in Brain Tumors – The JAK/STAT Story. Frontiers in Cancer Science 2015. \*co-first authors.

**Melanie SY Tan**, Edwin Sandanaraj\*, Yuk Kien Chong, Moogaambikai Thangaveloo, Wai Hoe Ng, Nguan Soon Tan, Carol Tang, Beng Ti Ang. Patient Stratification in Brain Tumors – The JAK/STAT Story. National Neuroscience Institute Research Day 2015. \*co-first authors.